NASA CONTRACTOR REPORT

NASA CR-1745

NASA CR-1745

STRUCTURAL DYNAMICS OF THE HELIOGYRO

by Richard H. MacNeal

Prepared by

THE MACNEAL-SCHWENDLER CORPORATION

Los Angeles, Calif. 90041

for

NATIONAL AERONAUTICS AND SPACE ADMINISTRATION • WASHINGTON, D. C. • MAY 1971

1. Report No.	2. Government Accession No.	3. Recipient's Catalog No.
NASA CR-1745		

4. Title and Subtitle	5. Report Date
STRUCTURAL DYNAMICS OF THE HELIOGYRO	May 1971
	6. Performing Organization Code
7. Author(s)	8. Performing Organization Report No.
Richard H. MacNeal	MS-73-1
	10. Work Unit No.
9. Performing Organization Name and Address	11. Contract or Grant No.
The MacNeal-Schwendler Corporation 7442 North Figueroa Street Los Angeles, California 90041	NAS7-699
	13. Type of Report and Period Covered
12. Sponsoring Agency Name and Address	Contractor Report
National Aeronautics and Space Administration Washington, D. C. 20546	14. Sponsoring Agency Code

15. Supplementary Notes

16. Abstract

The Heliogyro is a particular form of the solar sail in which the reflecting surface consists of a set of long, narrow and very thin blades that rotate about a central axis in the manner of a helicopter rotor. Blade pitch is the primary means of control. The structural dynamics of the Heliogyro are studied in this report in order to provide a basis for engineering development and to answer questions regarding concept feasibility. The topics that are examined include vibration modes, damping, coupling between blade pitch and blade bending, and dynamic response to maneuver commands. The results of a brief experimental program are presented and compared with analysis.

17. Key Words (Suggested by Author(s))	18. Distribution Statement
Heliogyro Rotating System Dynamics Centrifugal Structures Space Vehicles	Unclassified - Unlimited

19. Security Classif. (of this report)	20. Security Classif. (of this page)	21. No. of Pages	22. Price*
Unclassified	Unclassified	105	$3.00

*For sale by the National Technical Information Service, Springfield, Virginia 22151

TABLE OF CONTENTS

LIST OF TABLES

LIST OF FIGURES

LIST OF SYMBOLS

B_d	Viscous damping coefficient of damper
c	Blade chord
D	Plate bending stiffness
d	Diameter of roller
E	Elastic Modulus
f_r	Coefficient of reflectivity
f_{rx}	Inplane component of load per unit span due to radiation pressure
f_{rz}	Vertical component of load per unit span due to radiation pressure
f_x	Force component/unit length
$\overline{f}_x$	$f_x/\rho\Omega^2 chR$, scaled inplane load
f_y	Force component/unit length
f_z	Force component/unit length
$\overline{f}_z$	$f_z/\rho\Omega^2 chR$, scaled vertical load
G	Shear modulus
g	Acceleration constant; also damping coefficient
g_d	Damping coefficient of damper
g_e	Material damping coefficient
g_i	i = 1, 2, etc. modal damping
h	Blade thickness
h_f	Thickness of metal facing
I	$\frac{1}{12} hc^3$ chordwise moment of inertia
I_i	i = 1, 2, etc. modal inertia
I_ζ	Inplane inertia
K	$\frac{2EI}{\rho\Omega^2 chR^4}$, dimensionless inplane bending stiffness parameter
K_b	Brace stiffness

K_c	Centrifugal stiffness
K_d	Spring constant of damper
K_i	i = 1, 2, etc. modal stiffness
K_ζ	Inplane bending spring
ℓ_b	Distance between battens
m_c	Chordwise bending moment load per unit span
M_d	Moment applied to damper
M_β	Vertical bending moment
M_ζ	Inplane bending moment
m_θ	Pitching moment per unit length
$\bar{m}_\theta$	$m_\theta/\rho\Omega^2 I$, scaled pitching moment load
n	Parameter in Legendre's equation
p_a	Radiation pressure for absorbed light
p_d	Component of radiation pressure parallel to illumination
p_ℓ	Component of radiation pressure normal to illumination
p_n	Radiation pressure normal to blade surface
p_o	Radiation pressure for zero incidence angle and 100% reflectivity
p_r	Radiation pressure for reflected light
R	Blade radius
r	Spanwise position
r_b	Length of brace
R_c	Radius of curvature
T	Kinetic energy
t	time
T_o	Centrifugal tension at blade root

u	Inplane displacement (positive aft)
$\bar{u}$	u/R, dimensionless inplane displacement
V	Potential energy
v	Radial displacement
w	Vertical displacement (positive up)
$\bar{w}$	w/R, dimensionless vertical displacement
w_h	Wave height
x	Chordwise position (positive aft)
x_p	Distance from the center of pressure to the midchord
y	r/R, normalized spanwise position
z	Vertical position (positive up)
α	Coefficient of thermal expansion; also wave number, see Eqs. (128) and (129)
α_o	Blade arc
β	$\frac{\partial w}{\partial r}$ spanwise blade slope
β_o	$\frac{p_o R}{\sigma_o h}$ coning angle at blade root for zero pitch angle
β_p	Inclination of pitch axis
β_s	Blade static slope in vertical plane
γ	Incidence angle of illumination
ΔT	Difference in temperature between leading and trailing edges
ζ	$\frac{\partial u}{\partial r}$, inplane blade slope
ζ_o	Inplane slope at blade root
θ	Pitch
θ_c	Pitch control angle
θ_o	Pitch angle at blade root

λ	Wavelength
λ_s	Sail lightness number = $\frac{\text{radiation pressure}}{\text{solar gravitational force/unit area}}$
ρ	Density of blade material
σ_o	$\frac{1}{2}\rho\Omega^2R^2$, spanwise stress at blade root for a uniform blade
σ_r	Spanwise stress
σ_x	Chordwise stress
σ_y	Yield stress
τ	Ωt, dimensionless time; also shear stress
ψ	Ωt, blade azimuth angle relative to plane of illumination
Ω	Rotational speed (rad/unit time)
ω	Frequency (rad/unit time)
$\overline{\omega}$	ω/Ω, frequency in cycles per revolution

STRUCTURAL DYNAMICS OF THE HELIOGYRO

SUMMARY

The Heliogyro is a particular form of the solar sail in which the reflecting surface consists of a set of long, narrow and very thin blades that rotate about a central axis in the manner of a helicopter rotor. Blade pitch is the primary means of control. The structural dynamics of the Heliogyro are studied in this report in order to provide a basis for engineering development and to answer questions regarding concept feasibility. The topics that are examined include vibration modes, damping, coupling between blade pitch and blade bending, and dynamic response to maneuver commands. The results of a brief experimental program are presented and compared with analysis.

INTRODUCTION

The Heliogyro is a particular form of the solar sail, which is the name that has been given (Refs. 1, 2, 3) to a class of devices which develop useful mechanical force in space from solar radiation pressure. The principle of operation of the solar sail is illustrated in Figure 1. Light is partly reflected and partly absorbed at the surface of an object. The part that is reflected exerts a pressure

$$p_r = p_o f_r \cos^2\gamma \tag{1}$$

normal to the surface, where p_o is the total pressure for normal incidence due to reflected light, f_r is the coefficient of reflectivity, and γ is the incidence angle. The part that is absorbed exerts a pressure

$$p_a = \frac{1}{2} p_o (1 - f_r) \cos\gamma \tag{2}$$

in the direction of the incident radiation. The part that is absorbed is eventually reradiated diffusely from both sides of the reflecting surface.

The components of radiation pressure are combined as follows to obtain a drag pressure, p_d, in the direction of illumination and a lift pressure, p_ℓ, perpendicular to the illumination.

$$p_d = p_o\{f_r \cos^3\gamma + \frac{1}{2}(1-f_r)\cos\gamma\} \tag{3}$$

$$p_\ell = p_o(f_r \cos^2\gamma \sin\gamma) \tag{4}$$

The coefficient of reflectivity, f_r, is high for the metalized surfaces envisaged in the solar sail concept. It is commonly assumed equal to unity in preliminary design studies.

The lift and drag components of solar radiation pressure have a strong analogy with the lift and drag components of aerodynamic pressure, so that a pseudo-aerodynamic theory of solar sail behaviour can be developed. The lift force is particularly important because it provides the means for generating forces to accelerate or decelerate a body that is in a circular orbit around the sun.

The magnitude of the solar radiation pressure is not large by terrestrial standards. At the Earth's distance from the sun its average is equal to 0.90×10^{-4} dynes/cm^2 = 0.188×10^{-6} lb/ft^2 = $.1304 \times 10^{-8}$ psi. Very large surface areas are required to obtain enough thrust to be useful for propulsion. Fortunately for the solar sail concept, the technology is available for the manufacture of extremely thin reflecting surfaces. Standard commercially available 1/4 mil aluminized Mylar, for example, makes a solar sail that is quite competetive with other means of propulsion on long missions.

The fundamental performance parameter of the solar sail is the sail lightness number, λ_s, which is defined as the ratio of the solar radiation pressure to the solar gravitational force per unit area. Since both factors vary inversely as the square of the distance from the sun, the lightness number is constant within the solar system. The sail lightness number is related to the thickness, h, of the sail, and its weight density, ρg, by

$$\lambda_s = \frac{2.15 \times 10^{-6}}{(\rho g)h} \tag{5}$$

where the units of $(\rho g)h$ are lbs/in^2. The value of λ_s for 1/4 mil aluminized Mylar is approximately equal to 0.16.

Figure 2, taken from Ref. 4, shows a comparison of the propulsive efficiency of the solar sail and several other propulsion systems. Specific impulse is used as the measure of efficiency. It is seen that the specific impulse of the solar sail increases (linearly) with mission duration and that it outstrips all competing systems for mission durations greater than 1000 days. The range of values of lightness number used in Figure 2, $.25 < \lambda_s < 1.0$, extends from a value that is available with present technology to a value that seems feasible with future development. The performance ranges for the other propulsion system were selected in the same spirit.

Analyses of optimum interplanetary flight trajectories have been reported by several solar sail investigators (Refs. 5, 6, 7, 8), particularly for voyages to Mars and Jupiter. Applications of the solar sail concept for other purposes, including orientation control, station keeping, station changing, and micrometeoroid collection, have also been studied, Ref. 6 and 9.

In spite of favorable performance estimates, the solar sail was not initially given serious consideration, due to the absence of credible solutions for deploying, rigidizing and orienting the extremely large surface areas that are required. Table I shows a morphology of some of the choices that are available in the design of the solar sail. Early investigators favored the circular shape, which virtually defies deployment in large sizes. The more recent Heliogyro concept (Ref. 9), which employs the design choices underlined in Table I (very slender, centrifugal force, reflecting surface rotation) shows promise of providing practical solutions for the problems associated with large size.

The Heliogyro is, in effect, a helicopter rotor operating in a space environment. Its blades are made from thin reflecting sheets that are stowed on spools prior to deployment. The rotation of reflecting surfaces is achieved by pitching the blades about their lengthwise axes. Centrifugal force provides effective bending stiffness and torsional stiffness for the blades. A sketch of a two-bladed experimental model, proposed in Ref. 9, is shown in Figure 3. Concept models of much larger multi-bladed vehicles for manned interplanetary voyages are also described in Ref. 9.

The design concept of the Heliogyro borrows much from helicopter technology including the use of centrifugal force to rigidize the blades, and the use of blade pitch for control. The use of cyclic and collective pitch controls to produce lateral forces and moments and to impart initial spin during deployment are discussed in Ref. 9. Calculations are made there of deployment times, precession rates, and of the times required to perform such useful maneuvers as planetary escape. The results show that the maneuver performance is good and that the stress levels are low for vehicles ranging in size from the smallest up to several hundred thousand pounds gross weight, even though the latter may have rotor diameters of fifty miles or more. The calculations are, however, based on the usual assumption made in helicopter performance analysis that structural dynamic effects are negligible. Thus the rotor blades are assumed to respond instantly to pitch inputs, and pitching moments due to flapwise and chordwise motions are ignored even though the effective torsional stiffness provided by centrifugal force is very low. The means for providing damping in the absence of an aerodynamic environment were not discussed.

The purpose of the present report is to treat the structural dynamics of the Heliogyro in such a manner as to provide a basis for engineering development and to answer questions regarding concept feasibility that are raised by dynamic considerations. The subject will be treated by the techniques of helicopter rotor dynamics, but differences between an Earthbound and a space environment, and differences in scale and proportion require that the treatment start at an elementary level and that it carefully examine the basis of every assumption. It will be convenient, for the estimation of the magnitude of effects, to refer occasionally to the numerical values of parameters for a specific representative blade design. That design, whose properties are listed in Table 2, will be called the Sample Blade.

UNCOUPLED EQUATIONS OF MOTION

Since helicopter rotor blades are relatively slender (a condition which applies, a fortiori, to the Heliogyro blade), it is usual to analyze their motion by means of engineering beam theory. The notational system that will be used to describe blade motions is shown in Figure 4. The equilibrium position of the blade is assumed to lie in a plane perpendicular to the axis of rotation. The undeflected axis of the blade is assumed to be straight. The assumption of initial straightness, which is made for convenience in analysis, can be relaxed without difficulty. The independent degrees of freedom of the blade at points along its axis are its translations (u, v, and w), and its rotation, θ, about the blade axis. Distortion of the cross-sectional shape (e.g., by cambering) is neglected, or is treated by a secondary analysis. In the case of the Heliogyro, chordwise camber requires special consideration as will be shown later. Extensional strain parallel to the blade axis is neglected on the assumption that the extensional rigidity is very large compared to the bending and twisting rigidities. Vertical and inplane shearing flexibilities are similarly ignored.

All of the above assumptions, except as noted, self-evidently apply to the sample Heliogyro blade whose properties are listed in Table 2. In addition, the thinness of the blade permits us to ignore the elastic bending stiffness in a plane normal to the blade chord and the elastic torsional stiffness, in comparison with the corresponding centrifugal stiffening effects.

An uncoupled analysis of blade motions is one in which the differential equations for twist, θ, vertical deflection, w, and inplane deflection, u, are uncoupled. In such an analysis the coupling due to off-axis center of gravity location, and the nonlinear effects of finite motions, etc., are ignored. The uncoupled equations yield valuable information regarding vibration modes and the dynamic response to excitation. The uncoupled small-motion equations, which incorporate the assumptions which have been mentioned, are:

TWIST:

$$\underset{(2)}{-\frac{\partial}{\partial r}\left(I\sigma_r \frac{\partial}{\partial r}\right)} + \underset{(3)}{\rho\Omega^2 I\theta} + \underset{(4)}{\rho I\frac{\partial^2\theta}{\partial t^2}} = m_\theta \qquad (6)$$

VERTICAL DISPLACEMENT: ② ④

$$-\frac{\partial}{\partial r}\left(ch\sigma_r \frac{\partial w}{\partial r}\right) + \rho ch\frac{\partial^2 w}{\partial t^2} = f_z \qquad (7)$$

IN-PLANE DISPLACEMENT:

① ② ③ ④

$$\frac{\partial^2}{\partial r^2}\left(EI\frac{\partial^2 u}{\partial r^2}\right) - \frac{\partial}{\partial r}\left(ch\sigma_r \frac{\partial u}{\partial r}\right) - \rho ch\Omega^2 u + \rho ch\frac{\partial^2 u}{\partial t^2} = f_x \qquad (8)$$

The symbols that occur in the above equations are defined in the list of symbols. In particular, σ_r is the spanwise component of stress due to centrifugal force. The symbols ①, ②, ③, and ④ classify the terms according to their origin as follows:

① - terms derived from elastic stiffness

② - spanwise stiffness terms derived from rotation (centrifugal stiffening)

③ - local stiffness terms derived from rotation (gyroscopic stiffness terms)

④ - ordinary inertia terms..

The terms on the right hand side represent the loading per unit spanwise length and also the coupling effects that will be developed later. It will be noted that only the inplane displacement contains an elastic stiffness term. The gyroscopic stiffness term in the first equation (which is sometimes called the tennis racket effect) is stabilizing in the sense that it resists applied moment. The gyroscopic stiffness term in the inplane displacement equation is destabilizing but the combined effect of the second and third terms is stabilizing (or neutral in the case of rigid rotation about the z axis). The equations have been written so that they are correct when the blade properties (ρ, h, c, I, ξ) vary along the span. The blade properties will, however, be assumed to be constant in most calculations.

A set of boundary conditions is required in addition to the differential equations. At the outboard end the boundary conditions are that no concentrated forces are applied. At the inboard end the boundary conditions depend on the nature of the body located at the center, and on the number of blades connected to it. It is convenient, for initial treatment, to assume that the center body is massive so that translations (u, w) and the inplane rotation, ζ, are zero.

If many blades are present, these conditions are also correct in the presence of finite hub mass for many of the vibration modes (all except those with so-called cyclic and collective symmetry, ref. 10). The root end boundary condition on the pitch angle, θ, is that it must follow the motion imposed on it by the pitch control mechanism.

The boundary conditions should be applied at a short distance from the center line due to the finite length of the attachment fittings. Such offsets are important for helicopter rotor analysis. Due to the extreme length of Heliogyro blades, the boundary condition offsets are only a very small fraction of blade span. Their effects will be treated by perturbation techniques applied to the solutions for zero offset.

It is convenient, for the study of trends, to reduce the equations of motion to dimensionless form. This may be done by introducing the following scaling for the independent and dependent variables.

Independent variables:

$$y = \frac{r}{R} \tag{9}$$

$$\tau = \Omega t \tag{10}$$

Dependent variables:

$$\bar{u} = \frac{u}{R} \tag{11}$$

$$\bar{w} = \frac{w}{R} \tag{12}$$

In addition it will be assumed that the blade properties are uniform along the span. For that condition the spanwise stress due to centrifugal force is

$$\sigma_r = \frac{1}{2}\rho\Omega^2(R^2 - r^2) \tag{13}$$

Dimensionless equations of motion are then obtained by dividing equation (6) by $\rho\Omega^2 I$ and equations (7) and (8) by $\rho\Omega^2 chR$. The results are:

TWIST:

$$-\frac{1}{2}\frac{\partial}{\partial y}\left((1-y^2)\frac{\partial\theta}{\partial y}\right) + \theta + \frac{\partial^2\theta}{\partial\tau^2} = \bar{m}_\theta \tag{14}$$

VERTICAL DISPLACEMENT:

$$-\frac{1}{2}\frac{\partial}{\partial y}\left((1-y^2)\frac{\partial \bar{w}}{\partial y}\right)+\frac{\partial^2 \bar{w}}{\partial \tau^2}=\bar{f}_z \tag{15}$$

INPLANE DISPLACEMENT:

$$\frac{1}{2}\frac{\partial^2}{\partial y^2}\left(K\frac{\partial^2 \bar{u}}{\partial y^2}\right)-\frac{1}{2}\frac{\partial}{\partial y}\left((1-y^2)\frac{\partial \bar{u}}{\partial y}\right)-\bar{u}+\frac{\partial^2 \bar{u}}{\partial \tau^2}=\bar{f}_x \tag{16}$$

where $\bar{m}_\theta$, $\bar{f}_z$, and $\bar{f}_x$ are the scaled loads and K is a dimensionless parameter,

$$K=\frac{EI}{\frac{1}{2}\rho\Omega^2 chR^4}=\frac{1}{12}\frac{E}{\sigma_o}\left(\frac{c}{R}\right)^2 \tag{17}$$

σ_o is the spanwise stress at the blade root due to centrifugal force,

$$\sigma_o=\frac{1}{2}\rho\Omega^2R^2 \tag{18}$$

K, which is the only parameter appearing on the left hand side of the equations of motion, is a measure of the elastic chordwise bending stiffness relative to the stiffness provided by centrifugal force. Since equation (16) is dimensionless and since the range of y is $0 < y < 1$, the magnitude of K provides a direct indication of the relative magnitude of the elastic bending stiffness. For the sample blade whose properties are listed in Table 2,

$$K=\frac{1}{12}\frac{10^6}{10^3}\cdot\left(\frac{10}{10^4}\right)^2=.833\times 10^{-4} \tag{19}$$

For comparison, the value of K for a conventional helicopter blade is of the order of unity.

UNCOUPLED VIBRATION MODES

The homogeneous equations of motion, when written in dimensionless form, contain only a single parameter, and it has been shown that that parameter, K, is small for Heliogyro blades. If K is set equal to zero and if sinusoidal motion, $e^{i\bar{\omega}\tau}$, is assumed, the uncoupled homogeneous equations become

TWIST:

$$\frac{1}{2}\frac{d}{dy}\left((1-y^2)\frac{\partial\theta}{\partial y}\right) + (\bar{\omega}^2 - 1)\,\theta = 0 \tag{20}$$

VERTICAL DISPLACEMENT:

$$\frac{1}{2}\frac{d}{dy}\left((1-y^2)\frac{\partial\bar{w}}{\partial y}\right) + \omega^2\bar{w} = 0 \tag{21}$$

INPLANE DISPLACEMENT:

$$\frac{1}{2}\frac{d}{dy}\left((1-y^2)\frac{\partial\bar{u}}{\partial y}\right) + (\bar{\omega}^2 + 1)\,\bar{u} = 0 \tag{22}$$

All three equations are variations of Legendre's equation, for which the standard form is

$$\frac{d}{dy}\left((1-y^2)\frac{dx}{dy}\right) + n(n+1)x = 0 \tag{23}$$

The parameter n in equation (23) may be considered to be an eigenvalue whose value is determined by boundary conditions. For the range, $0 < y < 1$, the eigenvalues for zero displacement at $y = 0$ are the set of odd integers, and the eigenvalues for zero slope at $y = 0$ are the set of even integers. The corresponding eigenvectors are the Legendre polynomials, $P_n(y)$, listed below.

n	$P_n(y)$	$P_n(0)$	$P_n(1)$
0	1	1	1
1	y	0	1
2	$\frac{1}{2}(3y^2 - 1)$	-1/2	1
3	$\frac{1}{2}(5y^3 - 3y)$	0	1
4	$\frac{1}{8}(35y^4 - 30y^2 + 3)$	3/8	1
5	$\frac{1}{8}(63y^5 - 70y^3 + 15y)$	0	1

Formulas for the vibration mode frequencies, obtained by comparing equation (23) to equations (20), (21) and (22), are:

TWIST:

$$\bar{\omega} = \frac{\omega}{\Omega} = \sqrt{\frac{n(n+1)}{2} + 1} \tag{24}$$

VERTICAL DISPLACEMENT:

$$\bar{\omega} = \frac{\omega}{\Omega} = \sqrt{\frac{n(n+1)}{2}} \tag{25}$$

INPLANE DISPLACEMENT:

$$\bar{\omega} = \frac{\omega}{\Omega} = \sqrt{\frac{n(n+1)}{2} - 1} \tag{26}$$

The scaled frequency, $\bar{\omega}$, is the value of the vibration frequency in cycles per revolution. Table 3 gives the numerical values of $\bar{\omega}$ for the first four modes of each type with zero root end motion.

It is noteworthy that the vibration mode frequencies bear a fixed relationship to rotor speed, regardless of size, shape or blade material properties. It is fortunate, from the viewpoint of resonant excitation due to environmental effects, that none of the higher ($n > 1$) vertical and inplane mode frequencies are exact harmonics of rotor speed. The twist mode resonance at 4/rev. is not serious because damping can easily be introduced into the pitch degree of freedom, as will be shown.

The lowest vertical and inplane modes at $n = 1$ correspond to rigid body rotations of the blade about a fixed hub. The vertical mode frequency, which is at 1/rev. in a coordinate system that rotates with the blade, occurs at zero frequency and also at 2/rev. in a nonrotating coordinate system. These frequencies correspond to the precession and nutation of the vehicle as a whole.

Only two of the solutions with even order Legendre polynomials have practical significance. They are the lowest order (n = 0) twist mode which has a frequency of one cycle per revolution, and the lowest order vertical mode whose frequency is zero. The vertical mode is trivial since it simply describes rigid body translation parallel to the axis of rotation. The existence of the twist mode, on the other hand, demonstrates the important result that a cyclic pitch imposed at the blade root at a frequency of one cycle per revolution will result in a uniform response along the blade span. This kind of excitation is employed in several types of maneuvers, see reference 9.

At excitation frequencies other than 1/rev., the pitch response to excitation imposed at the root is not uniform due to the imbalance between the inertia and the local centrifugal stiffening terms. Figure 5 is a plot of the ratio of blade tip response to blade root excitation as a function of the exciting frequency, obtained by numerical integration of equation (20). The result for zero excitation frequency ($\theta_{tip}/\theta_{root} = .319$) is important because it is the steady state limit for collective pitch excitation.

The solutions that have been presented for uncoupled inplane modes are subject to the assumption that the elastic chordwise bending stiffness is zero. Except for the lowest mode, the error due to this assumption is unimportant for the very slender blades envisaged for the Heliogyro. The error in the lowest (n = 1) mode depends on the boundary condition for chordwise slope at the blade root. For modes with collective symmetry (modes in which all blades execute identical motions) the error is zero because the appropriate boundary condition, which is that the chordwise bending moment is zero, is satisfied by the assumed eigenvector. For all other types of modes, the appropriate boundary condition is that the chordwise slope is zero, which results in a finite value for the lowest mode frequency.

An analytical expression will be derived for the lowest mode frequency on the assumption that the chordwise bending stiffness parameter, K, is small but finite. The approach will be to derive an expression for the chordwise deflection that satisfies the boundary conditions at the root ($\bar{u} = 0$, $d\bar{u}/dy = 0$), that approximately satisfies the differential equation near the root, and that asymtotically approaches the straight line ($\bar{u} = y$) predicted for K = 0. The expression for deflection will then be substituted into a Rayleigh quotient to obtain an approximate frequency.

Neglecting inertia and local centrifugal stiffening terms in equation (16), the homogeneous differential equation for inplane bending near the root, $y << 1$, is approximately

$$K \frac{d^4\bar{u}}{dy^4} - \frac{d^2\bar{u}}{dy^2} = 0 \tag{27}$$

A solution which satisfies the differential equation and the boundary conditions, and that remains finite as y increases is

$$\bar{u} = \zeta_o \left\{ y - \sqrt{K} \left(1 - e^{-\frac{y}{\sqrt{K}}} \right) \right\} \tag{28}$$

Note that, for $y >> \sqrt{K}$, the deflection is approximately a straight line that intersects the y axis at $y = \sqrt{K}$.

The kinetic and potential energy functions for the blade are easily identified by examination of the terms in equation (16). They are

$$T = \frac{1}{2} \int_o^1 \bar{\omega}^2 \bar{u}^2 dy \tag{29}$$

$$V = \frac{1}{4} \int_o^1 \left[K \left(\frac{d^2\bar{u}}{dy^2} \right)^2 + (1-y^2) \left(\frac{d\bar{u}}{dy} \right)^2 - 2\bar{u}^2 \right] dy \tag{30}$$

The Rayleigh's quotient is

$$\bar{\omega}^2 = \frac{\int_o^1 \left[K \left(\frac{d^2\bar{u}}{dy^2} \right)^2 + (1-y^2) \left(\frac{d\bar{u}}{dy} \right)^2 - 2\bar{u}^2 \right] dy}{2 \int_o^1 \bar{u}^2 dy} \tag{31}$$

If equation (28) is substituted into equation (31), and if $\sqrt{K'}$ is treated as a small parameter such that higher order terms may be neglected in comparison with lower order terms, the resulting expression for the lowest inplane frequency is

$$\bar{\omega} = \sqrt{\frac{3}{2}\sqrt{K'}} \tag{32}$$

Straightforward analysis, reference 11, of a uniform articulated rotor blade with lag hinge offset, e, shows that the lowest inplane frequency is (approximately)

$$\bar{\omega} = \sqrt{\frac{3}{2}\frac{e}{R}} \tag{33}$$

By comparison of equations (32) and (33), the "effective" lag hinge offset for a Heliogyro blade is

$$e = R\sqrt{K'} \tag{34}$$

For the Sample Blade design, $K = .833 \times 10^{-4}$, so that $\bar{\omega} = \left(\frac{3}{2}(.833\times10^{-4})^{1/2}\right)^{1/2}$ = .1182/rev. From the form of equations (17) and (32), it is seen that the frequency of the lowest inplane mode is inversely proportional to the square root of the blade aspect ratio, R/c.

A rough estimate of the effect of chordwise bending stiffness on the higher modes can be obtained by substituting the assumed displacement function for K = 0 into the potential energy function, equation (30). The resulting frequency is

$$\bar{\omega} = \bar{\omega}_o(1 + \varepsilon) \tag{35}$$

where $\bar{\omega}_o$ is the frequency for K = 0 and

$$\varepsilon \simeq \frac{V_e}{2V_c} = \frac{\int_o^1 K\left(\frac{d^2\bar{u}}{dy^2}\right)^2 dy}{2\int_o^1 \left[(1-y^2)\left(\frac{d\bar{u}}{dy}\right)^2 - 2\bar{u}^2\right] dy} \tag{36}$$

As an example consider the second mode (n = 3) for which the deflection function (Legendre polynomial) is $\bar{u} = 5y^3 - 3y$.

For this function,

$$\left.\begin{aligned} (\bar{u})^2 &= 25y^6 - 30y^4 + 9y^2 \\ \left(\frac{d\bar{u}}{dy}\right)^2 &= 225y^4 - 90y^2 + 9 \\ \left(\frac{d^2\bar{u}}{dy^2}\right)^2 &= 900y^2 \end{aligned}\right\} \tag{37}$$

and the result is

$$\varepsilon = 52.5K \tag{38}$$

For the Sample Blade, $K = .833 \times 10^{-4}$ and $\varepsilon = .00436$. The importance of the chordwise bending stiffness increases as the mode index increases. For high order modes the eigenfunction is approximately a sine wave,

$$\bar{u} = \sin \frac{2\pi y}{\lambda} \tag{39}$$

where λ is the wavelength. An estimate of the effect on frequency is obtained by neglecting $2\bar{u}^2$ and replacing $1-y^2$ by $2/3$ in the denominator of equation (36). Thus

$$\varepsilon \simeq \frac{K\left(\frac{2\pi}{\lambda}\right)^4}{\frac{4}{3}\left(\frac{2\pi}{\lambda}\right)^2} = \frac{3\pi^2 K}{\lambda^2} \tag{40}$$

The condition under which the elastic energy and the potential energy of centrifugal stiffening are equal, is $\varepsilon = V_e/2V_c = 1/2$, or

$$\lambda = \pi\sqrt{6K} \tag{41}$$

For the Sample Blade, $K = .833 \times 10^{-4}$ and $\lambda = .0722$. The number of nodal points along the span is approximately equal to $2/\lambda$. This is a large number for the Sample Blade, again indicating that the elastic bending stiffness has a negligible effect on frequency in the practical range of excitation.

DAMPING DEVICES

Heliogyro blades have almost no inherent damping. Aerodynamic forces, which provide most of the damping for conventional helicopter rotors, are totally absent. The effectiveness of internal structural damping is small because elastic stiffness accounts for only a small part of the total stiffness. In fact, only the inplane modes have appreciable structural damping and then only in the higher modes. Damping for all other blade modes must be supplied by damping devices.

Damping is required in structures primarily for two reasons. The first is to limit the amplitude of the response of the vibration modes to sustained transient excitation (which over a long period of time may be regarded as either a periodic or as a random excitation). The second is to suppress instabilities involving structural deformation which may result from control feedback or nonconservative environmental processes.

Both of the above reasons apply to the Heliogyro. A primary source of transient excitation is the blade pitch control mechanism which can execute abrupt motions in response to maneuver commands. Another source of dynamic excitation is the solar illumination which can, in conjunction with cyclic blade pitch, produce periodic radiation pressure fluctuations at several of the lowest harmonic orders of rotor speed. Fortunately, as has been shown, there are no prominent resonances of vibration modes with the lower orders of rotor speed. Gravity gradient also produces periodic load fluctuations of relatively small size.

The primary means for combatting periodic excitation is to avoid resonances between exciting frequencies and natural modes. As long as this is done, periodic excitation produces no requirement for damping. The response to random excitation, on the other hand, is inversely proportional to the square root of the damping (as measured by the ratio of the modal damping force to the modal inertia force). Thus, even a very small amount of damping is effective in reducing the amplitude of response to sustained transient excitation.

The Heliogyro is potentially subject to structure-autopilot instability because it requires an autopilot in order to maintain trimmed flight and to execute coordinated maneuvers. Even though the gain of the autopilot may be very small at frequencies corresponding to the higher vibration modes, some small level of structural damping is required in order to avoid instability.

Thermal expansion is a source of instability that has been troublesome for long booms on space vehicles. This mode of instability involves differential thermal expansion between the illuminated and nonilluminated sides of the boom, which produces a change in the illumination incidence angle which, in turn, changes the temperature distribution. Thermal time lag plays an important role in determining the phase of the feedback. Fortunately for the Heliogyro, differential thermal expansion between the leading and trailing edges of the blades is very small so long as the blades are reasonably flat, and the thermal time lag is small due to the thinness of the blades. Nevertheless, some small amount of damping is probably required to prevent this kind of instability.

Since it has been determined that damping devices are required, it is pertinent to seek practical ways of providing them and to estimate the damping levels that can be achieved. The most desirable locations for the damping devices are at the ends of the blade. Distribution of devices along the blade is undesirable because they will increase the bulk of the stowed configuration and will reduce the reliability of deployment. The blade tip is not a practical location for damping devices because significant forces cannot be produced there except at the expense of a significant tip mass. The most practical location for damping devices is at the blade root attachment, which, incidentally, is the location chosen for conventional helicopter rotor blades.

As long as the motions of the blade are substantially uncoupled, separate devices must be provided for pitch, vertical displacement and inplane displacement. A higher level of damping can be provided for pitch than for the other degrees of freedom, which is fortunate because of the important role played by pitch motions in maneuver control.

Pitch Damping

Damping is conveniently provided for the pitch degree of freedom by means of a parallel combination of a spring and a dashpot between the control actuator and the blade as shown in Figure 6. In order to achieve maximum damping, the damper spring should be of the order of magnitude of the blade torsional restraint due to centrifugal force ($\rho\Omega^2 IR$), and the time constant of the damper (B_d/K_d) should be of the order of the period of one of the lower torsional modes. A parametric investigation was made of the idealized model shown in Figure 6 in order to determine an optimum damper combination. The criterion used was the number of revolutions for the blade tip motion to damp to within 10% of its steady state value in response to a collective pitch input. The collective pitch input was a ramp function that achieved its final value in one-half revolution, as shown in Figure 6. Results for a typical case are shown in Figure 7 where the blade tip response, θ_{tip}, and also the blade root response just outboard of the damper, θ_o, are plotted versus time measured in rotor revolutions. The results for all cases are summarized in Figure 8 where it is seen that the selection of the damper parameters is not critical.

An eigenvalue analysis was also made made of the configuration whose transient results are shown in Figure 7 in order to determine the effects of the damper on the torsional vibration modes. The results are presented in Table 4.

The table shows, as does Figure 7, that only the lowest mode has significant response after two revolutions. Comparison of the frequencies listed in Table 4 with the results for the blade without damper given in Table 3, shows that the damper slightly reduces the frequencies of the lowest two modes. The increases shown for the 3rd and 4th modes are the result of finite element approximation.

It is instructive to calculate the physical magnitudes for the damper and the spring for the Sample Blade whose properties are listed in Table 2. The control stiffness is

$$K_d = 2\rho\Omega^2 IR = \frac{1}{6}\Omega^2 \rho c^3 hR$$

$$= \frac{1}{3}\sigma_o \frac{c^3 h}{R} \qquad (42)$$

$$= \frac{1}{3} \times (1000) \times \frac{(120)^3 \times .25 \times 10^{-3}}{120{,}000} = 1.2 \text{ in-lb/rad.}$$

The control damping is

$$B_d = \frac{2\pi}{\Omega} K_d = \frac{2\pi}{.0316} \times 1.2 = 242 \text{ in-lb/rad/sec} \qquad (43)$$

The control stiffness, and consequently also the control moment, is extraordinarily small in view of the size and weight of the rotor blade, indicating that the pitch control mechanism will be delicate and that friction about the control axis must be minimized. Perhaps the best way to achieve the required control stiffness and damping is by means of the output impedance of an electric motor which can, with appropriate servo control, be adjusted to virtually any value. The effect of friction can be minimized simply by increasing the magnitude of the control stiffness at the expense of a decrease in the damping decay rate, as shown by Figure 8. A design concept for a complete Heliogyro blade retention system will be introduced after the means for damping inplane and vertical blade motions have been discussed.

Inplane Damping

Inplane bending deflections are the only blade motions that have appreciable structural damping. The theory presented earlier for the effect of elastic stiffness on inplane mode frequencies can also be used to estimate mode damping. If g_e is the structural damping coefficient of the elastic material, then the modal damping parameter is, approximately,

$$g = \frac{V_e}{V_c} g_e \qquad (44)$$

where V_e/V_c is the ratio of the elastic energy to the potential energy of centrifugal stiffening. From equations (36) and (38), the energy ratio for the second inplane mode is

$$\frac{V_e}{V_c} = 105K \qquad (45)$$

where K is the inplane bending stiffness parameter. For the Sample Blade, $K = .833 \times 10^{-4}$, so that

$$g = 105 \times .833 \times 10^{-4}\, g_e$$

$$= .00872\, g_e \tag{46}$$

Thus, the effective damping of the second mode is less than 1% of the material damping. The effectiveness of structural damping increases rapidly for higher modes, as indicated by equation (40). It is also high for the lowest mode but it cannot be considered adequate due to the very low natural frequency of this mode.

A practical design concept for an inplane damping device is a damper that resists relative rotational motion between the blade root and the center body. The damper must have some stiffness in order to maintain the azimuth angles between blades (provided that there are more than three blades).

An idealized model for the inplane motion of the rotor blade when vibrating in its first mode is shown below.

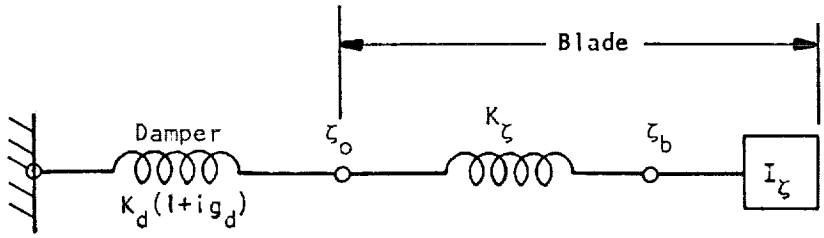

The damper is represented by a spring whose value is given an imaginary part to represent hysteresis damping. The blade is represented by its inertia for rigid body rotation about the blade root, I_ζ, and by a spring K_ζ, that is calculated from the inertia and the frequency of the lowest mode

$$K_\zeta = \omega^2 I_\zeta \tag{47}$$

Using dimensionless coefficients,

$$I_\zeta = 1/3 \tag{48}$$

and, from equation (32)

$$\bar{\omega}^2 = \frac{3}{2}\sqrt{K} \tag{49}$$

Thus, in dimensionless form,

$$K_\zeta = \frac{1}{2}\sqrt{K} \tag{50}$$

The damping of the first mode is, approximately, for $g_d << 1$,

$$g_i = \frac{V_d}{V_d + V_\zeta} g_d \tag{51}$$

where V_d is the energy stored in K_d and V_ζ is energy stored in K_ζ. Since the energy distribution of springs in series is inversely proportional to their stiffnesses

$$g_i = \frac{K_\zeta}{K_d + K_\zeta} g_d \tag{52}$$

Evidently maximum damping is achieved when K_d is small compared to K_ζ.

An idealized model for vibration in the second inplane mode is shown below

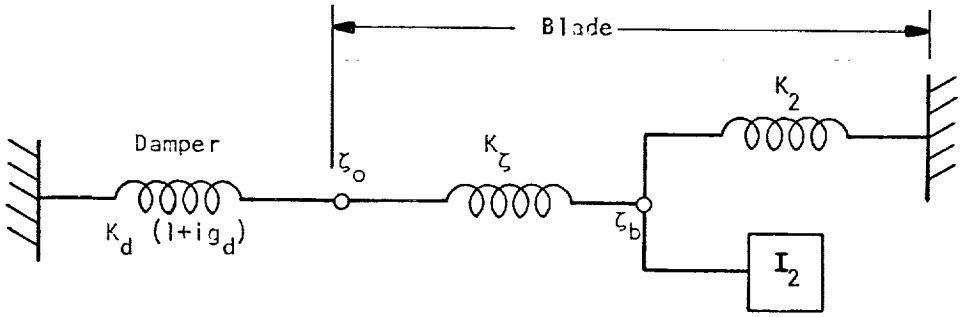

The blade is represented by its modal mass, I_2, and modal stiffness, K_2, referred to the slope, ζ_b, at a point near the root. The equivalent elastic coupling spring, K_ζ, that was calculated from the properties of the first mode, is connected between the damper and the blade. The modal mass is calculated from the deflection function $\bar{u} = \zeta_b(y - \frac{5}{3}y^3)$ and the kinetic energy equivalence,

$$T = \frac{1}{2} I_2 \bar{\omega}_2^2 \zeta_b^2 = \frac{1}{2}\int_o^1 \bar{\omega}_2^2 \bar{u}^2 dy \tag{53}$$

Thus, in dimensionless units,

$$I_2 = \int_o^1 (y - \frac{5}{3} y^3) dy = \frac{4}{63} \tag{54}$$

and

$$K_2 = \bar{\omega}_2^2 I_2 = 5 \times \frac{4}{63} = \frac{20}{63} \tag{55}$$

The damping of the second mode is, for $g_d \ll 1$,

$$g_2 = \frac{V_d}{V_d + V_\zeta + V_2} g_d \tag{56}$$

where, in addition to previously defined terms, V_2 is the energy stored in K_2. Let

$$\bar{K}_\zeta = \frac{K_\zeta K_d}{K_\zeta + K_d} \tag{57}$$

be the equivalent stiffness of K_d and K_ζ in series. Then

$$\left.\begin{aligned} V_d + V_\zeta + V_2 &= \frac{1}{2} \zeta_b^2 (K_2 + \bar{K}_\zeta) \\ \text{and} \\ V_d + V_\zeta &= \frac{1}{2} \zeta_b^2 \bar{K}_\zeta \end{aligned}\right\} \tag{58}$$

so that, using equations (51), (52) and (58)

$$\begin{aligned} g_2 &= \frac{V_d}{V_d + V_\zeta} \cdot \frac{V_d + V_\zeta}{V_d + V_\zeta + V_2} \cdot g_d \\ &= \frac{K_\zeta}{K_d + K_\zeta} \cdot \frac{\bar{K}_\zeta}{K_2 + \bar{K}_\zeta} \cdot g_d \\ &= \frac{K_\zeta}{K_d + K_\zeta} \cdot \frac{g_d}{1 + K_2\left(\frac{1}{K_d} + \frac{1}{K_\zeta}\right)} \end{aligned} \tag{59}$$

The maximum value of g_2, obtained by differentiating equation (59) with respect to K_d, occurs when

$$K_d = K_\zeta \left(\frac{K_2}{K_2 + K_\zeta} \right)^{1/2} \tag{60}$$

For very slender blades, $K_\zeta << K_2$, so that nearly optimum second mode damping is obtained by setting $K_d = K_\zeta$. Using this value in equations (52) and (59),

$$\left.\begin{aligned} g_1 &= \frac{1}{2} g_d \\ g_2 &= \frac{\frac{1}{2} g_d}{1 + \frac{2K_2}{K_\zeta}} = \frac{\frac{1}{2} g_d}{1 + \frac{80}{63\sqrt{K}}} \end{aligned}\right\} \tag{61}$$

For the Sample Blade $\sqrt{K} = .00931$, so that

$$g_2 = \frac{\frac{1}{2} g_d}{137} \tag{62}$$

A typical value of g_d for a good elastomeric material, such as silicone rubber, is 0.30. For this value of material damping the modal dampings for the Sample Blade are $g_1 = .15$ and $g_2 = .00109$. The corresponding times to half amplitude, measured in revolutions, are

$$\left.\begin{aligned} t_1 &= \frac{\ln 2}{\pi g_1 \bar{\omega}_1} = 12.5 \text{ revs} \\ t_2 &= \frac{\ln 2}{\pi g_2 \bar{\omega}_2} = 90.7 \text{ revs} \end{aligned}\right\} \tag{63}$$

The relatively long decay time for the 2nd mode is a direct result of blade slenderness as expressed by the elastic stiffness parameter $\sqrt{K}$. From the definition of K, equation (17),

$$\sqrt{K} = \frac{c}{R}\sqrt{\frac{E}{12\sigma_o}} \tag{64}$$

Thus, other factors remaining equal, the damping of the second inplane mode (and of higher modes) is approximately proportional to the ratio of blade chord to blade span. The inability to provide adequate damping for inplane modes may set a limit to blade aspect ratio.

Somewhat better results can be achieved with viscous dampers. A configuration using two springs and two viscous dampers is shown below

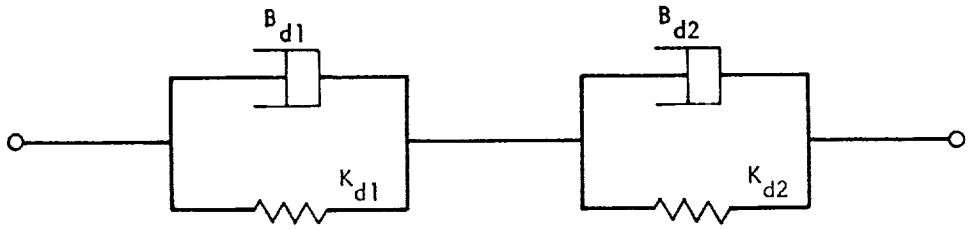

An eigenvalue analysis was made for the inplane vibration modes of the Sample Blade design using this damper configuration with the following dimensionless component values

$$\left.\begin{aligned} K_{d1} &= K_{d2} = 2K_{\zeta} \\ \frac{\bar{\omega}_1 B_{d1}}{K_{d1}} &= \frac{4}{3} \\ \frac{\bar{\omega}_2 B_{d2}}{K_{d2}} &= \frac{3}{2} \end{aligned}\right\} \qquad (65)$$

The springs were selected to be equal and to give the same stiffness as the hysteresis damper described earlier. The dashpots were selected to provide maximum damping for the first and second modes. The results of the analysis are shown in Table 5. It will be noted that the presence of the damper slightly reduces the lowest mode frequency (see discussion following equation (34)). The increase in the higher mode frequencies over the values for the blade without

bending stiffness, see Table 3, is partly due to bending stiffness but mostly due to finite difference approximation. The damping for the first mode is slightly less than that for the silicone rubber damper but the damping of the second mode is substantially larger. Unfortunately the vibration frequencies for real blades are so low (their periods are of the order of minutes) that the physical realization of viscous dampers may not be practical.

As in the case of the pitching modes, it is instructive to estimate the physical magnitudes of parameter values. The physical value of the damper spring for the Sample Blade is

$$K_d^* = \rho ch\Omega^2 R^3 K_d$$

$$= \left(2\sigma_o\right)\left(chR\right)\left(\frac{1}{2}\sqrt{K}\right)$$

$$= 2000 \times 3600 \times .004655$$

$$= 33600 \text{ in-lb/rad.} \qquad (66)$$

This stiffness can, for example, be provided by an extensional spring with a spring constant equal to 336 lb/in located ten inches from the hinge axis. It will be shown later that a damper containing less than one cubic inch of silicone rubber will satisfy strength requirements.

Vertical Damping

A problem encountered in designing a damper for vertical blade motions is that the blade has essentially no bending stiffness to react the moment applied by a rotational damper. Effective bending stiffness can, however, be provided by structural reinforcement over a short span of blade at the root end. A design concept is shown in the following sketch.

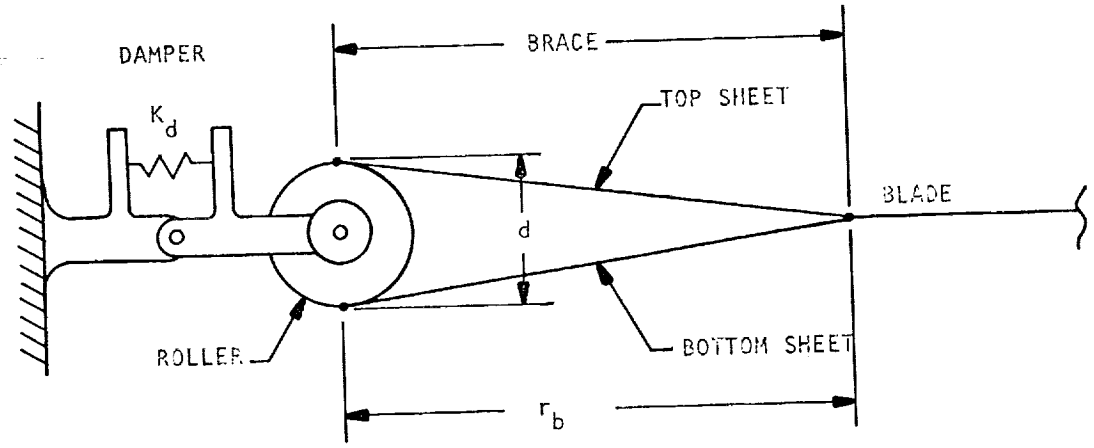

The reinforcement consists of a brace made from two thin sheets of material similar to the blade material. Additional spanwise reinforcing fibers are attached to the sheets. In the stowed configuration, the bottom sheet is back-rolled under the top sheet.

If the brace and the damper were infinitely rigid, the blade would be provided with a flap hinge offset at a distance r_b from the roller, and the flapping moment at the roller would be

$$M_r = r_b T_o \beta_o \tag{67}$$

where T_o is the centrifugal tension and β_o is the flapping angle just outboard of the flap hinge. An idealized model for vertical blade motion, including an elastomeric damper and a brace with finite stiffness is shown below.

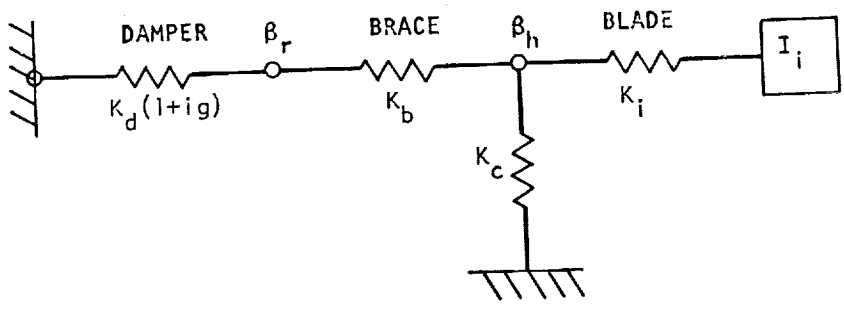

(68)

In the model I_i and K_i are the modal inertia and stiffness of the ith mode referred to $\beta_h = \frac{w_h}{r_b}$, the normalized displacement at the hinge. K_c is the centrifugal stiffness associated with the increment of span occupied by the brace. Its value, in physical units, is

$$K_c^* = r_b T_o \tag{69}$$

or, in dimensionless form,

$$K_c = \frac{y_b}{2} \tag{70}$$

where $y_b = r_b/R$. The value of the brace stiffness is, in physical units

$$K_b^* = \frac{(EA)_b d^2}{2r_b} \tag{71}$$

and, in dimensionless form

$$K_b = \frac{1}{4y_b} \frac{(EA)_b}{\sigma_o ch} \left(\frac{d}{R}\right)^2 \tag{72}$$

$(EA)_b$ is the extensional stiffness of one sheet.

The modal inertia, I_i, can, as in the case of inplane bending, be evaluated from the spanwise integral of kinetic energy. Assuming that the mode shapes are adequately described by the Legendre polynomials discussed earlier, the dimensionless values of the modal inertias and stiffnesses for the first two modes, referred to blade flapping, β_o, just outboard of the hinge are

$$\left.\begin{aligned} I_{10} &= \frac{1}{3} \\ I_{20} &= \frac{4}{63} \\ K_{10} &= \bar{\omega}_1^2 I_{10} = \frac{1}{3} \\ K_{20} &= \bar{\omega}_2^2 I_{20} = \frac{24}{63} \end{aligned}\right\} \tag{73}$$

A transformation of these quantities to the normalized hinge displacement, β_h, is provided by the ratio of the moment on the roller, M_r, given by equation (67) to the generalized force acting on β_o,

$$M_o = K_{io}\beta_o \tag{74}$$

In dimensionless form, the moment on the roller is

$$M_r = \frac{y}{2}\beta_o \tag{75}$$

The blade inertia, I_i, and stiffness, K_i, in the idealized model are, therefore,

$$\begin{aligned} I_i &= \left(\frac{M_r}{M_o}\right)^2 I_{io} = \left(\frac{y_b}{2K_{io}}\right)^2 I_{io} \\ K_i &= \left(\frac{M_r}{M_o}\right)^2 K_{io} = \left(\frac{y_b}{2K_{io}}\right)^2 K_{io} \end{aligned} \tag{76}$$

Substituting from equation (73) into equation (76)

$$\begin{aligned} I_1 &= \frac{3}{4} y_b^2 \\ I_2 &= \frac{63}{576} y_b^2 \\ K_1 &= \frac{3}{4} y_b^2 \\ K_2 &= \frac{63}{96} y_b^2 \end{aligned} \tag{77}$$

As in the case of inplane motion, the ratio of modal damping to material damping is approximately equal to the ratio of the energy stored in the damper spring to the total potential energy. Thus

$$g_i = \frac{V_d g_d}{V_d + V_b + V_c + V_i} \tag{78}$$

The simple idealized model can readily be analyzed to produce the energy ratio in terms of stiffnesses. If it is assumed that $y_b << 1$, then, to a good approximation,

$$g_i = g_d \frac{K_i}{K_d}\left(\frac{\bar{K}_b}{K_c + \bar{K}_b}\right)^2 \tag{79}$$

where $\bar{K}_b = K_b K_d / K_b + K_d$. Cursory examination of equation (79) shows that maximum damping is obtained by making K_b large. This may result in a significant weight penalty so that selection of an optimum design involves a tradeoff between weight and damping.

As an example for the purpose of estimating the order of magnitude of damping that can be expected, consider the Sample Blade with a brace described by the following parameters:

$$d = 1.0 \text{ ft}$$

$$r_b = 50 \text{ ft}$$

$$E_b = 30 \times 10^6 \text{ psi (steel)}$$

$$A_b = .010 \text{ in}^2$$

Then the dimensionless stiffness of the brace is

$$K_b = \frac{1}{4x.005} \times \frac{300,000}{30} \times \left(\frac{1}{10^4}\right)^2 = 50 \times 10^{-4}$$

The weight of the brace is 3.6 lbs which is 1.9% of the blade weight. The blade stiffness parameters are, from equations (70) and (77),

$$K_1 = .1875 \times 10^{-4}$$

$$K_2 = .1642 \times 10^{-4}$$

$$K_c = 25 \times 10^{-4}$$

An optimum value of K_d can be found for given values of K_b and K_c. For the

parameters that have been assumed, the optimum value is near

$$K_d = 20 \times 10^{-4}$$

The corresponding values of modal damping are, assuming an elastomeric damper with $g_d = 0.30$,

$$g_1 = 3.73 \times 10^{-4}$$

$$g_2 = 3.27 \times 10^{-4}$$

These values are only about one-third as large as the damping for the second inplane mode. They can be increased at the expense of an increase in brace length and brace weight or by an increase in the diameter of the roller. The diameter of the roller can be increased, in the deployed configuration, by the extension of arms that are stowed inside the roller.

The physical value of the damper stiffness is

$$K_d^* = 14{,}400 \text{ in-lb/rad}$$

which is about four-tenths of the value of the inplane damper stiffness.

Damping of Modes that Involve Rotations of the Center Body

If all blades are identical, certain types of modes will exist in which the inplane and vertical dampers discussed above are ineffective. They are modes in which, due to the symmetry of the blade motions, the blade bending moments are zero at the center of rotation. There are two classes of such modes as shown in Figure 9.

It will be noted that the modes of each class involve a rotation of the center body. It would, therefore, appear feasible to damp them by attaching damping devices to the center body, or by attaching devices, such as gyroscopes, that provide a significant impedance against which the blade dampers can react.

Unfortunately the size of the center body will probably be so small compared to the blade radius, that appreciable damping cannot be provided in this manner without a large weight penalty.

A more fruitful approach is to alter the characteristics of the blades so that the bending moments at the hub do not vanish in any modes, except, of course, in the lowest modes which correspond to rigid body motion of the entire vehicle. For a two-bladed rotor, this can be accomplished by making one blade longer than the other so that the center body is no longer at the center of rotation. For multibladed rotors, a convenient technique is to taper the chord of some of the blades so as to alter their mode frequencies. (Simply changing blade length will not significantly alter the mode frequencies.) For example, the second vertical mode of a blade whose chord is linearly tapered to a value of zero at the tip is 1.955/rev compared to 2.449/rev for a uniform blade, and the second inplane mode is 1.68/rev compared to 2.236/rev. These differences are large enough so that, considering the relatively small influence that hub rotational constraints have on blade mode frequencies, the modes of the tapered and uniform blades will be virtually uncoupled. Thus, one set of blades will be nearly motionless in the modes of the other set and the dampers will be effective. An attractive configuration is a symmetrical six bladed rotor with three uniform blades and three tapered blades. Rotors with fewer blades must be unsymmetrical in order to make the dampers effective for all modes.

One last mode of interest which is not damped by any of the techniques discussed so far, is the nutation mode of a vehicle with three or more blades, in which the entire vehicle vibrates as a rigid body at approximately two cycles per revolution. In the rotating system this mode appears as a blade flapping mode at one cycle per revolution. Active control feedback can be used to damp the nutation mode. Also it may be feasible to damp the nutation mode by means of a tuned absorber that consists of a long boom attached to the center body in the direction of the spin axis.

A solution to the damping problem which has the advantage that it applies to all modes that involve rotations of the center body, including the nutation mode, is to employ an auxilliary set of counter-rotating blades. The counter-rotating blades, which must have their own dampers, need only be large enough to provide an appreciable impedance to hub rotation. They can be fabricated from high strength materials in order to minimize weight.

BLADE RETENTION SYSTEM

The need for blade dampers about all three rotational axes has been identified and appropriate values of stiffness and damping have been calculated for the Sample Blade design in the preceding section. The recommended properties of the dampers are as follows:

Motion	Damper Type	Spring Constant (in-lb/rad)	Damping Constant
Pitch	Electric Motor	1.2	B_d = 242 in-lb/rad/sec
Vertical	Silicone Rubber	14,400	g_d = 0.3
Inplane	Silicone Rubber	33,600	g_d = 0.3

It is evident, from comparison of the spring constants that the friction about the pitch axis should be as small as possible. Additional requirements for the blade retention system are that it support the centrifugal load (30 lbs), that it accommodate blade motions of the required amounts, and that it withstand environmental hazards. The major environmental hazards are shock and vibration (during launch) and micrometeoroids.

The available pitch motion should be large in order to maximize maneuver capability. At least 45° should be provided. The required vertical flapping accommodation can be estimated to be a reasonable factor times the steady coning. Table 2 records the blade root tension (30 lbs) and the total thrust for normal solar illumination (.0188 lbs) on the Sample Blade. Thus, assuming that the center body is much heavier than the blades, the root coning angle is

$$\beta_o = \frac{.0188}{30} = .000626 \text{ rad}$$

It seems reasonably conservative to assume dynamic flapping of equal magnitude so that the total required flap angle accommodation is approximately .0013 radian = .075°.

The required inplane bending moment can be estimated from the analysis of maneuvers. A reasonably severe maneuver (sudden application of cyclic pitch) is studied in a later section of this report. The results show that the peak in-plane bending moment is 13.5 in-lbs per radian of applied cyclic pitch. It seems reasonably conservative, therefore, to take twice this value, 27.0 in-lbs, as the design inplane bending moment for the damper. The corresponding angular deflection of the damper is

$$\Delta\zeta_d = \frac{27}{33,600} = .000802 \text{ rad.}$$

We are now able to calculate the required volume of silicone rubber for the vertical and inplane dampers. From the equivalence of two energy expressions

$$V = \frac{1}{2}\frac{\tau^2}{G} Vol = \frac{1}{2}\frac{M_d^2}{K_d}, \tag{80}$$

the required volume of material is

$$Vol = \frac{G}{\tau^2}\frac{M_d^2}{K_d} \tag{81}$$

where G is the shear modulus and τ is the allowable shear stress. The shear modulus for silicone rubber is approximately 100 psi. A conservative estimate of the fatigue endurance limit is 5 psi. The required volume of material for the inplane damper is, therefore,

$$Vol = \frac{100}{(5)^2} \times \frac{(27.0)^2}{33,600} = .087 \text{ in}^3.$$

The flapping moment at the roller for a rigid damper and a rigid brace is, from equation (67),

$$M_r = r_b T_o \beta_o = 600 \times 30 \times .0013 = 23.4 \text{ in-lb.}$$

For the damper design studied in the previous section, the moment applied to the flexible damper is 36% of this value, or 8.4 in-lb. The required volume of material for the vertical damper is, therefore,

$$\text{Vol} = \frac{100}{(5)^2} \times \frac{(8.4)^2}{14{,}400} = .020 \text{ in}^3.$$

A design concept for the blade retention system is shown in Figure 10. It is similar, in many respects, to retention systems currently in use on several light helicopters. Centrifugal tension is taken by three stranded wire cables which can accomodate large pitch motions without appreciable torque. The maximum pitch angle is approximately ±55°. The assembly includes only a single bearing which carries no thrust. The values of the design shear loads for the bearing, which are equal to the design bending moments for the damper divided by the moment arm (ten inches), are 2.7 lbs. inplane and .84 lbs. vertically. Assuming that the bearing radius is 1/4" and that the coefficient of friction is 0.02, the maximum friction torque is

$$T = \sqrt{(2.7)^2 + (.84)^2} \times \frac{1}{4} \times .02 = .014 \text{ in-lb.}$$

The corresponding break-away pitch angle is .014/1.2 = .0116 rad = 0.67°, which is certainly tolerable.

The pitch drive shaft passes through a central hole in the pitch bearing and is attached directly to the rotor of an electrical motor. The friction loads on the drive shaft should be negligible.

The pitch case, the meteoroid shield and the droop stop are designed to protect the mechanism from environmental hazards.

FORCES DUE TO SOLAR ILLUMINATION

Figure 11 shows the coordinate geometry for a rotating blade that is coned through an angle β with respect to the plane of rotation and subsequently pitched through an angle θ with respect to a tangent to the cone of rotation. A further rotation, ζ, about the normal to the blade produces no change in the radiation pressure and need not be considered. The illumination lies in the $\bar{x},z$ plane at an angle γ with respect to the axis of rotation.

The following expression is derived in ref. 9 for the normal pressure on the blade surface under the assumption that the coefficient of reflectivity is unity.

$$p_n = p_o[(\sin\theta \sin\psi - \cos\theta \sin\beta \cos\psi) \sin\gamma + \cos\theta \cos\beta \cos\gamma]^2 \quad (82)$$

where $\psi = \Omega t$, is the azimuth angle relative to the plane of illumination. The components of vertical and inplane load for use in structural dynamics, equations (7) and (8), are

$$\left.\begin{aligned} f_{rz} &= p_n c \cos\theta \\ f_{rx} &= p_n c \sin\theta \end{aligned}\right\} \quad (83)$$

The moment about the pitch axis due to solar illumination is zero provided that the reflectivity of the surface is uniform and that the blade is not cambered in the chordwise direction. The effects of such nonuniformities will be discussed later.

Equations (82) and (83) are sufficiently general for most purposes. They are, however, nonlinear in the motions (θ, β), so that it is desirable for convenience in analysis to derive linearized expressions for the loads under the assumptions of small motion. Some expressions are presented in Table 6 for a number of different cases. Since β is always very small, case 5 of Table 6 is sufficiently general for all practical cases. It shows that, if θ varies cyclicly through a large angle, $\theta = \theta_c \sin\psi$, and if the illumination is not parallel to the axis of rotation, the vertical exciting force will include harmonic components with prominent amplitudes up to the fourth harmonic, and that the inplane exciting force will include prominent harmonics up to the fifth.

Another important fact is that, since β is very small and may be neglected in comparison with θ, the significant coupling is from the pitch degree of freedom to the vertical and inplane degrees of freedom and not otherwise. Even so, the magnitudes of the coupling coefficients are very small when expressed in dimensionless form. For example, considering case 4 in Table 6

$$\overline{f}_{rx} = \frac{f_{rx}}{\rho\Omega^2 chR} = \theta \cos^2 \gamma \bullet \frac{p_o R}{2\sigma_o h} = \theta_o \cos^2 \gamma \bullet \frac{\beta_o}{2} \tag{84}$$

where β_o is the blade root coning angle under the assumptions that the center body is much heavier than the blades and that the illumination is parallel to the axis of revolution. For the Sample Blade design the value of β_o is 6.26×10^{-4} rad.

MECHANICAL COUPLING DUE TO BLADE DEFLECTIONS

The equations of motion for a rotating beam that is slightly curved include small terms that couple the vertical, inplane, and pitching motions. Since the curvature of Heliogyro blades is small, the coupling due to curvature would be only a slight concern if the torsional stiffness were not also very small. It is seen, however, from equations (6) and (8) that the ratio of the effective torsional stiffness ($\sigma_r I$) to the inplane bending stiffness (EI) is equal to the spanwise strain which, of course, is small. Thus, a detailed analysis is required in order to determine the significance of the coupling terms.

It is shown in the Appendix that the pitching moment per unit length due to curvature may be expressed as

$$m_\theta = \frac{\partial \beta}{\partial r} M_\zeta - \frac{\partial \zeta}{\partial r} M_\beta \tag{85}$$

where β and ζ are vertical and inplane slopes of the blade (see Figure 4) and M_β and M_ζ are the vertical and inplane bending moments. The bending moments are related to blade curvature via the bending stiffness. Ignoring the flapwise bending stiffness about an axis lying in the blade chord, and assuming that the pitch angle, θ, is small, the relationships are

$$M_\zeta = EI\left(\frac{\partial \zeta}{\partial r} - \theta \frac{\partial \beta}{\partial r}\right) + M_{\zeta o} \tag{86}$$

$$M_\beta = -EI\theta \frac{\partial \zeta}{\partial r} - \theta M_{\zeta o} \tag{87}$$

Substitution of equations (86) and (87) into equation (85) produces the result

$$m_\theta = EI\theta\left[\left(\frac{\partial \zeta}{\partial r}\right)^2 - \left(\frac{\partial \beta}{\partial r}\right)^2\right] + EI\frac{\partial \beta}{\partial r}\frac{\partial \zeta}{\partial r} + M_{\zeta o}\left(\frac{\partial \beta}{\partial r} + \theta \frac{\partial \zeta}{\partial r}\right) \tag{88}$$

Equations (86) and (87) are correct to second order in the motions (ζ, β, θ) and equation (88) is substantially correct to third order. The quantity $M_{\zeta o}$ is the chordwise bending moment due to initial stress. Its major source is the lack of straightness introduced in the manufacturing process. When the blade is deployed it is straightened by centrifugal force, and the initial curvature is

converted, almost completely, into a chordwise bending moment. Subsequent pitching of the blade rotates the moment to produce a vertical component as well.

Coriolis forces are another source of coupling between the inplane and vertical motions. For an undeflected blade the Coriolis forces acting in the inplane and radial directions are

$$\left.\begin{aligned} f_x &= 2\rho ch\Omega \frac{\partial v}{\partial t} \\ f_y &= -2\rho ch\Omega \frac{\partial u}{\partial t} \end{aligned}\right\} \tag{89}$$

where u and v are respectively the inplane and radial displacements. When the blade is flapped through an angle β, the velocity normal to the blade, $\frac{\partial w}{\partial t}$, has a component $-\beta\frac{\partial w}{\partial t}$ in the radial direction and the radial force, f_y, has a component $-\beta f_y$ normal to the blade. Thus the normal and inplane components of Coriolis force are

$$\left.\begin{aligned} f_{cx} &= -2\rho ch\Omega\beta \frac{\partial w}{\partial t} \\ f_{cz} &= 2\rho ch\Omega\beta \frac{\partial u}{\partial t} \end{aligned}\right\} \tag{90}$$

The additional normal and inplane loads due to equations (86), (87) and (90) are

$$f_z = 2\rho ch\Omega\beta \frac{\partial u}{\partial t} + \frac{\partial^2}{\partial r^2}\left(EI\theta \frac{\partial^2 u}{\partial r^2} + \theta M_{\zeta_o}\right) \tag{91}$$

$$f_x = -2\rho ch\Omega\beta\frac{\partial w}{\partial t} + \frac{\partial^2}{\partial r^2}\left(EI\theta \frac{\partial^2 w}{\partial r^2} - M_{\zeta_o}\right) \tag{92}$$

The dimensionless forms of the coupling terms given by equations (88), (91) and (92) are

$$\bar{m}_\theta = \frac{m_\theta}{\rho\Omega^2 I} = \frac{E\theta}{2\sigma_o}\left[\left(\frac{\partial\zeta}{\partial y}\right)^2 - \left(\frac{\partial\beta}{\partial y}\right)^2\right] + \frac{E}{2\sigma_o}\frac{\partial\beta}{\partial y}\frac{\partial\zeta}{\partial y} + \frac{M_{\zeta_o}R}{2\sigma_o I}\left(\frac{\partial\beta}{\partial y} + \theta\frac{\partial\zeta}{\partial y}\right) \tag{93}$$

(① ② ③)

$$\overline{f}_z = \frac{f_z}{\rho\Omega^2 chR} = \underset{④}{\beta \frac{\partial \overline{u}}{\partial \tau}} + \underset{⑤}{\frac{1}{2}\frac{\partial^2}{\partial y^2}\left[K\theta \frac{\partial^2 \overline{u}}{\partial y^2}\right]} - \underset{⑥}{\frac{\theta M_{\zeta o}}{2\sigma_o chR}} \tag{94}$$

$$\overline{f}_x = \frac{f_x}{\rho\Omega^2 chR} = \underset{⑦}{-\beta \frac{\partial \overline{w}}{\partial \tau}} + \underset{⑧}{\frac{1}{2}\frac{\partial^2}{\partial y^2}\left[K\theta \frac{\partial^2 \overline{w}}{\partial y^2}\right]} - \underset{⑨}{\frac{M_{\zeta o}}{2\sigma_o chR}} \tag{95}$$

The significance of each term is determined by comparing its size with the terms on the left hand sides of equations (14), (15) and (16). The latter terms are of the order of the scaled deformations (θ, $\overline{w}$, and $\overline{u}$).

The properties of the Sample Blade design will be used in order to obtain a quantitative evaluation of the coupling effects. In so doing it will be assumed that the vertical deflection is of the same order as the static deflection

$$\beta_s = \frac{\beta_o}{1 + y} \tag{96}$$

and that the inplane deflection is of similar size. The latter assumption will be justified later. It will also be assumed that θ is of the order of unity. The value of β_o for the Sample Blade is 6.26×10^{-4} rad. Using this value and the properties listed in Table 2, it is found that the order of magnitude of the terms in equations (93), (94) and (95) are

term ① : 1.9×10^{-4}

② : 1.9×10^{-4}

③ : $.0125\ M_{\zeta o}$

④ : $6 \times 10^{-4}\ \overline{u}$

⑤ : $.4 \times 10^{-4}\ \overline{u}$

⑥ : $.14 \times 10^{-6}\ M_{\zeta o}$

⑦ : $6 \times 10^{-4}\ \overline{w}$

⑧ : $.4 \times 10^{-4}\ \overline{w}$

⑨ : $.14 \times 10^{-6}\ M_{\zeta o}$

All of the coupling terms, except possibly those involving $M_{\zeta o}$, are small compared to the terms in the uncoupled equations, and they may safely be neglected. They are, in fact, much smaller than the corresponding terms for a conventional helicopter blade. Terms ① and ② are potentially significant terms when β and ζ have larger values as will be shown later in connection with an experimental blade that was tested in a spin chamber.

As has been mentioned, a major source for $M_{\zeta o}$ is unavoidable chordwise curvature built into the blade during manufacture. Thus, assuming that the blade is straightened by centrifugal force during deployment

$$M_{\zeta o} = \frac{EI}{R_c} \tag{97}$$

where R_c is the initial radius of curvature. Substitution into the third term of equation (93) gives

$$\bar{m}_{\theta 3} = \left(\frac{E}{2\sigma_o}\right)\left(\frac{R}{R_c}\right)\left(\frac{\partial \beta}{\partial y} + \theta \frac{\partial \zeta}{\partial y}\right) \tag{98}$$

Static vertical deflection, as given by equation (96), therefore, produces a moment load distribution

$$\bar{m}_{\theta 3} = -\left(\frac{E}{2\sigma_o}\right)\left(\frac{R}{R_c}\right)\frac{\beta_o}{(1 + y)^2} \tag{99}$$

Figure 12 shows the pitch distribution that results from application of a load, $\bar{m}_\theta = 1/(1 + y)^2$. Using Figure 12 and equation (99), the pitch angle at the tip due to a constant initial radius of curvature is

$$\theta_t = .225 \left(\frac{E}{2\sigma_o}\right)\left(\frac{R}{R_c}\right)\beta_o \tag{100}$$

For the Sample Blade design

$$\theta_t = .225 \times (500) \times 6.26 \times 10^{-4}\left(\frac{R}{R_c}\right)$$

$$= .0705\left(\frac{R}{R_c}\right)\text{radian.}$$

It should be possible, using only moderately careful calibration procedures, to ensure that the initial radius of curvature is greater than 50,000 ft, a value which corresponds to a tangent offset of about one inch in 100 ft. Using this value

$$\theta_t = .0705 \times \left(\frac{10,000}{50,000}\right) = .0141 \text{ rad} = .81°$$

A static twist of this magnitude is probably insignificant. Initial curvature may be a problem for longer blades, particularly because the coning angle increases with radius according to the formula

$$\beta_o = \frac{p_n R}{\sigma_o h} \tag{101}$$

The corresponding pitch angle at the tip is

$$\theta_t = .225\left(\frac{E p_n}{2\sigma_o^2}\right)\left(\frac{R^2}{R_c h}\right) \tag{102}$$

Note that the pitch angle is directly proportional to the square of the radius and inversely proportional to the thickness. Note also that it is inversely proportional to the elastic energy density, $\sigma_o^2/2E$, so that materials with high energy storage capacity are good candidates for Heliogyro blades.

Another potential source of steady chordwise bending moment is differential thermal expansion. If a linear temperature gradient across the blade chord is assumed, the steady chordwise moment is

$$M_{\zeta o} = EI\frac{\alpha \Delta T}{c} \tag{103}$$

where α is the coefficient of thermal expansion and ΔT is the difference in temperature between the leading and trailing edges. The corresponding static blade twist is

$$\theta_t = .225\left(\frac{E}{2\sigma_o}\right)\left(\frac{R}{c}\right)\alpha \Delta T \beta_o \tag{104}$$

For the Sample Blade, assuming $\alpha = 15 \times 10^{-6}/°F$,

$$\theta_t = .225 \times (500) \times (1000) \times \left(15 \times 10^{-6}\right) \times 6.26 \times 10^{-4} \Delta T$$

$$= 1.058 \times 10^{-3} \Delta T$$

The temperatures of the leading and trailing edges cannot be appreciably different if the chordwise camber is small. This subject will be discussed later.

Another effect of chordwise camber is to produce a chordwise shift in the center of radiation pressure. The resulting pitching moment load is

$$m_\theta = p_n c x_p = \frac{\sigma_o h \beta_o c x_p}{R} \tag{105}$$

where x_p is the distance from the center of pressure to the midchord. In dimensionless form

$$\overline{m}_\theta = \frac{p_n c x_p}{\rho \Omega^2 I} = 6\left(\frac{R}{c}\right)\left(\frac{x_p}{c}\right) \beta_o \tag{106}$$

Let it be assumed that the center of pressure is located at the same percent chord from root to tip. The blade pitch deflection for a unit dimensionless moment is plotted in Figure 12. Using Figure 12 and equation (106), the twist angle at the tip is

$$\theta_t = 3.93\left(\frac{R}{c}\right)\left(\frac{x_p}{c}\right)\beta_o \tag{107}$$

For the Sample Blade design

$$\theta_t = 3.93 \times 1000 \times 6.26 \times 10^{-4}\left(\frac{x_p}{c}\right)$$

$$= 2.46\left(\frac{x_p}{c}\right) \text{ radian.}$$

The center of pressure shift should, therefore, be restricted to a few percent of chord in order to limit blade twist to an acceptable value. As in the case of initial chordwise curvature, the problem becomes more severe for longer blades. Substituting for β_o from equation (101) gives

$$\theta_t = 3.93\left(\frac{p_n}{\sigma_o}\right)\left(\frac{R^2}{ch}\right)\left(\frac{x_p}{c}\right) \tag{108}$$

It is seen that the effect is reduced by using higher strength materials.

Equations (102) and (108) provide practical limits to the blade radius, which can be surpassed only by providing the blade with additional torsional stiffness. Although it is not particularly difficult to develop concepts for torsional reinforcement that can be stowed in a rolled up configuration, the resulting increases in weight and complexity are not attractive. The analysis that has been presented shows that such measures are probably unnecessary for blades in the size range of the Sample Blade.

A large offset in the center of pressure can also produce significant dynamic coupling. From the expression for the vertical component of radiation pressure given by case 4 in Table 6, the pitching moment load is

$$m_\theta = p_o c x_p[(\theta \sin\psi - \beta\cos\psi)\sin 2\gamma + \cos^2\gamma] \tag{109}$$

or, in dimensionless form,

$$\bar{m}_\theta = 6\left(\frac{R}{c}\right)\left(\frac{x_p}{c}\right)\beta_o[(\theta \sin\psi - \beta\cos\psi)\sin 2\gamma + \cos^2\gamma] \tag{110}$$

For the Sample Blade

$$\bar{m}_\theta = 3.76\,\frac{x_p}{c}\,[(\theta \sin\psi - \beta\cos\psi)\sin 2\gamma + \cos^2\gamma] \tag{111}$$

For $\gamma = 45°$, $\psi = 90°$, and $\beta = 0$, the destabilizing moment load due to θ is

$$\bar{m}_\theta = 3.76\left(\frac{x_p}{c}\right)\theta \tag{112}$$

The effect is significant, when compared with the other terms in the equation of motion for pitch, only when the center of pressure offset is of the order of several percent. Similar effects can be expected from a shift in the location of the center of gravity. The magnitude of the center of gravity offset can, however, be limited to a very small value by proper balance procedures during manufacture.

The main conclusions that have been reached regarding mechanical coupling effects are that initial blade chordwise curvature and blade center of pressure shifts must be controlled. The required tolerances appear to be quite easy to achieve for the Sample Blade design but they become increasingly difficult for longer blades.

CHORDWISE CURL

The significance of a chordwise shift of the center of pressure relative to the midchord was examined in the preceding section where it was shown that the shift should be limited to a few percent of blade chord (for the Sample Blade design). An important cause of center of pressure shift is chordwise camber, or curl, as illustrated in the following diagram.

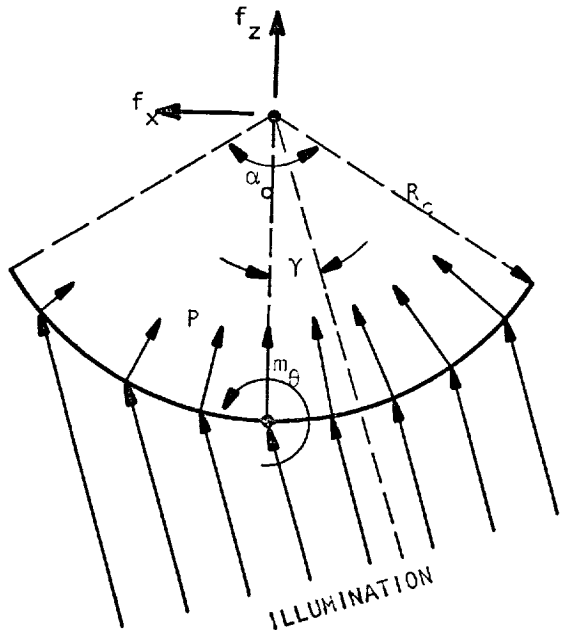

The blade chord is assumed to form a circular arc of radius R_c. The angle of the illumination with respect to a normal to the blade at its midspan is γ. Since the radiation pressure is normal to the local blade surface, the resultant of the radiation pressure passes through the center of curvature and the moment about the blade midspan axis per unit span is

$$m_\theta = R_c f_x \tag{113}$$

where f_x is the horizontal component of the resultant. From the diagram

$$f_x = R_c \int_{-\alpha_o/2}^{\alpha_o/2} p \sin\alpha \, d\alpha \tag{114}$$

and, from equation (1), assuming complete reflection,

$$p = p_o \cos^2 (\gamma - \alpha) \tag{115}$$

Solution of the above three equations gives

$$m_\theta = \frac{2}{3} p_o R_c^2 \left(\frac{c}{2R_c}\right)^3 \sin 2\gamma \tag{116}$$

where c is the blade chord. The vertical component of force is approximately, for small α_o,

$$f_z = p_o c \cos^2\gamma \tag{117}$$

Hence, the per unit forward shift in the center of pressure is

$$\frac{x_p}{c} = \frac{m_\theta}{c f_z} = \frac{c \tan \gamma}{6R_c} \tag{118}$$

The maximum pitching moment occurs when $\gamma = 45°$. For this condition $x_p/c = c/6R_c$. A reasonable design criterion for the Sample Blade design is that $x_p/c < 0.01$. The corresponding requirement on blade chordwise curvature is that $R_c/c > 16.67$.

Chordwise curvature is the result of differential chordwise strain through the thickness of the blade, which can be produced by manufacturing procedures or by environmental effects. The latter, which are probably the more important, include thermal expansion and changes in the crystal structure of the metallic coating due to prolonged exposure to solar radiation. For example, solar protons will gradually erode a surface that is exposed to sunlight thereby producing a dissymmetry that will produce unsymmetrical thermal expansion, even if the temperature is uniform throughout the cross-section. At the present time we do not know the limits of the differential strain that can be produced by prolonged exposure in the space environment. We can, however, determine an effective upper limit to the moment that can be produced, as established by the yield strength of the material. Structural reinforcement can then be designed that will exhibit less than the permitted chordwise curvature while carrying the limit moment.

As an example, consider the Sample Blade design which has a Mylar core with two external layers of pure aluminum as shown below.

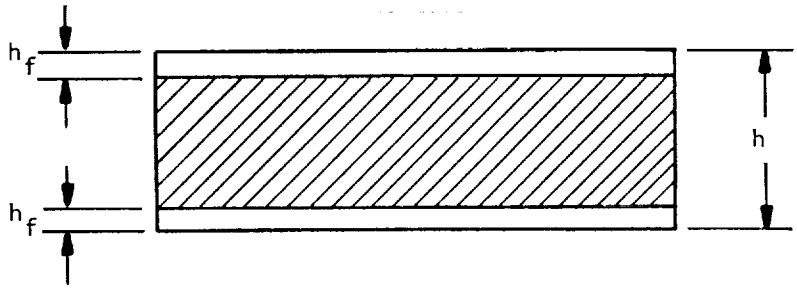

Let it be assumed that the top layer is stressed in tension to the yield stress and that the bottom layer is stressed in compression to the yield stress. The central core is assumed to be unstressed. The chordwise moment per unit span is

$$m_c = h\, h_f\, \sigma_y \tag{119}$$

where σ_y is the yield stress.

The moment produced by differential expansion of the surface layers is resisted by the bending stiffness of the core material and by the chordwise component of centrifugal force which produces a chordwise tension stress (Ref. 9),

$$\sigma_x = \frac{1}{2}\rho\Omega^2\left(\left(\frac{c}{2}\right)^2 - x^2\right) \tag{120}$$

where x is measured from the mid-chord. It is easily shown that neither effect is sufficient to reduce the chordwise curvature to an acceptable level and that reinforcing members are required.

Figure 13 shows a design concept for a chordwise reinforcing member, or batten, that was developed at Astro Research Corporation as part of the effort described in this report. Each batten consists of a thin film of Kapton on one side of which a carbon coating has been deposited. Chemical interaction between the Kapton and the carbon produces a large prestress which, upon release of one edge of a strip of the coated film causes it to roll into a tight scroll

of approximately 1/8 inch diameter. A volatile material which diffuses rapidly in vacuum provides a temporary bond on one edge of the strip so that it may conveniently be rolled in a flattened condition into the stowage roll.

Structural test of a sample scroll showed that it had a bending stiffness $(EI)_b$ equal to 6.39 lb-in^2 and that its maximum bending moment capacity, as limited by local crippling, was 0.265 lb-in. The mass per unit length of the scroll was 1.46×10^{-4} lb/in.

It is important to attach the batten to the blade in such a way as to permit differential expansion in the chordwise direction between the blade and the batten. This can be done by slotting the batten scroll near the edge that is attached to the blade. If the scroll is slotted, the total bending stiffness is the sum of the stiffnesses of the blade and of the batten. Since the latter is much larger than the former, the chordwise bending moment developed per unit span is

$$m_c = \frac{(EI)_b}{R_c \ell_b} \tag{121}$$

where ℓ_b is the distance between battens. Thus, from equations (119) and (121)

$$\ell_b = \frac{(EI)_b}{R_c h\, h_f\, \sigma_y} \tag{122}$$

For the Sample Blade, using the batten design concept that has been described and the design criteria that have been suggested, the parameters in equation (122) are

$$(EI)_b = 6.39 \text{ lb-in}^2$$

$$R_c = 16.67 \text{ c} = 2000 \text{ in}$$

$$h = 2.5 \times 10^{-4} \text{ in}$$

$$h = .15 \times 10^{-4} \text{ cm} = .0591 \times 10^{-4} \text{ in}$$

$$\sigma_y = 5000 \text{ psi (pure aluminum)}.$$

The required batten spacing is

$$\ell_b = \frac{6.39}{2000 \times 2.5 \times 10^{-4} \times .0591 \times 10^{-4} \times 5000}$$

$$= 432 \text{ in} = 36.0 \text{ ft.}$$

The bending moment carried by each batten is $M_c = (EI)_b/R_c = .0032$ in-lb, which is well below its capacity. The weight of each batten is $120 \times 1.46 \times 10^{-4} = .01753$ lb. The required number of battens is 10,000/36 = 278. The total weight of all battens is $.01753 \times 278 = 4.88$ lb, which is 2.5% of the blade weight.

Since the batten spacing is large compared to the chord, the manner in which blade deformations are restrained by the battens should be investigated. This may be done by examining the following differential equation which governs the deflection of the blade normal to its surface.

① ② ③ ④ ⑤

$$D\left[\frac{\partial^4 w}{\partial x^4} + 2\frac{\partial^4 w}{\partial x^2 \partial r^2} + \frac{\partial^4 w}{\partial r^4}\right] - \frac{\partial}{\partial r}\left(\sigma_r h \frac{\partial w}{\partial r}\right) - \frac{\partial}{\partial x}\left(\sigma_x h \frac{\partial w}{\partial x}\right) = p_n \qquad (123)$$

where

$$D = \int_{-h/2}^{h/2} \frac{Ez^2}{1-\nu^2}\, dz \qquad (124)$$

is the bending stiffness. Since the curvature in the spanwise direction is small, terms ② and ③ may be neglected. Term ⑤ is very small, because σ_x is very small (see equation (120) and may be neglected.

The boundary conditions are that the vertical displacement is restrained by battens at $r = r_1$ and at $r = r_1 + \ell_b$ and that the leading and trailing edges are free. The normal pressure, p_n, is very small, but differential expansion of the blade produces an initial curvature whose effect may be represented by placing bending loads equal to m_c on the leading and trailing edges. For simplicity, it will be assumed that the battens are undeflected and that the deflection of the blade varies sinusoidally in the spanwise direction. Thus

$$w = w_m(x) \sin\left(\frac{\pi \Delta r}{\ell_b}\right) \qquad (125)$$

where $\Delta r = r - r_1$. With this assumption, and omitting the terms that have been declared negligible, the differential equation is

$$D \frac{\partial^4 w_m}{\partial x^4} + \left(\frac{\pi}{\ell_b}\right)^2 \sigma_r h \, w_m = 0 \tag{126}$$

At the leading and trailing edges, $x = \pm\frac{c}{2}$, the boundary conditions are

$$\left.\begin{aligned} \frac{\partial^2 w_m}{\partial x^2} &= \frac{m_c}{D} \\ \frac{\partial^3 w_m}{\partial x^3} &= 0 \end{aligned}\right\} \tag{127}$$

where, again, curvature in the spanwise direction has been neglected. Equations (126) and (127) constitute a two-point boundary value problem that is analogous to the problem of a uniform beam with end moments on an elastic foundation. The solution to the problem is

$$w_m = \frac{-m_c}{D\alpha^2}\left[\frac{\cos \alpha x - \dfrac{\sin \frac{\alpha c}{2}}{\sinh \frac{\alpha c}{2}} \cosh \alpha x}{\cos \frac{\alpha c}{2} + \sin \frac{\alpha c}{2} \operatorname{ctnh} \frac{\alpha c}{2}}\right] \tag{128}$$

where

$$\alpha = \left(\frac{\pi^2 \sigma_r h}{D \ell_b{}^2}\right)^{1/4} \tag{129}$$

For Heliogyro blades, $\frac{\alpha c}{2}$ is a large number which results in simplification. For the Sample Blade

$$D \simeq 2.75 \times 10^{-6} \text{ lb-in}$$

$$\sigma_r = 750 \text{ psi (at midspan)}$$

$$h = 2.5 \times 10^{-4} \text{ in}$$

$$\ell_b = 432 \text{ in}$$

$$c = 120 \text{ in}$$

so that

$$\alpha = 1.38 \text{ in}^{-1}$$

and

$$\frac{\alpha c}{2} = 82.9$$

Thus, in equation (128) $\text{ctnh } \frac{\alpha c}{2} \simeq 1.0$ and $\cosh \alpha x / \sinh \frac{ac}{2} \ll 1$ except very near the edges. The resulting simplified expression for the deflection is

$$w_m = \frac{-m_c}{D\alpha^2} \cdot \frac{\cos \alpha x}{\cos \frac{\alpha c}{2} + \sin \frac{\alpha c}{2}} \tag{130}$$

which shows that the chordwise deflection shape is a wave. The chordwise wavelength $\lambda = 2\pi/\alpha$ is equal to 4.56 inches for the Sample Blade. The wave height is

$$w_h = \frac{m_c}{D\alpha^2} \cdot \frac{1}{\cos \frac{\alpha c}{2} + \sin \frac{\alpha c}{2}} \tag{131}$$

Since $\frac{\alpha c}{2}$ is a large number, the wave height can change a large amount for a small change in α. The maximum value is

$$w_{hm} = \frac{m_c}{D\alpha^2} \tag{132}$$

For the Sample Blade, $m_c = h\, h_f\, \sigma_y = 7.39 \times 10^{-6}$ in-lb/in, and

$$w_{hm} = \frac{7.39 \times 10^{-6}}{2.75 \times 10^{-6} \times (1.38)^2} = 1.41 \text{ in.}$$

It remains to examine whether a wave of this height produces a significant shift in the center of pressure. It may be noted in this connection, that the wave height is directly proportional to batten spacing, as may be seen from equations (129) and (132). Thus the wave height can be reduced by reducing the batten spacing.

An analysis of the radiation pressure acting on a wavy surface whose deflection is

$$w = w_h \left[\cos \alpha x - \frac{\sin \frac{\alpha c}{2}}{\sinh \frac{\alpha c}{2}} \cosh \alpha x \right] \tag{133}$$

produces, under the assumption that $\frac{\partial w}{\partial x} << 1$, the result that the pitching moment per unit span about the mid chord is

$$m_\theta = c p_o w_h \sin 2\gamma \left[\cos \frac{\alpha c}{2} - \sin \frac{\alpha c}{2} \right] \tag{134}$$

Note that the magnitude of the moment fluctuates between $\pm c p_o w_h \sin 2\gamma$ for small variations in the physical parameters because $\alpha c/2$ is a large number. This characteristic may, in itself, be relied upon to produce an average pitching moment load over a relatively long blade span that is much smaller than its maximum value. The maximum value of m_θ is

$$m_\theta = \sqrt{2}\, c p_o w_h \sin 2\gamma \tag{135}$$

The per unit shift in the center of pressure is, from equations (117) and (135)

$$\frac{x_p}{c} = \frac{m_\theta}{c f_z} = 2\sqrt{2} \frac{w_h}{c} \tan \gamma \tag{136}$$

Thus, for the Sample Blade and the condition of maximum moment ($\gamma = 45°$),

$$\frac{x_p}{c} = 2\sqrt{2} \times \frac{1.41}{120} = .0333$$

Considering that a very severe differential strain condition (yield stress on top and bottom surfaces) has been assumed and that the effects of the variations in physical parameters have been ignored, this result shows that the center of pressure shift under practical conditions is probably negligible. A more important concern may be the presence of deep spanwise ridges in the blade which will produce chordwise shrinkage and which will tend to invalidate the assumption of specular reflection which is made in performance calculations. A shorter distance between battens will tend to alleviate the problem, but a better solution is to establish a less conservative estimate of differential expansion by further research.

DYNAMIC RESPONSE DURING MANEUVERS

A major concern in the design of a flexible vehicle is the extent to which structural flexibility will interfere with the response of the vehicle to maneuver commands. This is particularly true of the Heliogyro because of the extreme flexibility of its blades. Accordingly, it was deemed important to perform an analysis of the dynamic response during maneuvers under the present study.

The primary means for exerting forces on the vehicle in the plane of rotation is cyclic blade pitch, as shown in Figure 14a. A simple application is shown in Figure 14b, where cyclic pitch is used to change the orbital altitude of a vehicle in a polar orbit. Note that the frequency of the cyclic pitch input should be equal to $\Omega - \psi$, where $\dot{\psi}$ is the orbital frequency, in order to align the resultant control force with the orbital velocity at all times.

The theory for calculating the longitudinal and lateral forces due to cyclic pitch is relatively simple if it is assumed that the blade is rigid. Consider, for example, the case of axial illumination and small pitch angle. Then, the total force on the blade in the chordwise direction is, from Table 6, case 4,

$$F_x = p_o R c \theta \tag{137}$$

The force components in the longitudinal and lateral directions ($\bar{x}$ and $\bar{y}$ in Figure 11) are

$$\begin{aligned} F_{long} &= F_x \sin \Omega t \\ F_{lat} &= -F_x \cos \Omega t \end{aligned} \tag{138}$$

Let the blade pitch be cyclicly excited at frequency $\Omega + \omega_o$, such that

$$\theta = \theta_c \sin (\Omega + \omega_o) t \tag{139}$$

Then, combining the above equations and resolving the products of trigonometric functions into sum and difference terms,

$$\left.\begin{aligned} F_{long} &= \frac{1}{2} p_o Rc\theta_c [\cos \omega_o t - \cos (2\Omega + \omega_o)t] \\ F_{lat} &= -\frac{1}{2} p_o Rc\theta_c [\sin \omega_o t + \sin (2\Omega + \omega_o)t] \end{aligned}\right\} \quad (140)$$

The high frequency terms have little significance and they will, in any event, be cancelled out when the effects of three or more blades are added. The low frequency terms are the desired control forces.

The elastic response to the sudden application of cyclic pitch was analyzed during the present study by means of a digital computer simulation. The pitch input was assumed to be a sine wave which is modulated by an envelope function that rises to its full amplitude in one-half revolution, see Figure 15a. Three different cases were analyzed corresponding to different values of the frequency of the sine wave. Blade pitch was assumed to produce a component of force in the inplane direction according to equation (137), which is the appropriate expression for the case of axial illumination and small pitch motions.

The simulation included a single blade, with properties identical to those of Sample Blade design. The center body was assumed to be massive compared to the blades so that the translational motions at the blade root could be rigidly restrained in the simulation. It is evident from the symmetry of the applied load, see Figure 14a, that the inplane bending slope, ζ, should also be rigidly restrained at the blade root.

Mechanical coupling between blade motions was ignored in view of the demonstration (see section on MECHANICAL COUPLING DUE TO BLADE DEFLECTIONS) that these effects can be made negligible for the Sample Blade by careful construction. As a result vertical deflections could be ignored entirely since they were not coupled, either directly or indirectly, to the source of dynamic excitation.

Dampers were included at the blade root for torsional and inplane bending motions. The properties of the dampers that were used and the damping that they provided for the lowest four modes of each type are given in Tables 4 and 5.

The analytical model included ten blade stations located at the following spanwise positions:

STA	1	2	3	4	5	6	7	8	9	10
y = r/R	.005	.010	.020	.040	.080	.150	.30	.50	.70	.90

Note the concentration of stations near the blade root in order to provide adequate simulation for the rapid decay of chordwise bending moment.

The results of the analysis are presented in Figures 15a thru 15ℓ for the case in which the frequency of the cyclic pitch excitation is equal to the rotational speed. The response of various quantitites are plotted for the first twenty revolutions following the initiation of the maneuver. The plots were produced by a computer, which accounts for the somewhat unconventional scaling practices that are evident.

The blade pitch response is shown in Figures 15b, c and d, where it is seen that the pitch motion achieves its steady state value (within ±10%) in about five revolutions.

The inplane blade deflections at 50% and 90% span are shown in Figures 15e and 15f. The presence and the decay of the low frequency (.105/rev) inplane mode are evident in these plots. Note also that the amplitude of motion at the tip is comparable in magnitude to the static vertical tip displacement ($.694\ R\beta_o$) when the magnitude of the pitch input is one radian. This is the order of magnitude of dynamic chordwise motion that was assumed earlier in estimating mechanical coupling effects.

The inplane and axial components of force that exist at the blade root are shown in Figures 15g and 15h. The axial component was obtained by summing the axial component of Coriolis force, f_y in equation (89), along the blade span. The inplane component is the sum of the inplane bending shear and the inplane component of centrifugal force at the blade root. It is seen that the axial component is, surprisingly, about twice as large as the inplane component.

The forces at the blade root are resolved into components parallel to non-rotating axes in Figures 15i and 15j. Note the presence of the steady component of longitudinal force and the existence of the 2/rev oscillations as predicted

by rigid blade theory. It is seen that the low frequency component of the longitudinal force settles down to the neighborhood of its final value within about five revolutions. The gradual decay of the high frequency transients can also be detected.

The inplane bending moment near the blade root is plotted in Figures 15k and 15ℓ, where it is seen that the bending moment decays to 10% of its value at the root in only 2% of the span. The peak magnitude of the inplane moment at the root is

$$M_\zeta = .006\ p_o R^2 c\ \theta_c$$
$$= 13.5\ \theta_c \text{ in-lb}$$

The corresponding displacement of the tension axis, as a fraction of blade chord, is

$$\frac{x_t}{c} = \frac{M_\zeta}{Tc} = \frac{13.5\ \theta_c}{30 \times 120} = .00375\ \theta_c$$

Thus, even a one radian pitch amplitude produces a shift in the tension axis that is negligibly small.

The longitudinal and lateral force resultants produced by the simulation study are compared with the results of rigid blade theory in Figure 16 for three values of the cyclic pitch frequency, ω. The 2/rev components of force were filtered from the results of the simulator study. It is seen that, in all cases, control is established within approximately one revolution and that the steady state is achieved (within ±10%) in about five revolutions. It will be noted that the steady state forces for the flexible blade exceed those for the rigid blade when the pitch frequency is greater than one/rev, and are less than those for the rigid blade when the pitch frequency is less than one/rev. This result is explained by Figure 5.

EXPERIMENTAL PROGRAM

An experimental program, which was designed to demonstrate the deployment concept and the control of blade pitch, was conducted at Astro Research Corporation as part of the present study. It was realized in advance that it would be impossible to simulate the proper values of the critical dynamic parameters (K, β_o) in an Earth environment. At the same time it was hoped that the experiment might provide a verification of the theory of dynamic response. As matters turned out the experiment was, in fact, a critical test of the theory for dynamic coupling effects due to blade deflections.

The experimental apparatus consisted of an 18 ft. diameter spin chamber in which a model of the Heliogyro blade was deployed from a spool. The spin chamber was not evacuated, but since it was enclosed and rotated at the same velocity as the experimental model, the velocity of the enclosed air relative to the blade was substantially zero and the aerodynamic effects (virtual mass and damping) could be neglected.

A diagram of the test set up and the parameters that define the experiment are shown in Figure 17. It will be noted that the deployment spool is offset a considerable distance from the axis of rotation. Note also that the pitch axis of the blade is tangent to the surface of the spool and that it is inclined downward at an angle that is somewhat less than the root coning angle of the fully deployed blade. A number of experiments were conducted including unwinding and rewinding the blade, steady cyclic pitch oscillations, and abrupt changes in collective pitch. A motion picture was produced that demonstrates successful accomplishment of these maneuvers.

The experimental blade consisted of a .001 inch thick strip of Kapton about 2 inches wide and 77 inches long. Photographs of the deployed blade made from motion picture frames at two different pitch angles are shown in Figure 18. The inplane deformation of the blade is clearly visible in the lower photograph. The blade was painted in order to enhance its visibility and to provide lateral markings for the observation of pitching motions. The paint, which was applied to one side only, also produced chordwise camber.

The frames of a motion picture showing the response of the blade to an abrupt change in collective pitch from zero degrees to twenty-five degrees were analyzed to produce a time history of the pitching motion at the 50% span and at the blade tip. The results of a digital computer simulation are compared with the experimental measurements in Figure 19. The agreement between analysis and experiment is seen to be only fair. It will be shown that the most likely reasons for the observed discrepancies are nonlinear effects, not accounted for in the analysis, and the extreme sensitivity of the response to the angle of depression of the pitch axis.

The most important dimensionless modeling parameters for comparing the dynamic response of different blades are the inplane bending stiffness parameter, K, and the steady coning angle at the blade root, β_o. The values of these parameters for the Sample Blade and the experimental blade are compared below.

	Sample Blade	Experimental Blade	Experimental Blade / Sample Blade
K	$.833 \times 10^{-4}$	.454	5440
β_o	6.26×10^{-4}	.1967	314

The conclusion stated earlier, that dynamic coupling due to blade deflections is unimportant for the Heliogyro, obviously does not apply to the experimental blade. The coupling terms in question are written in dimensionless form in equations (93), (94) and (95). If small dynamic motions are assumed, the important terms are those that contain the static coning angle $\beta_s = \partial \bar{w}_s / \partial y$. They are

$$\bar{m}_\theta = - \frac{E(\beta_s')^2}{2\sigma_o} \theta + \frac{E\beta_s'}{2\sigma_o} \frac{\partial \zeta}{\partial y} \tag{141}$$

$$\bar{f}_z = \beta_s \frac{\partial \bar{u}}{\partial \tau} \tag{142}$$

$$\bar{f}_x = - \beta_s \frac{\partial \bar{w}}{\partial \tau} + \frac{1}{2} \frac{\partial^2}{\partial y^2} (K\beta_s' \theta) \tag{143}$$

where $\beta_s' = \frac{\partial \beta_s}{\partial y} = \frac{\partial^2 \bar{w}_s}{\partial y^2}$.

The analysis was performed including the above terms. The boundary condition at the blade root accounted for the angle between the blade twist axis and the applied pitch axis. Thus the inplane blade slope at the root is

$$\zeta_o = \frac{\partial \bar{u}}{\partial y} = -\theta_c \sin (\beta_o - \beta_p) \tag{144}$$

The sensitivity of the analysis to the inclination of the pitch axis, β_p, is indicated in Figure 20 where it is seen that a change in β_p of one degree produces a 20 degree change in the peak pitch angle at the tip.

Since the peak transient pitch angle at the tip is actually rather large (72°) the error produced by the small angle assumption in the analysis cannot be neglected. Furthermore, the peak magnitude of the inplane bending moment at the blade root is large enough to produce buckling at the edges of the blade, thereby altering the inplane bending stiffness of the experimental model significantly.

The effects of finite elastic torsional stiffness and of the added mass due to the air were investigated and were found to be unimportant. The most probable reasons for the differences between the analytical and experimental results are the effects of large dynamic motions, the effects of large initial deflections, and the sensitivity of the response to the inclination of the pitch axis.

CONCLUSIONS

A number of fundamental topics concerning the structural dynamics of the Heliogyro have been examined. These topics include

— Uncoupled vibration modes

— Means for providing damping

— Coupling between the blade motions

— Transient response to maneuver commands.

On the basis of the results of the study it may be concluded that:

1. Resonances between the harmonics of rotor speed and the blade vibration modes are easily avoided.
2. Damping can be provided for all degrees of freedom. The damping in pitch is sufficient to produce convergence to within 10% of steady state in about five revolutions. The damping that can be provided (with very little added weight) for inplane and vertical vibrations is about an order of magnitude smaller but it is probably adequate. Damping for the rigid body nutation mode requires active control feedback or an auxilliary passive damping device connected to the center body.
3. The major source of coupling between the blade motions is solar radiation pressure which produces inplane and vertical forces due to pitching motion. This source is utilized in orientation and control of the vehicle.
4. Pitching moments due to vertical and inplane blade deflections can be held to an unimportant level for blades that are the size of the Sample Blade (10,000 ft radius) by careful design and manufacture. The major sources of unwanted pitching moments are a chordwise shift in the location of the center of pressure due to chordwise camber, and an initial chordwise radius of curvature in the as-manufactured blade. Suppression of chordwise camber requires chordwise bending members (battens) at frequent intervals. The design of a satisfactory batten which increases

the weight of the Sample Blade by 2.5% has been demonstrated. The control of initial chordwise curvature to the level required by the Sample Blade does not appear to be difficult.

5. Undesirable dynamic coupling effects (pitching moments) increase in severity with increases in blade radius. For example, the steady pitch angle at the blade tip due to center of pressure shift, x_p, is, from equation (108),

$$\theta_t = 3.93\left(\frac{p_n}{\sigma_o}\right)\left(\frac{R^2}{ch}\right)\left(\frac{x_p}{c}\right)$$

and the steady pitch angle at the tip due to initial chordwise radius of curvature, R_c, is, from equation (102),

$$\theta_t = .225\left(\frac{Ep_n}{2\sigma_o{}^2}\right)\left(\frac{R^2}{R_c h}\right)$$

It is seen that in both cases the pitch angle increases in proportion to the square of the span, R, and inversely as the thickness, h. The remedies, in addition to suppressing the primary sources, x_p and $1/R_c$, are to increase the blade chord, c, and, more importantly, to increase the blade centrifugal stress, σ_o. Thus, the development of higher strength materials will enhance the feasibility of designing longer blades. Another remedy, which has the undesirable effects of increasing the weight and complexity of the blade, is to provide torsional stiffness by means of structural reinforcement.

6. The effect of blade flexibility on the ability to provide lateral control forces by means of cyclic pitch is slight. Effective response to an abrupt command is achieved (within ±10%) in about five revolutions. The effect of rotor size on control effectiveness is small.

In summary, it is concluded that no structural dynamic reasons to doubt the feasibility of the Heliogyro in sizes up to 10,000 ft radius have been discovered. On the other hand, the development of very much larger sizes will depend, in part, on the ability to minimize undesirable dynamic effects.

REFERENCES

1. Cotter, T., "Solar Sailing", Sandia Corporation Research Coloquium SCR-78, April, 1959, Office of Technical Services, Dept. of Commerce, Washington, D.C.

2. Garwin, "Solar Sailing, A Practical Method of Propulsion within the Solar System", Jet Propulsion, March, 1958.

3. Tsu, T., "Interplanetary Travel by Solar Sails", ARS Journal, June, 1959.

4. MacNeal, R. H., "Comparison of the Solar Sail with Electric Propulsion Systems", MacNeal-Schwendler Corp. MSR-13, February, 1969.

5. Gordon, B. J., "A Study of Interplanetary Travel by Solar Sail", M. S. Thesis, Air University, USAF, Wright-Patterson Air Force Base, Ohio, August, 1961.

6. MacNeal, R. H., Hedgepeth, J. M., and Schuerch, H. U., "Heliogyro Solar Sailer Summary Report", NASA Contractor Report CR-1329, June 1969.

7. Kelley, H. J., "Gradient Theory of Optimal Flight Paths", ARS Journal, Vol. 30, p. 947-954, October, 1960.

8. Hedgepeth, J. M., and Benton, M. D., "Analysis of Planetary Flyby Using the Heliogyro Solar Sailer", Astro Research Corporation ARC-R-296, August, 1968.

9. MacNeal, R. H., "The Heliogyro - An Interplanetary Flying Machine", NASA Contractors Report CR-84460, June, 1967.

10. MacNeal, R. H., "Direct Analog Method of Analysis of the Vertical Flight Dynamic Characteristics of the Lifting Rotor with Floating Hub", Journal of the American Helicopter Society, Vol. 3, October, 1958.

11. Gessow, A., and Myers, G. C., Aerodynamics of the Helicopter, The MacMillan Company, New York, 1952, p. 177.

APPENDIX

THE TWISTING MOMENT IN A SLIGHTLY CURVED BEAM

Consider a beam whose axis is slightly deflected from the r-axis, as shown in the following sketch.

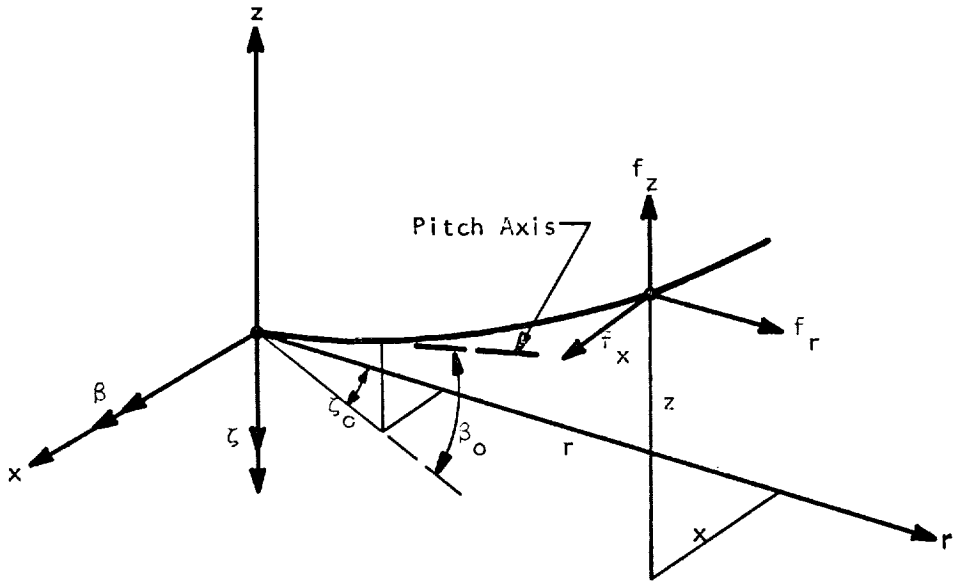

The angles β_o and ζ_o, which define the orientation of the pitch axis at the root end, are small. Thus, to first order in the angles, the moment about the pitch axis is

$$M_a = M_r + \zeta_o M_x + \beta_o M_z \qquad \text{(A-1)}$$

The moments about the x, r and z axes due to running loads applied to the centroidal axis of the beam are, from elementary mechanics,

$$M_x = \int_0^R (-f_r z + f_z r)dr \tag{A-2}$$

$$M_r = \int_0^R (f_x z - f_z x)dr \tag{A-3}$$

$$M_z = \int_0^R (-f_x r + f_r x)dr \tag{A-4}$$

Upon substitution into equation (A-1):

$$M_a = \int_0^R [f_x z - f_z x + \zeta_o (-f_r z + f_z r) + \beta_o (-f_x r + f_r x)]dr \tag{A-5}$$

Assuming that x, z, f_x, f_z, and ζ_o and β_o are of first order and that f_r and r are of zero order, it is seen that all of the terms in equation (A-5) are of second order. Equation (A-5) is inconvenient for use in an analysis where the other effects are expressed by partial differential equations because of the presence of β_o and ζ_o. It can, however, be converted into a more amenable form by applying the rules for integration by parts. First, however, it is convenient to rewrite equation (A-5) in terms of the offset distances

$$\begin{aligned} \bar{z} &= z - \beta_o r \\ \bar{x} &= x - \zeta_o r \end{aligned} \tag{A-6}$$

from a line tangent to the pitch axis at the root. Thus,

$$M_a = \int_0^R [f_x \bar{z} - f_z \bar{x} + f_r (x\beta_o - z\zeta_o)]dr \tag{A-7}$$

The formula for integration by parts is

$$\int_a^b udv = uv\Big|_a^b - \int_a^b vdu \tag{A-8}$$

The formula will be applied in the following manner to the terms in equation (A-7):

Term	u	dv	du	v
$f_x\bar{z}$	$\bar{z}$	$f_x dr$	$(\beta - \beta_o)dr$	$-\int_r^R f_x dr = -F_x$
$f_z\bar{x}$	$\bar{x}$	$f_z dr$	$(\zeta - \zeta_o)dr$	$-\int_r^R f_z dr = -F_z$
$f_r(x\beta_o - z\zeta_o)$	$x\beta_o - z\zeta_o$	$f_r dr$	$(\zeta\beta_o - \beta\zeta_o)dr$	$-\int_r^R f_r dr = -T$

The quantities F_x, F_z and T that appear above are respectively the total inplane force, the total vertical force, and the total axial tension at a distance r along the blade. The result of the integration by parts is

$$M_a = \left| - \bar{z}F_x + \bar{x}F_z - T(x\beta_o - z\zeta_o) \right|_o^R + \int_o^R [F_x(\beta - \beta_o) - F_z(\zeta - \zeta_o) + T(\zeta\beta_o - \beta\zeta_o)]dr \quad \text{(A-9)}$$

The boundary terms vanish because $\bar{z}$, $\bar{x}$, x, and z are zero at r = 0, and F_x, F_z and T are zero at r = R. The inplane force, F_x, and the vertical force F_z, are partly carried by centrifugal tension and partly carried by beam shear. Thus,

$$F_x = T\zeta - \frac{\partial M_\zeta}{\partial r} \quad \text{(A-10)}$$

and

$$F_z = T\beta - \frac{\partial M_\beta}{\partial r} \quad \text{(A-11)}$$

where M_ζ and M_β are respectively the inplane and vertical bending moments. Upon substitution of equations (A-10) and (A-11) into equation (A-9), it is seen that all of the terms proportional to T cancel each other so that

$$M_a = \int_o^R [-\frac{\partial M_\zeta}{\partial r}(\beta - \beta_o) + \frac{\partial M_\beta}{\partial r}(\zeta - \zeta_o)]dr \quad \text{(A-12)}$$

Integration of this equation by parts produces the result

$$M_a = \int_o^R (M_\zeta \frac{\partial \beta}{\partial r} - M_\beta \frac{\partial \zeta}{\partial r})dr \quad \text{(A-13)}$$

Since the origin can be shifted without changing the form of the result, it is seen that the running pitching moment load is

$$m_\theta = M_\zeta \frac{\partial \beta}{\partial r} - M_\beta \frac{\partial \zeta}{\partial r} \qquad \text{(A-14)}$$

The term indicated in equation (A-14) can be added directly to the differential equation for pitch.

TABLE 1

SOLAR SAIL DESIGN MORPHOLOGY

SHAPE	MEANS OF RIGIDIZING	MEANS OF ORIENTING
CIRCULAR ↓ RECTANGULAR ↓ VERY SLENDER	ELASTICITY ELECTROSTATIC FORCE MAGNETIC FORCE CENTRIFUGAL FORCE	AREA SHADING CENTER OF GRAVITY MOVEMENT REFLECTING SURFACE ROTATION

TABLE 2

PROPERTIES OF SAMPLE BLADE DESIGN	
Blade Chord (uniform)	10 ft.
Blade Radius	10,000 ft.
Blade Material	1/4 mil Mylar with 1500 A° aluminum coating each side.
Chordwise Bending Moment of Inertia	36 in^4
Surface Density	1.34×10^{-5} psi
Modulus of Elasticity (Composite)	1.0×10^{6} psi
Rotational Speed, Ω	.0316 rad/sec
Rotational Period	3.31 minutes
Blade Root Stress*	1000 psi
Blade Root Tension	30 lbs.
Blade Weight	194 lbs.
Total Thrust for Normal Solar Illumination	.0188 lb.
Sail Lightness Number, λ_s	0.16
Blade Root Coning Angle	6.26×10^{-4} rad.

* Based on 1/4 mil thickness.

TABLE 3

UNCOUPLED BLADE FREQUENCIES

$\bar{\omega} = \omega/\Omega$			
n	TWIST	VERTICAL	INPLANE
1	$\sqrt{2} = 1.414$	1.0	0
3	$\sqrt{7} = 2.646$	$\sqrt{6} = 2.449$	$\sqrt{5} = 2.236$
5	$\sqrt{16} = 4.000$	$\sqrt{15} = 3.873$	$\sqrt{14} = 3.742$
7	$\sqrt{29} = 5.385$	$\sqrt{28} = 5.291$	$\sqrt{26} = 5.099$

TABLE 4

FREQUENCIES AND DAMPING FOR BLADE
PITCH MODES WITH A CONTROL DAMPER,

$$\frac{K_d}{\rho\Omega^2 IR} = 2.0; \quad \frac{B_d}{K_d} = \frac{2\pi}{\Omega}$$

Mode Number	Frequency Cycles/Rev.	Damping g	Revolutions to 1/2 Amplitude
1	1.368	.0845	1.91
2	2.618	.1024	.825
3	4.022	.0863	.636
4	5.455	.0680	.596

TABLE 5

FREQUENCIES AND DAMPING FOR INPLANE
MOTIONS OF THE SAMPLE BLADE WITH A DAMPER
WHOSE PROPERTIES ARE GIVEN IN EQUATION 65.

Mode Number	Frequency Cycles/Rev.	Damping g	Revolutions to 1/2 Amplitude
1	.1053	.1167	18.0
2	2.276	.00236	41.0
3	3.834	.00196	29.5
4	5.342	.00159	26.1

TABLE 6

FORMULAS FOR VERTICAL AND INPLANE LOADING DUE TO SOLAR ILLUMINATION

ASSUMPTION				f_{rz}	f_{rx}
CASE	θ	β	γ		
1.	0	0	any	$p_o c \cos^2\gamma$	0
2.	0	$\ll 1$	any	$p_o c[\cos^2\gamma - \beta \sin 2\gamma \cos \psi]$	0
3.	any	any	0	$p_o c \cos^2\beta \cos^3\theta$	$p_o c \cos^2\beta \cos^2\theta \sin \theta$
4.	$\ll 1$	$\ll 1$	any	$p_o c[(\theta \sin \psi - \beta \cos \psi)\sin 2\gamma + \cos^2\gamma]$	$p_o c\, \theta \cos^2\gamma$
5.	any	$\ll 1$	any	$p_o c \cos \theta \left[(\sin \theta \sin \psi \sin \gamma + \cos \theta \cos \gamma)^2 - \beta \sin \gamma \left(\frac{1}{2} \sin 2\theta \sin 2\psi \sin \gamma + 2 \cos^2\theta \cos \psi \cos \gamma\right)\right]$	$f_{rz} \tan \theta$

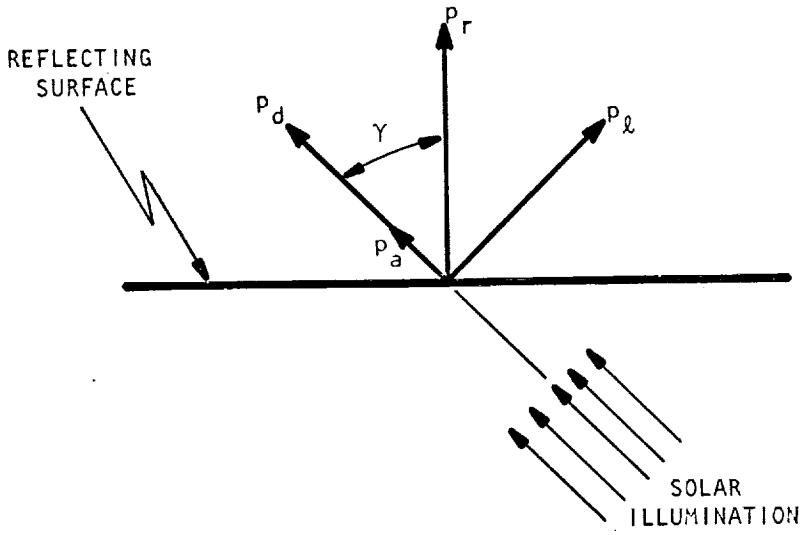

Figure 1. Solar Radiation Pressure on a Reflecting Surface

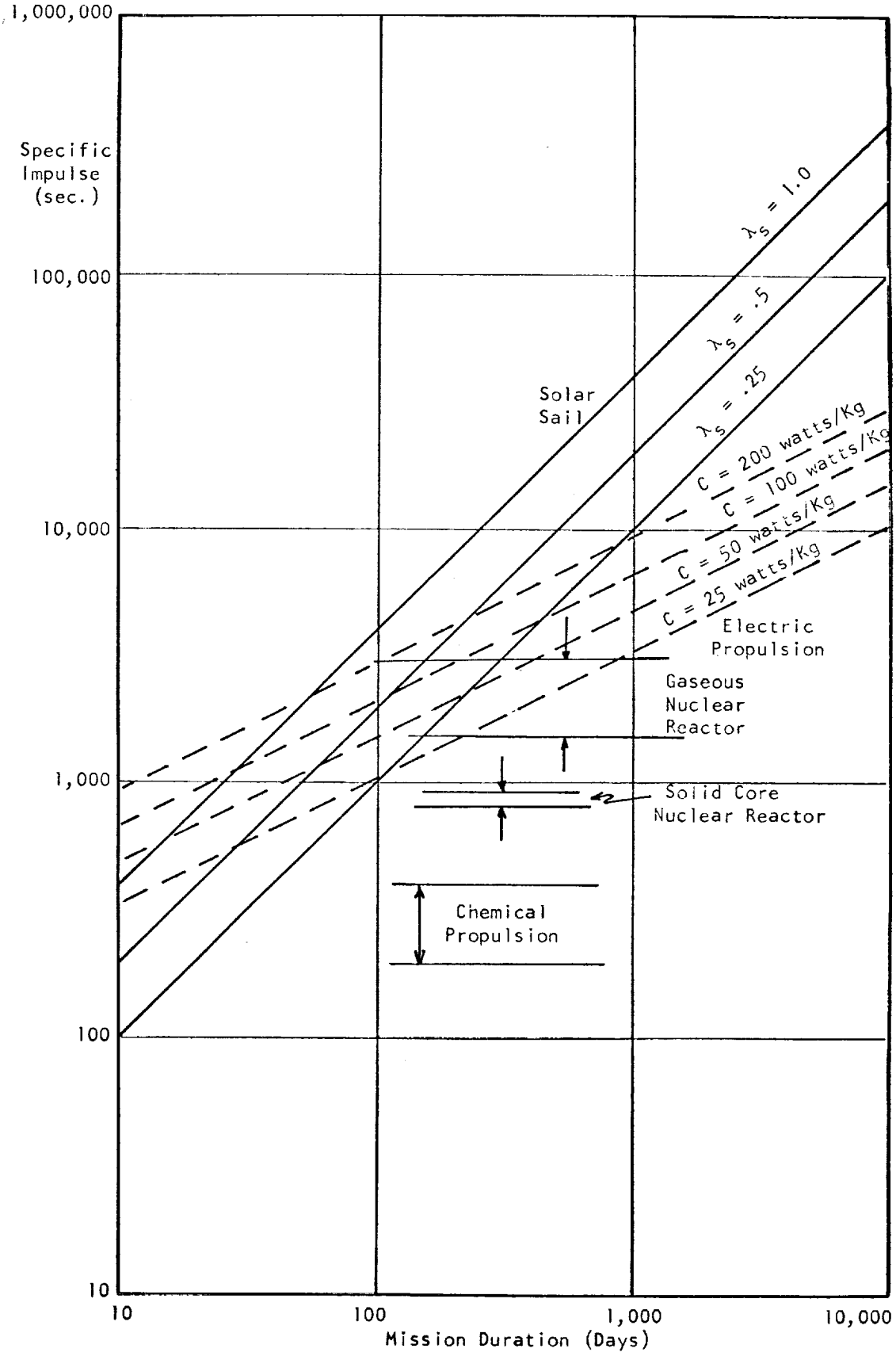

FIG. 2. SPECIFIC IMPULSE VS MISSION DURATION FOR VARIOUS PROPULSION SYSTEMS OPERATING IN THE VICINITY OF THE EARTH'S ORBIT

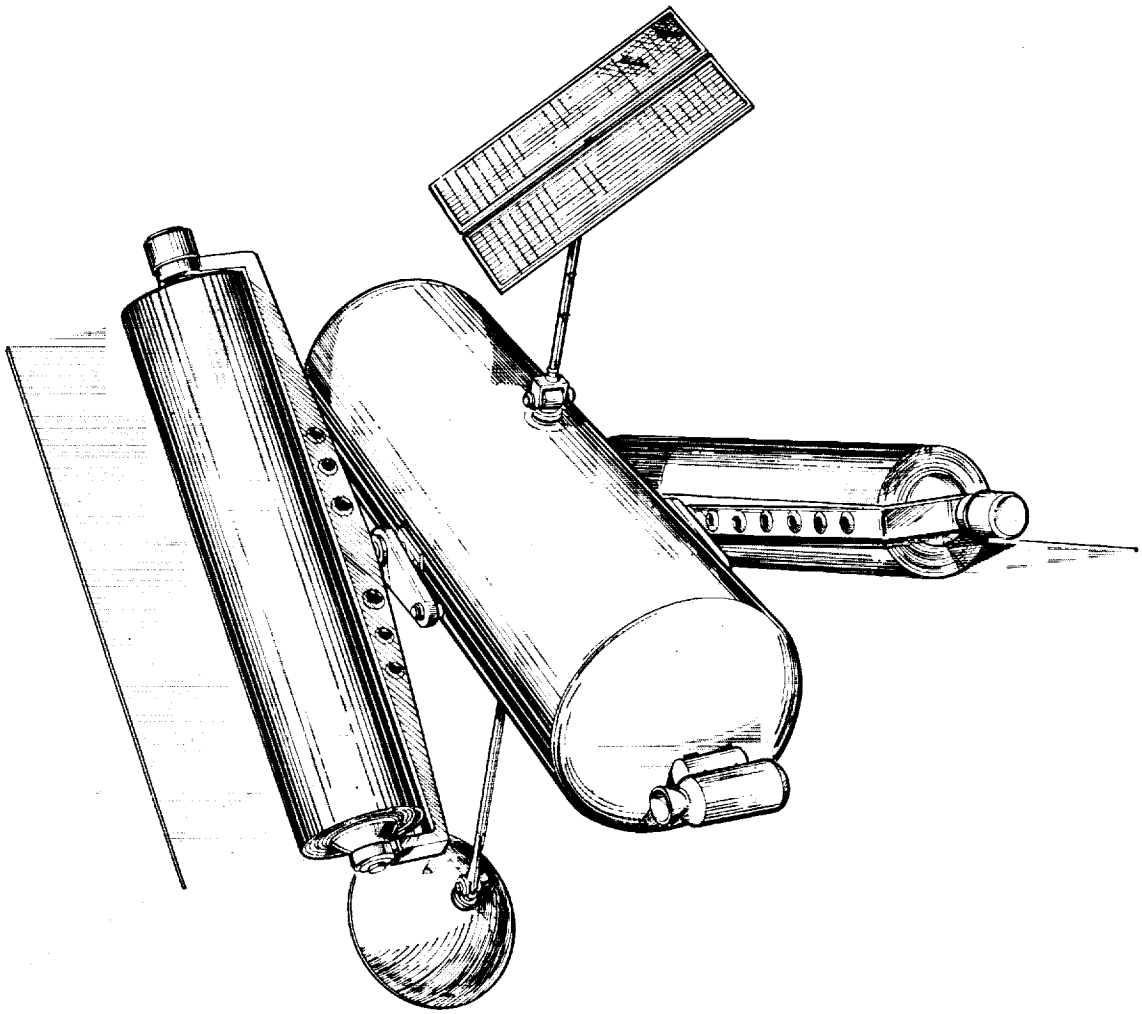

Figure 3. Sketch of Experimental Two-Blader

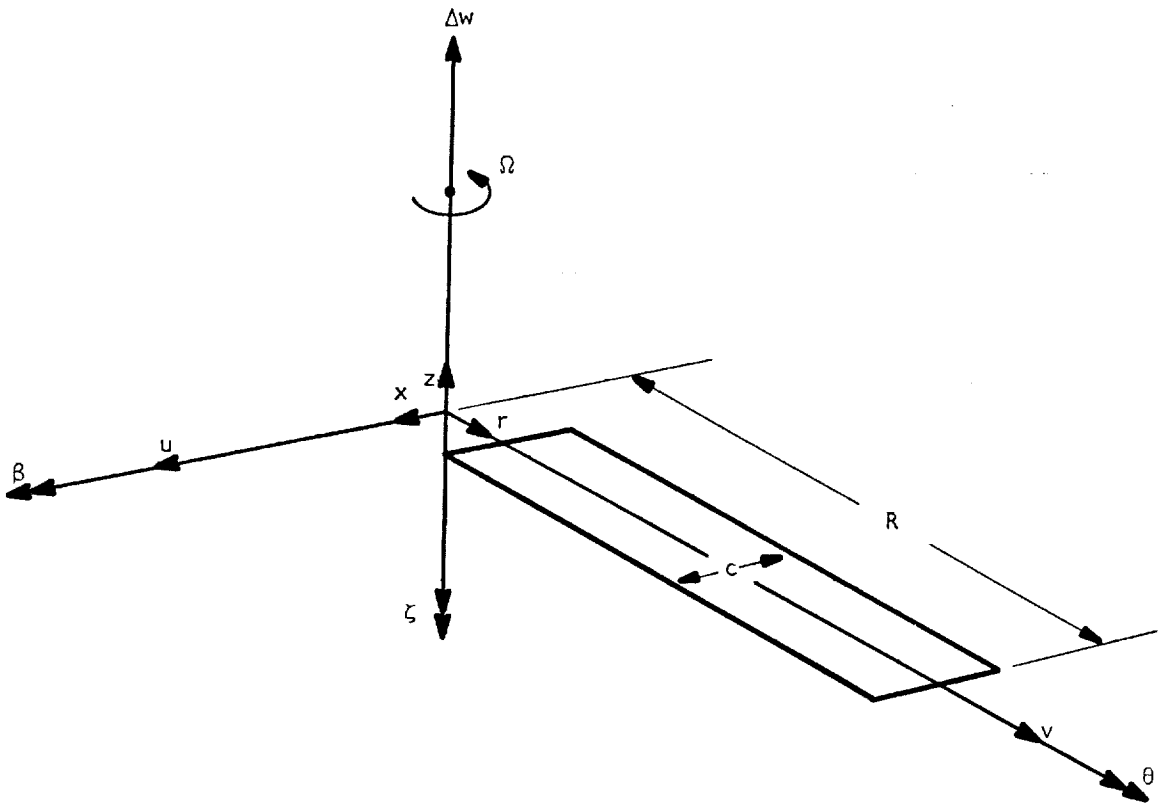

Figure 4. Rotor Blade Coordinate Notation

Figure 5. Blade Tip Pitch Response due to Sinusoidal Excitation at the Blade Root

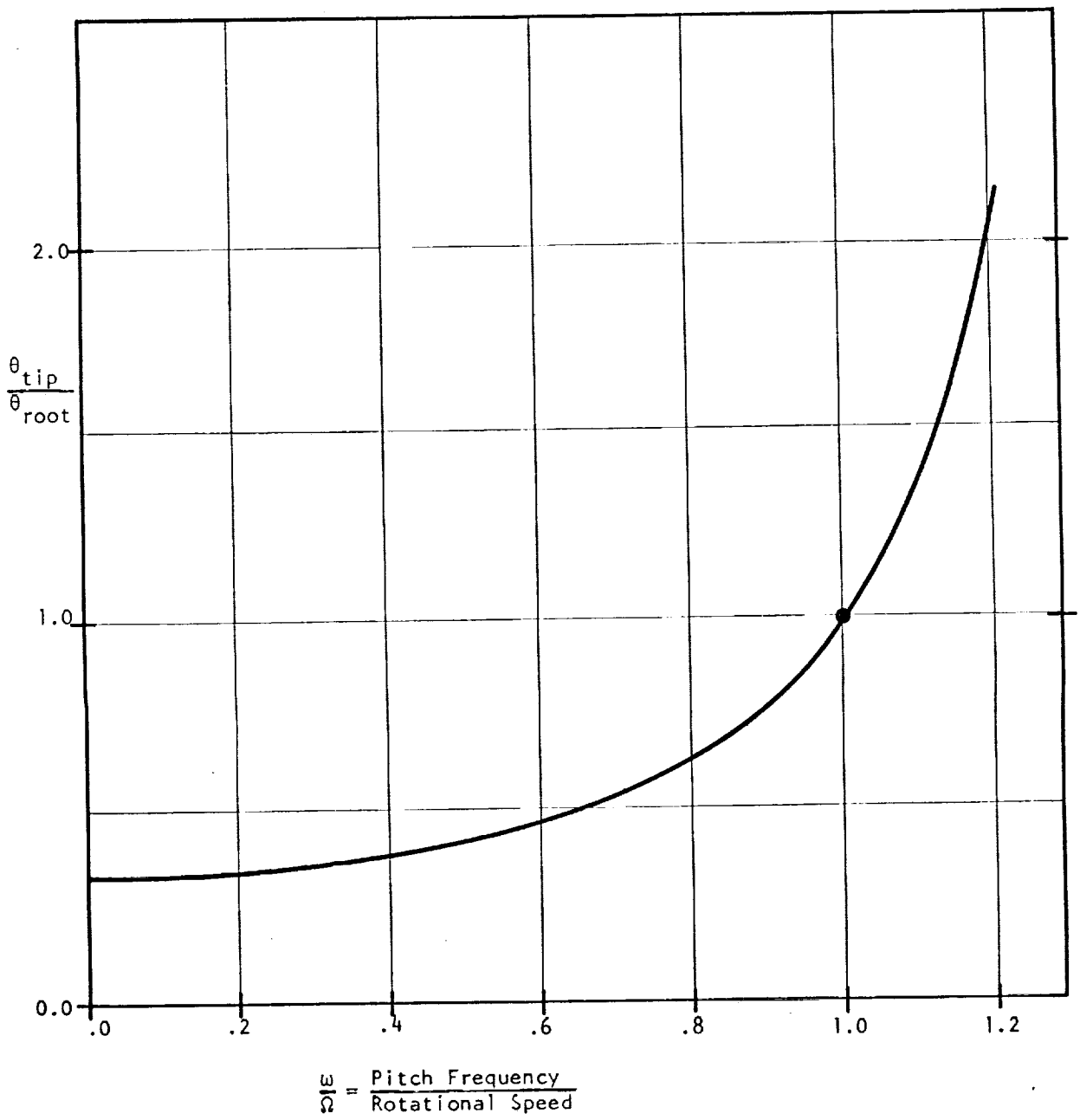

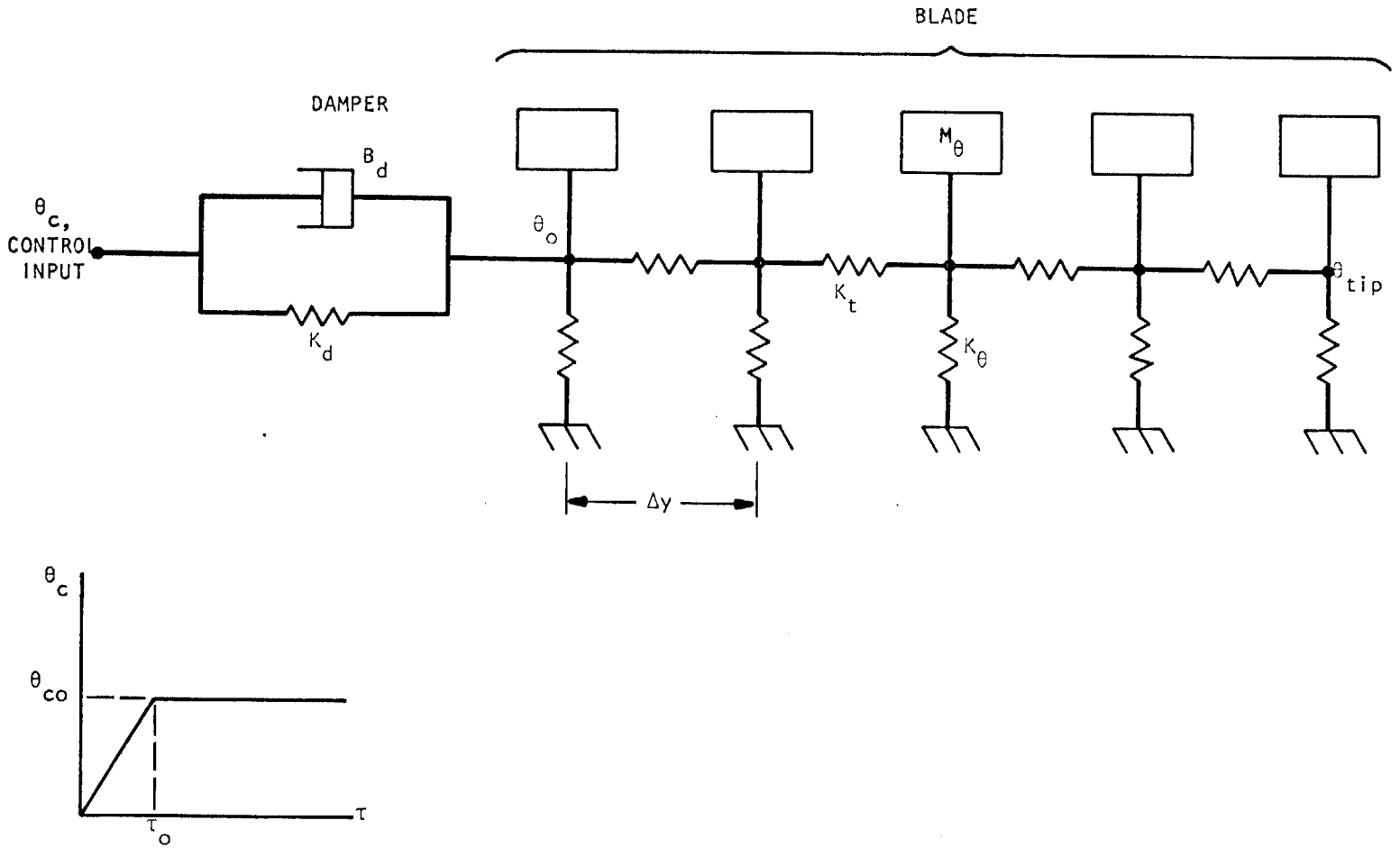

Figure 6. Idealized Model for Blade Pitch

$$M_\theta = \Delta y;\ K_\theta = \Delta y;\ K_t = \frac{1-y^2}{2\Delta y}$$

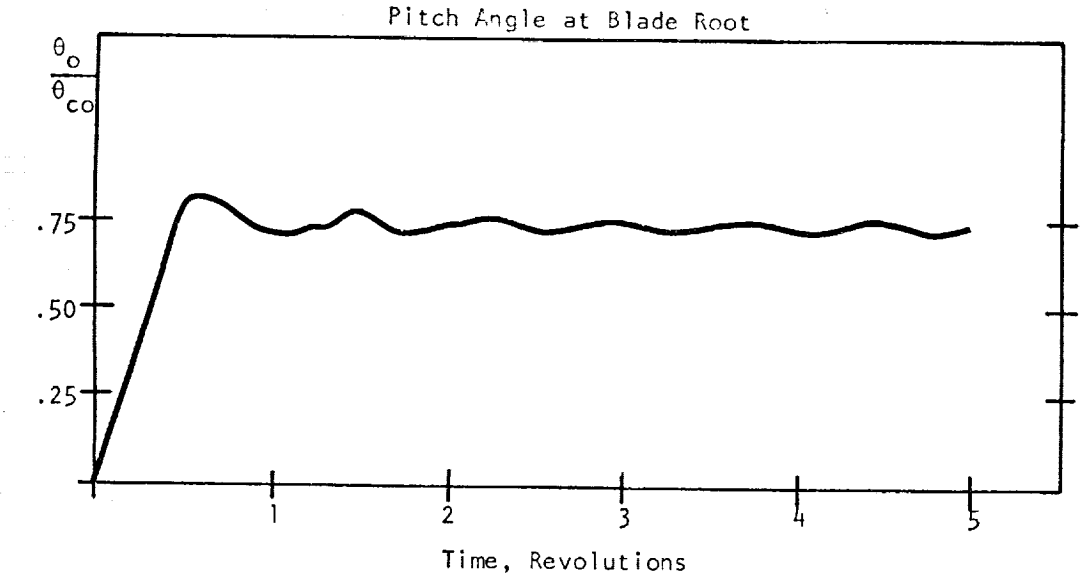

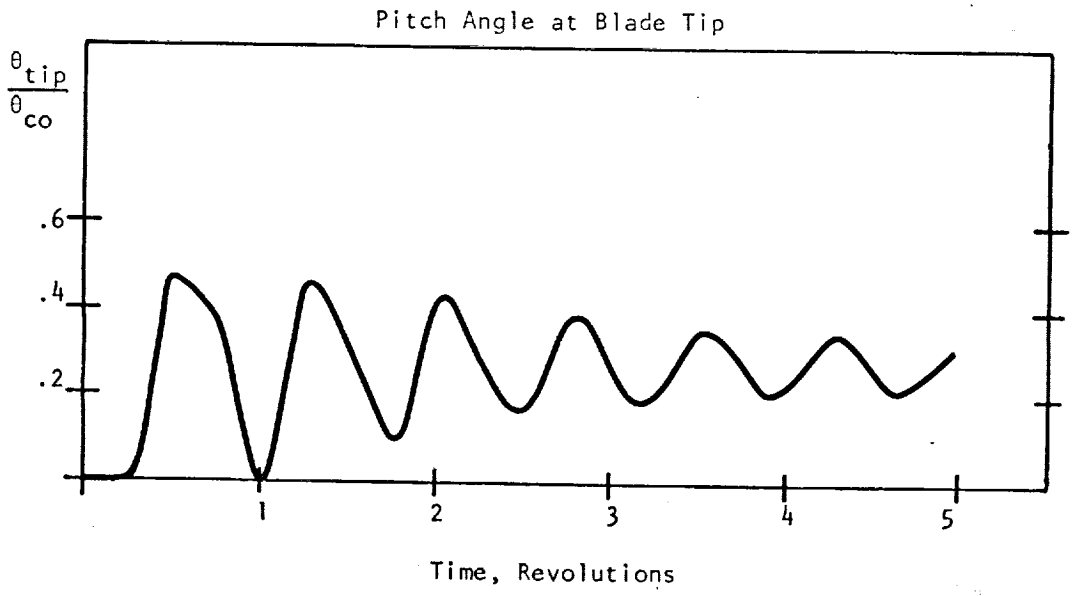

Figure 7. Blade Torsional Response to Ramp Collective Input

$$\frac{K_d}{\rho\Omega^2 IR} = 2.0; \quad \frac{B_d}{K_d} = \frac{2\pi}{\Omega}$$

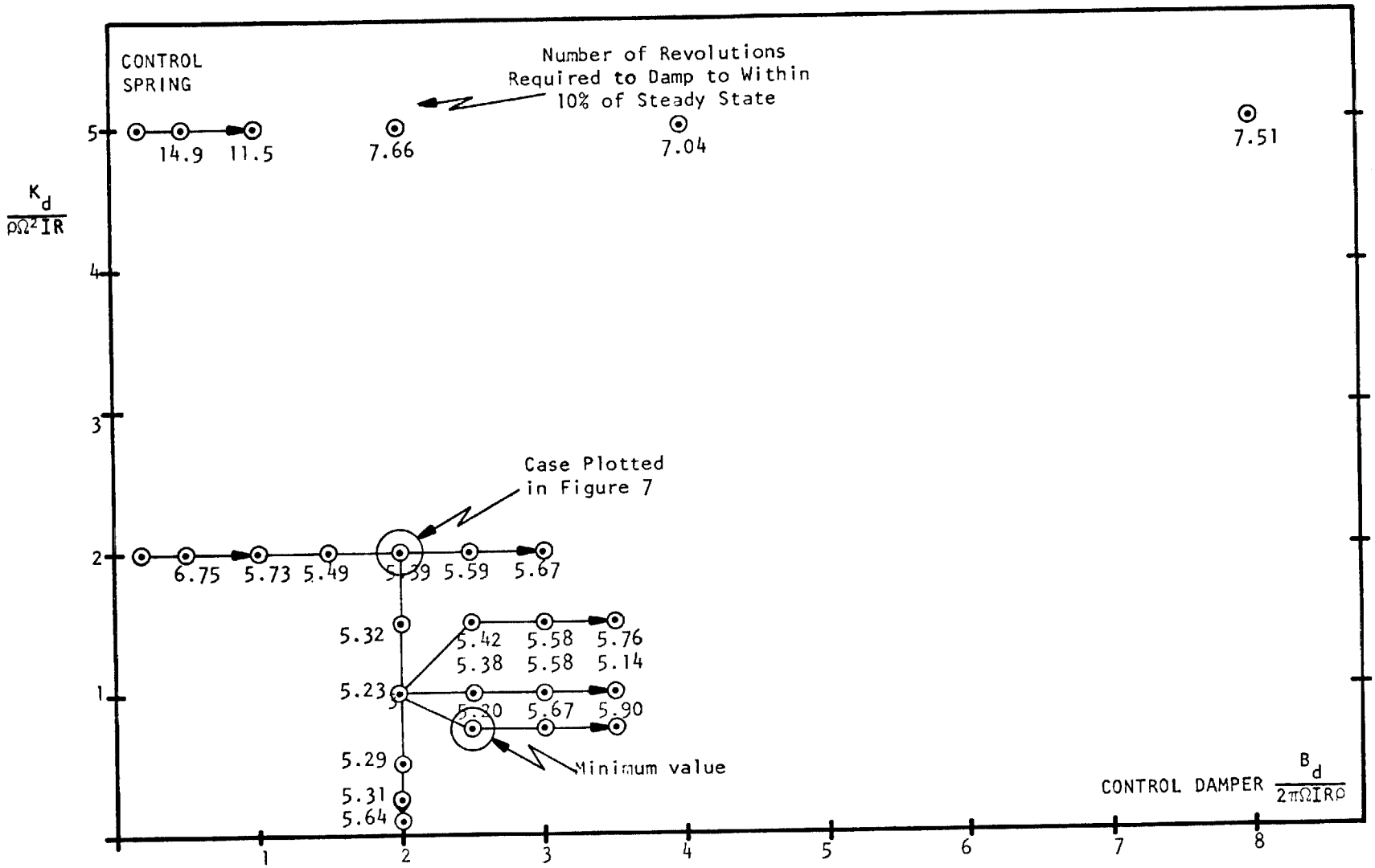

Figure 8. Results for Control Damper Optimization Study

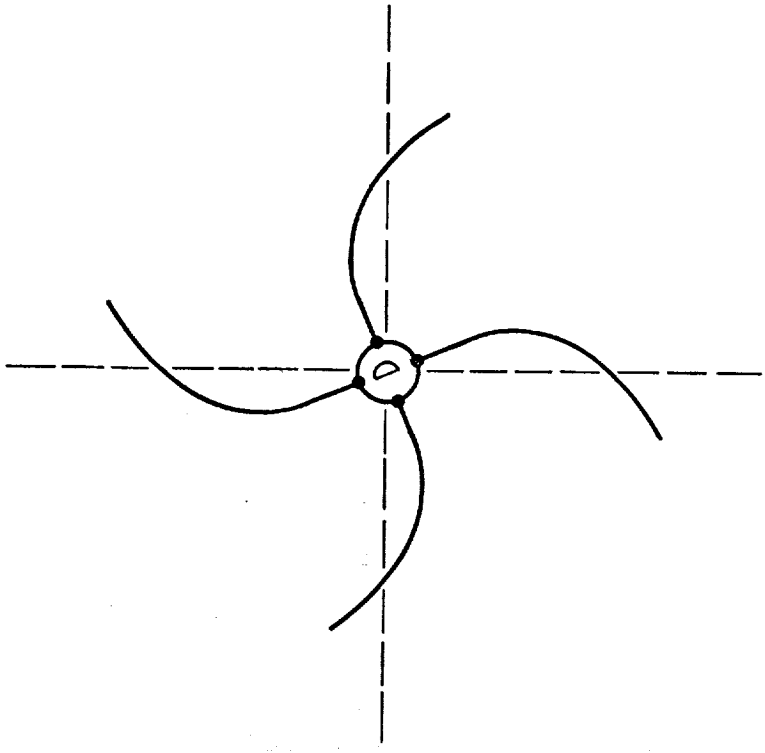

(a) 2nd Collective Inplane Mode

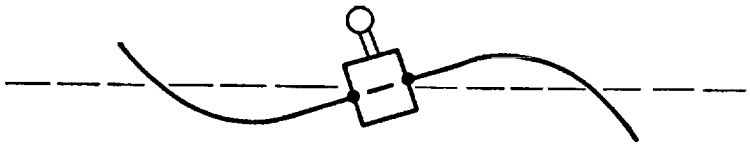

(b) 2nd Cyclic Vertical Mode

Figure 9. Blade Modes that Result in Rotations of the Center Body

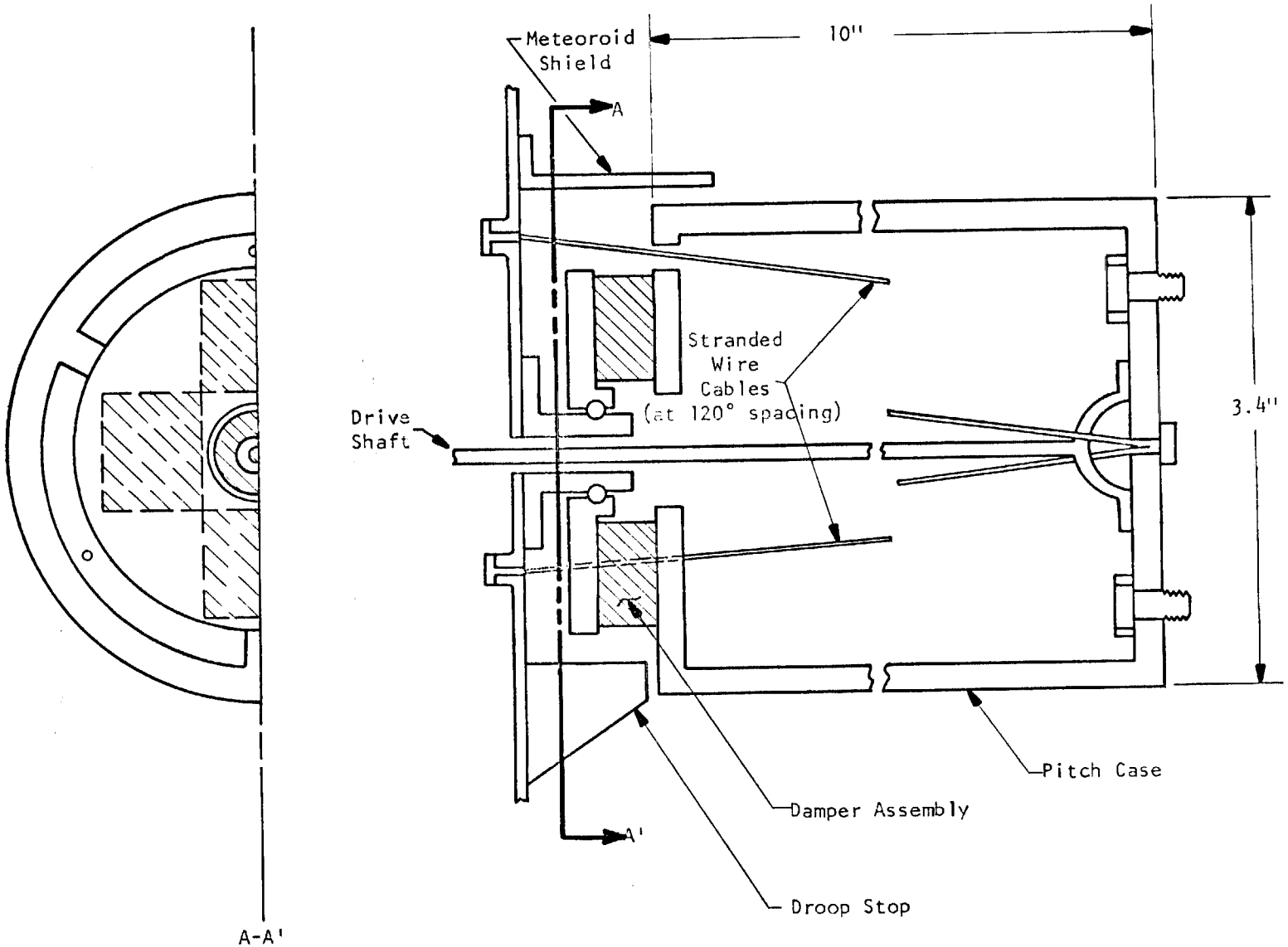

Figure 10. Blade Retention System

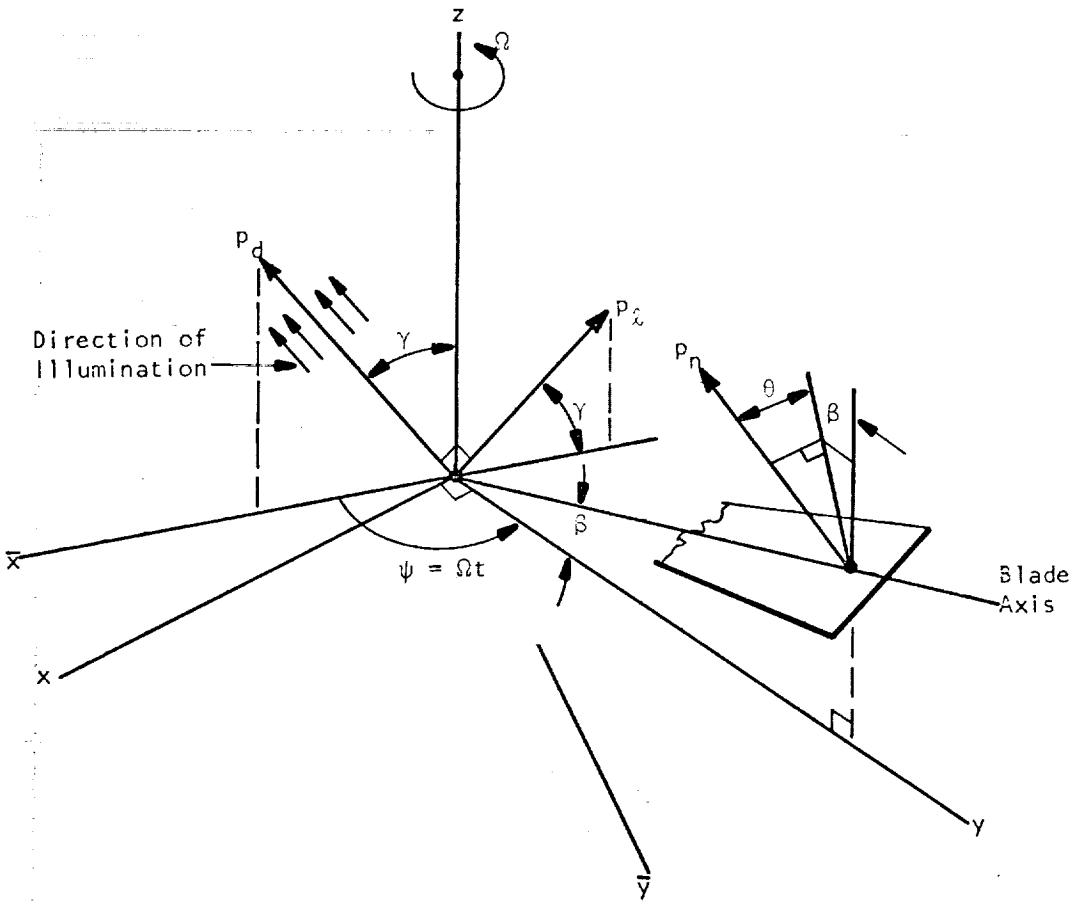

Figure 11. Coordinate Geometry for Rotating Blade

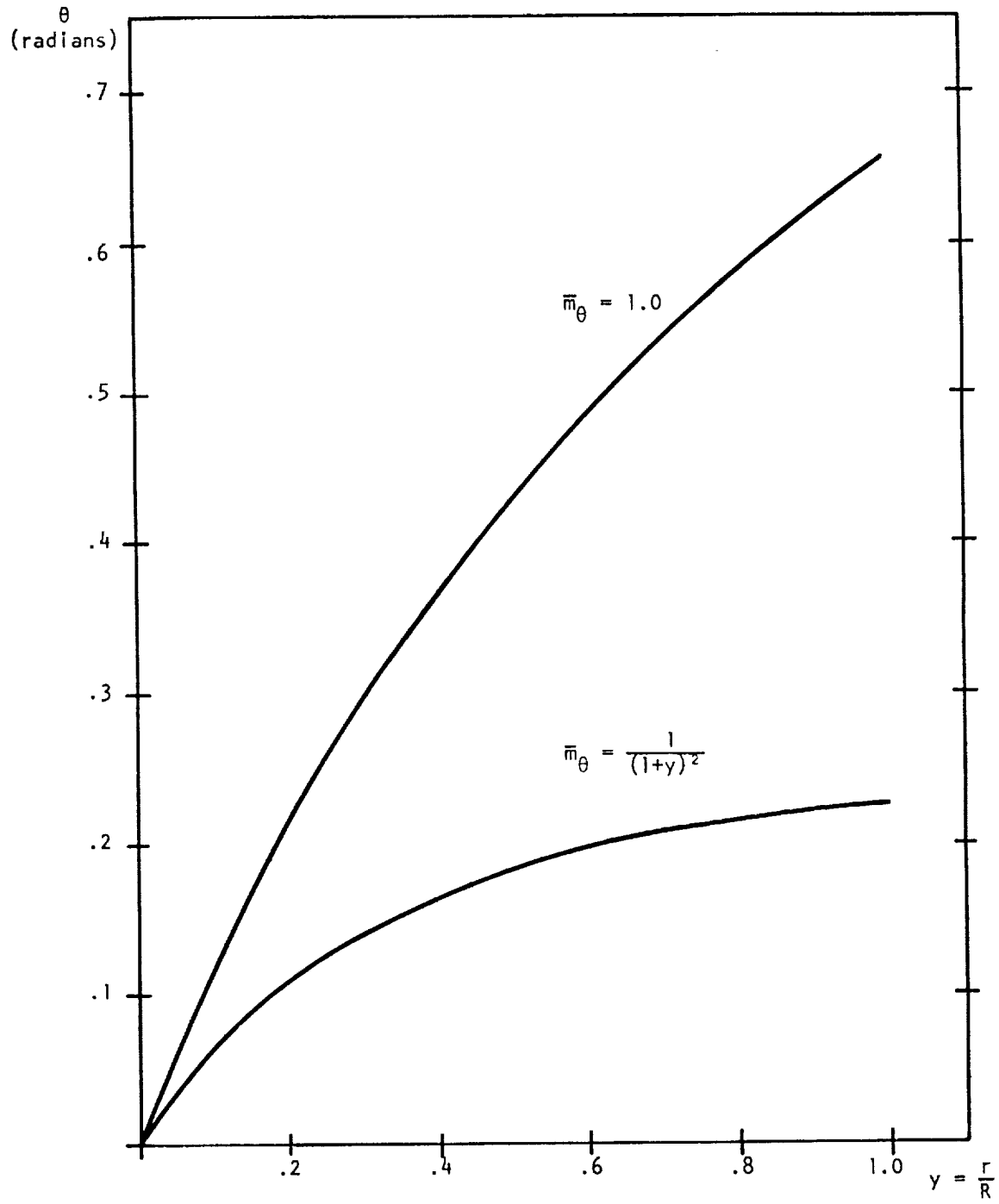

Figure 12. Pitch Distribution Due to Static Applied Load

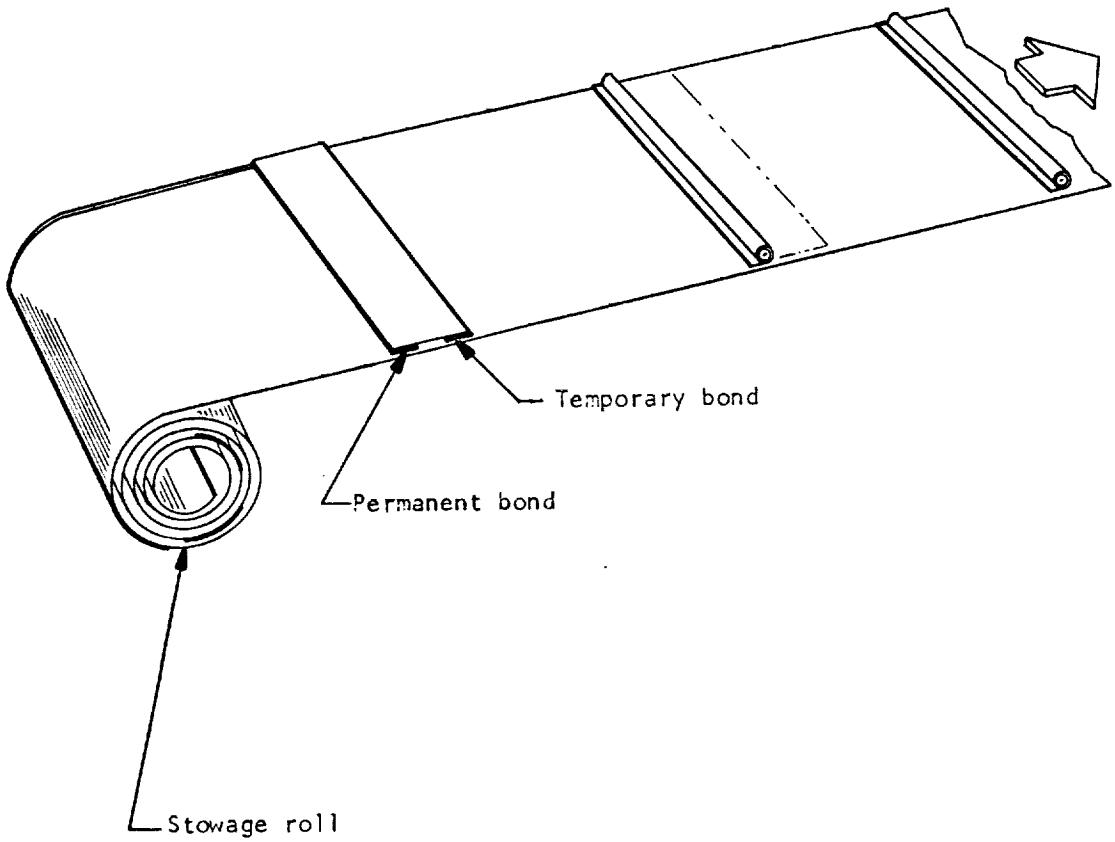

Figure 13. Deployable Transverse Batten Concept

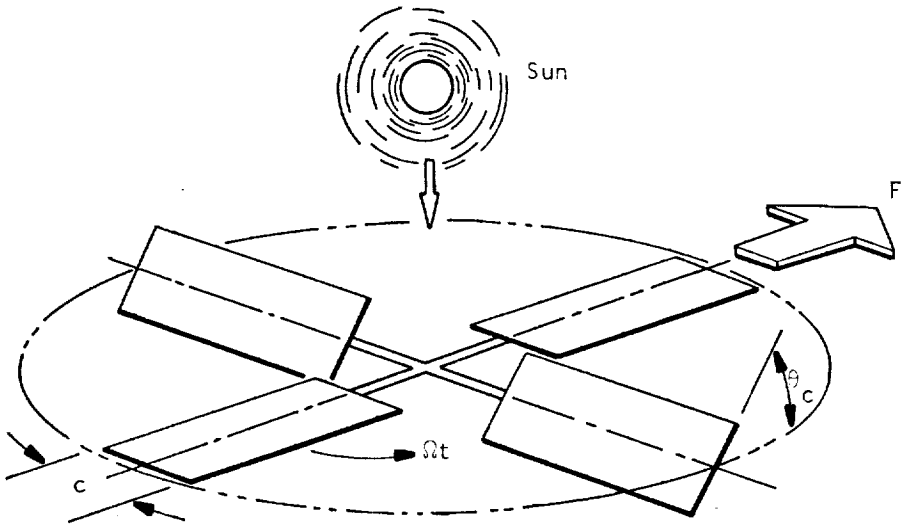

(a) Lateral Force Produced by Cyclic Pitch

$\theta = \theta_c \sin \Omega t$

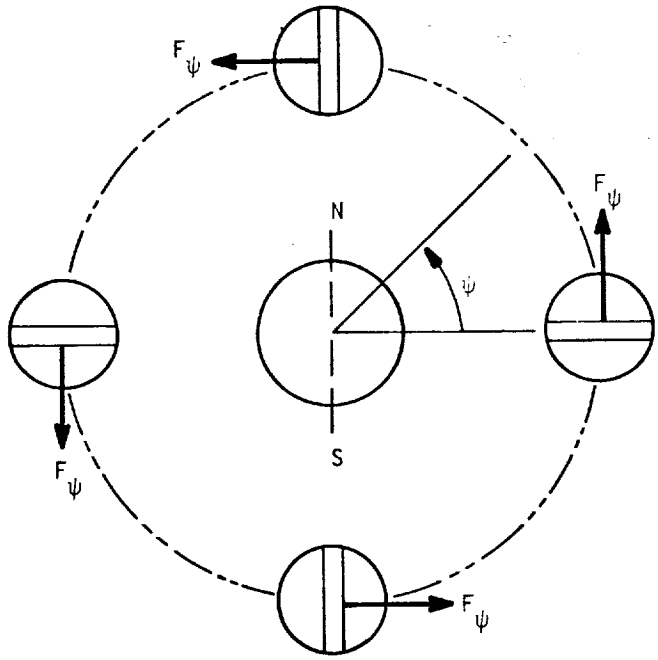

(b) Use of Cyclic Pitch to Change Orbital Altitude in a Polar Orbit

Figure 14. Lateral Vehicle Control

(a) Cyclic Pitch Input

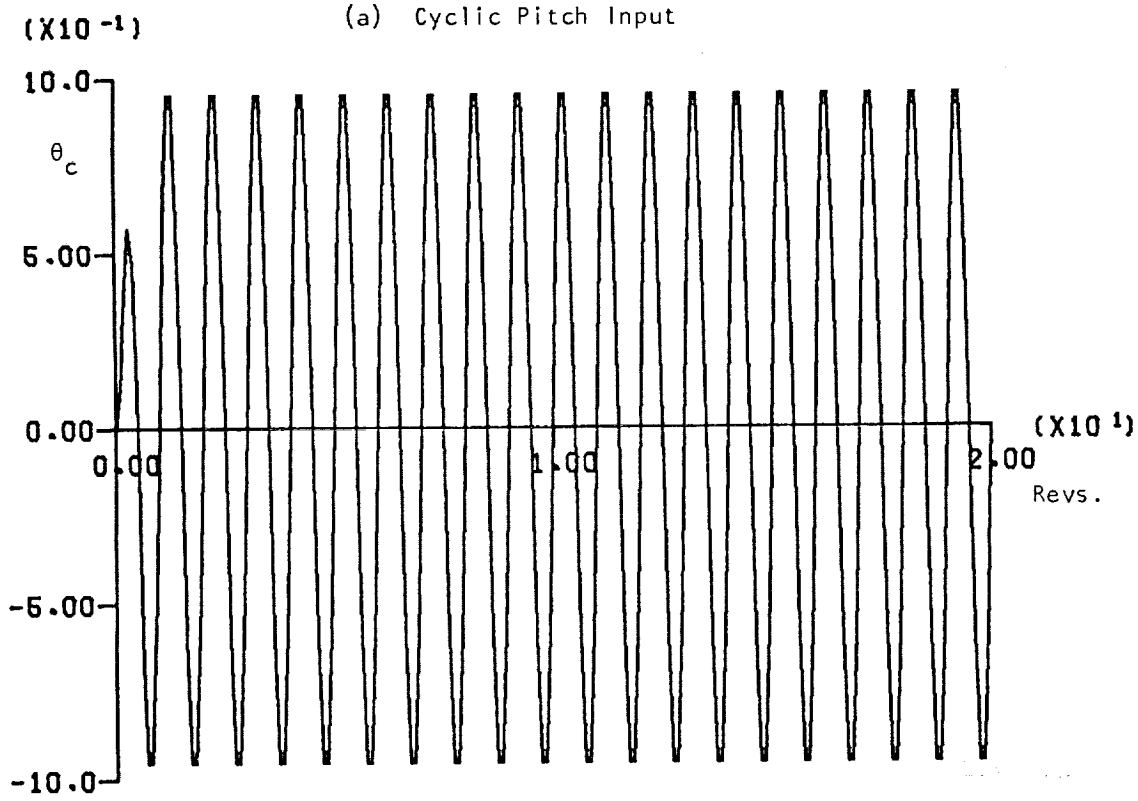

(b) Pitch Angle at Blade Root

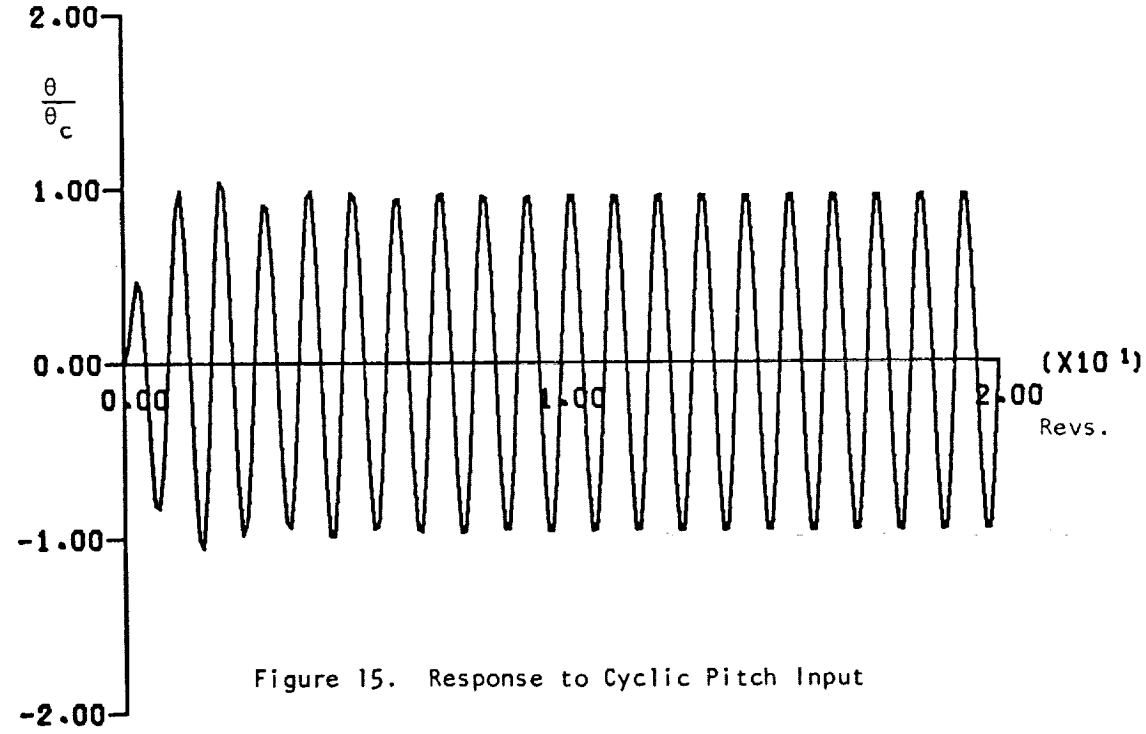

Figure 15. Response to Cyclic Pitch Input

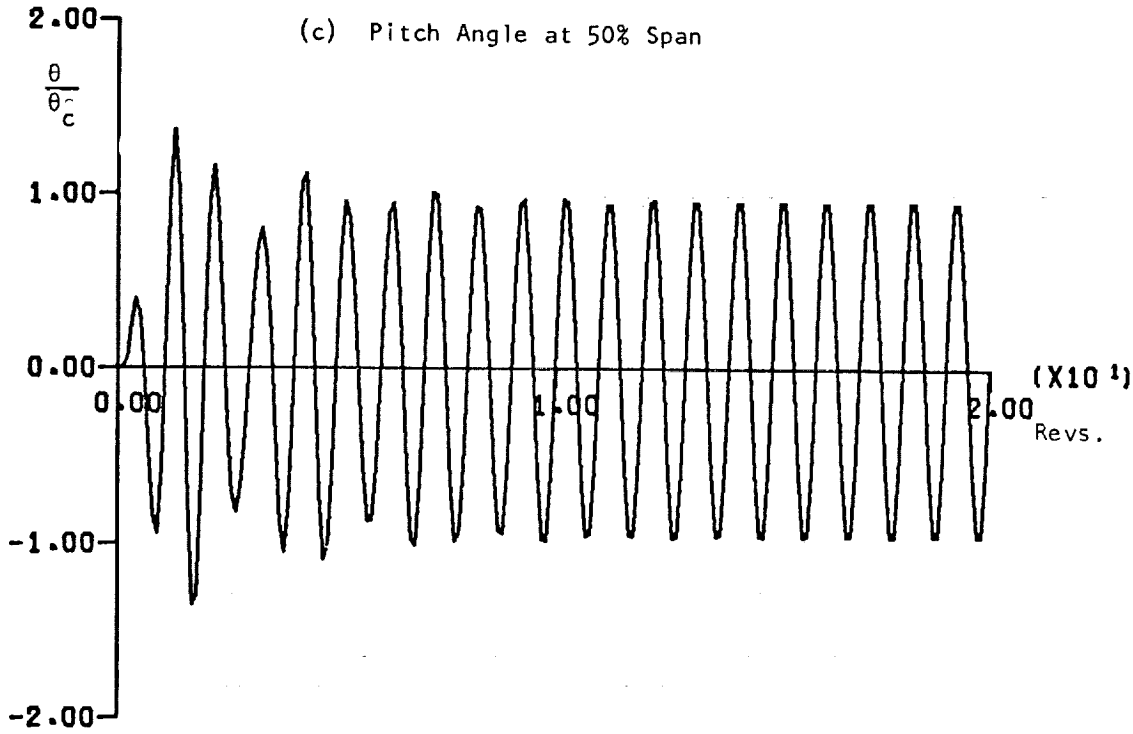

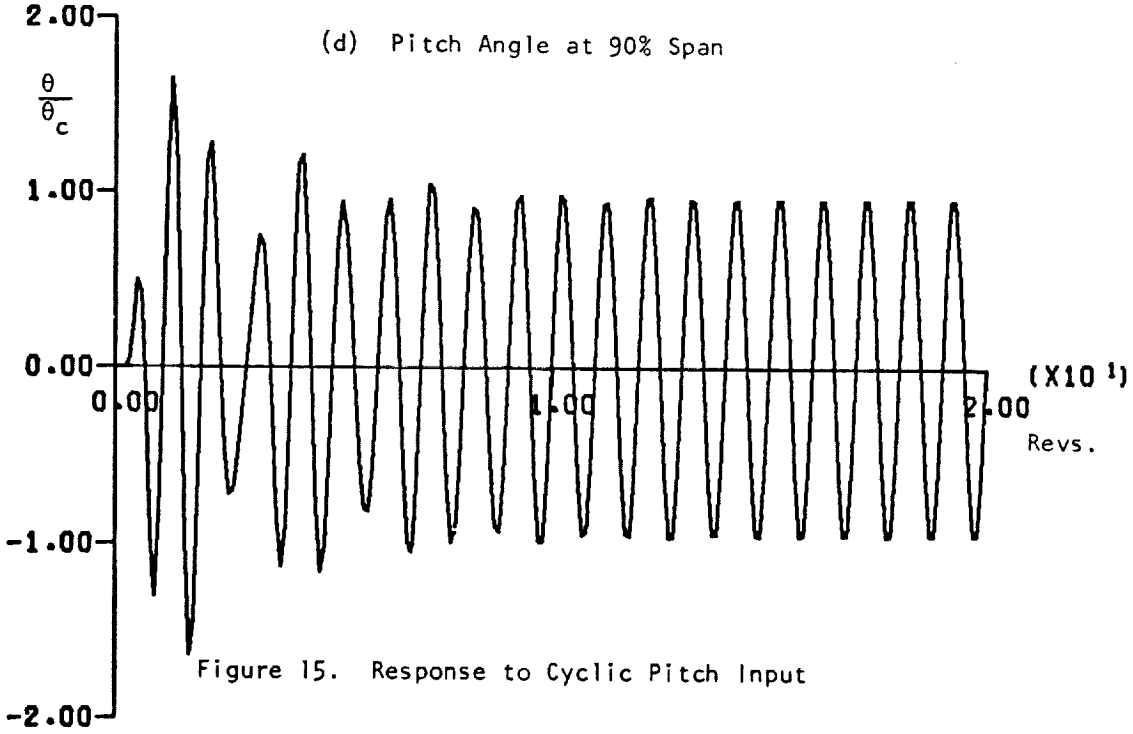

Figure 15. Response to Cyclic Pitch Input

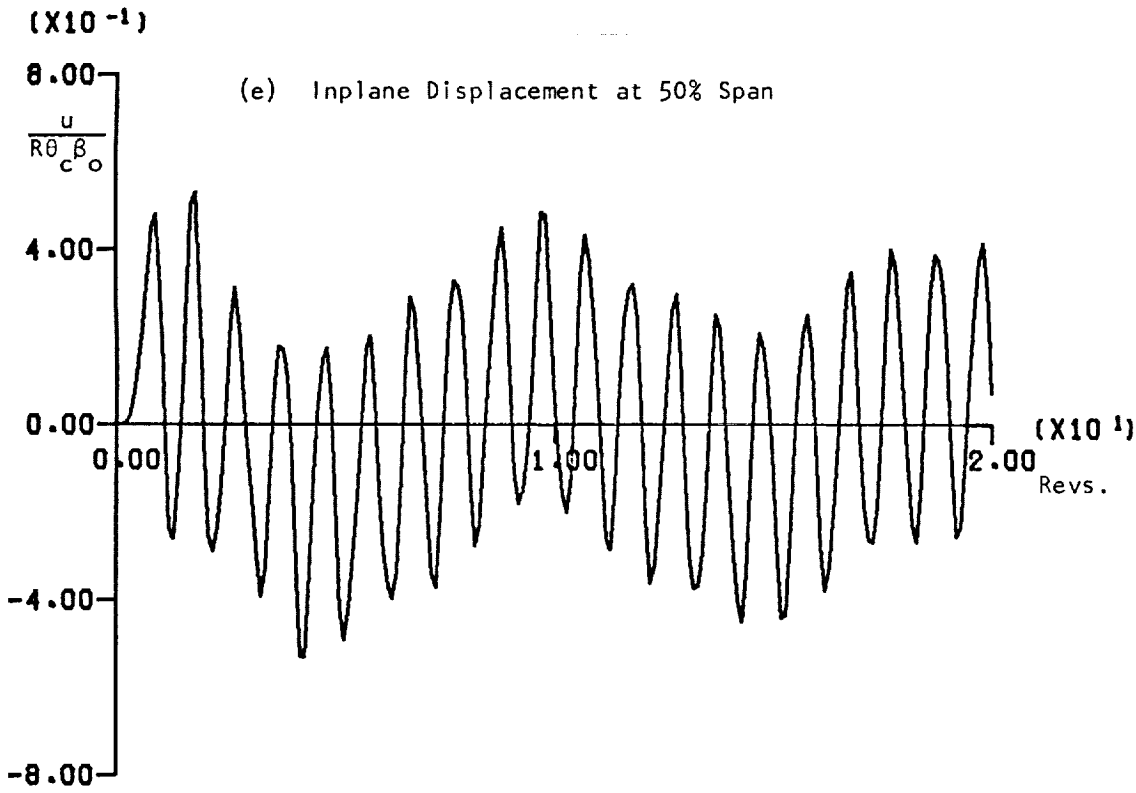

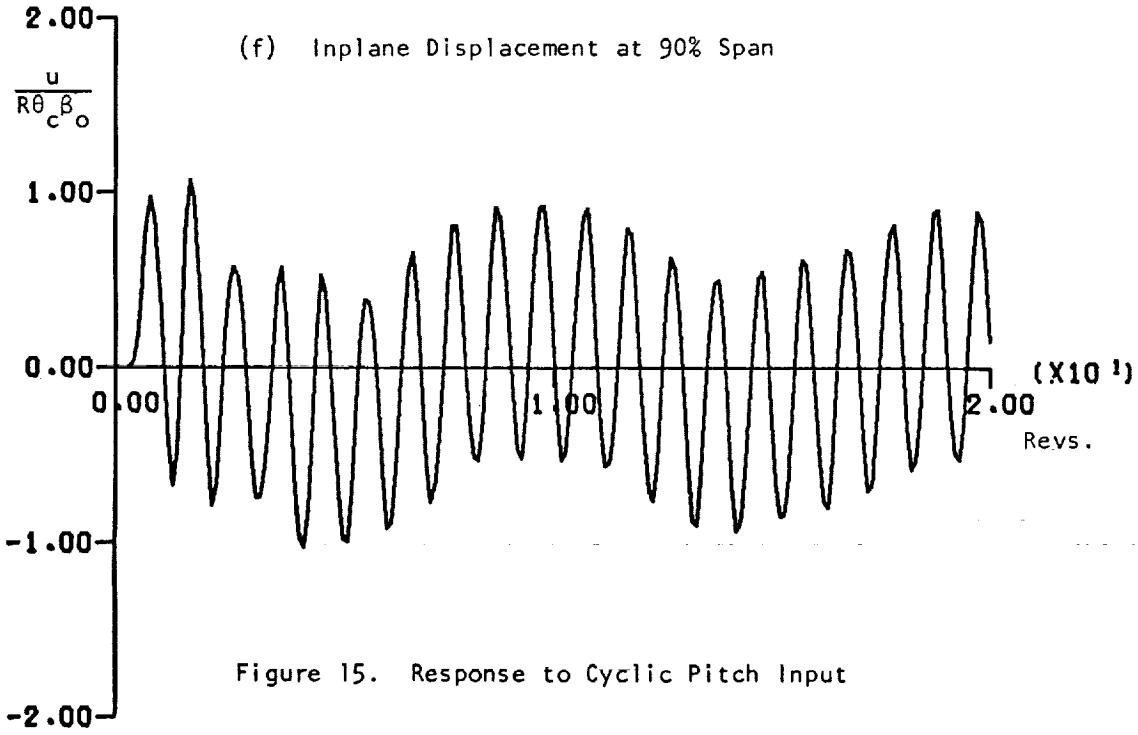

Figure 15. Response to Cyclic Pitch Input

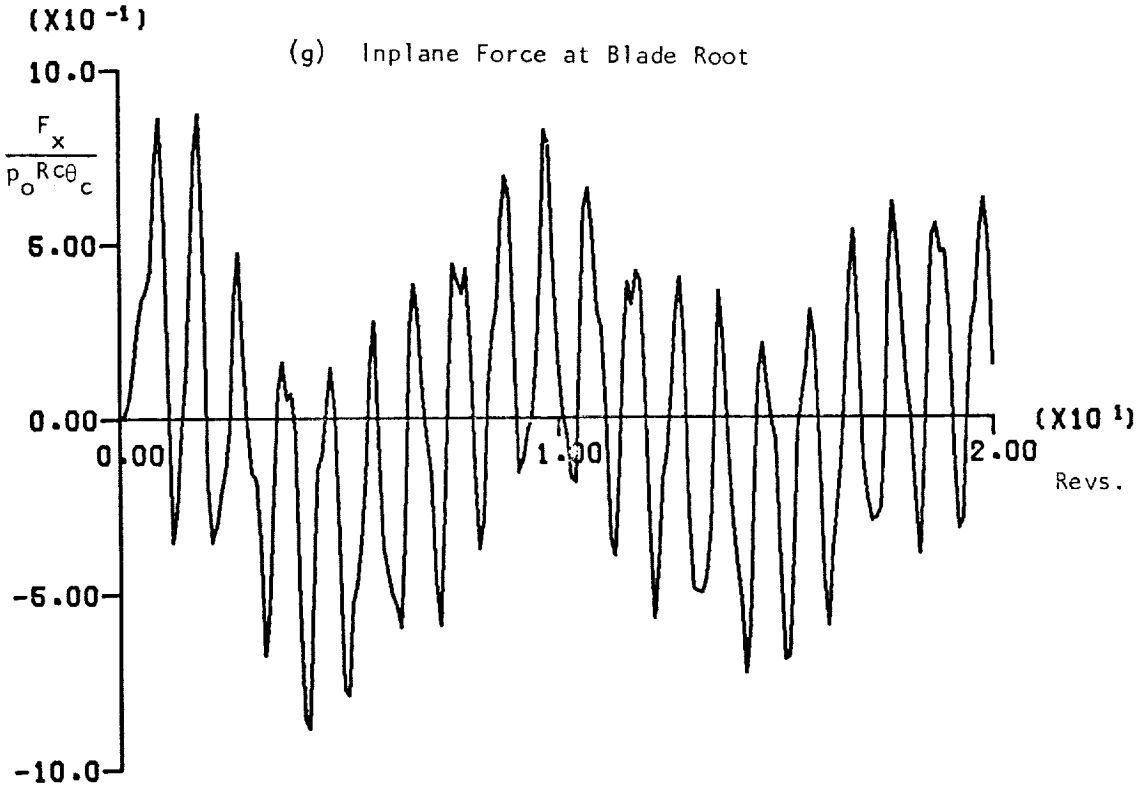

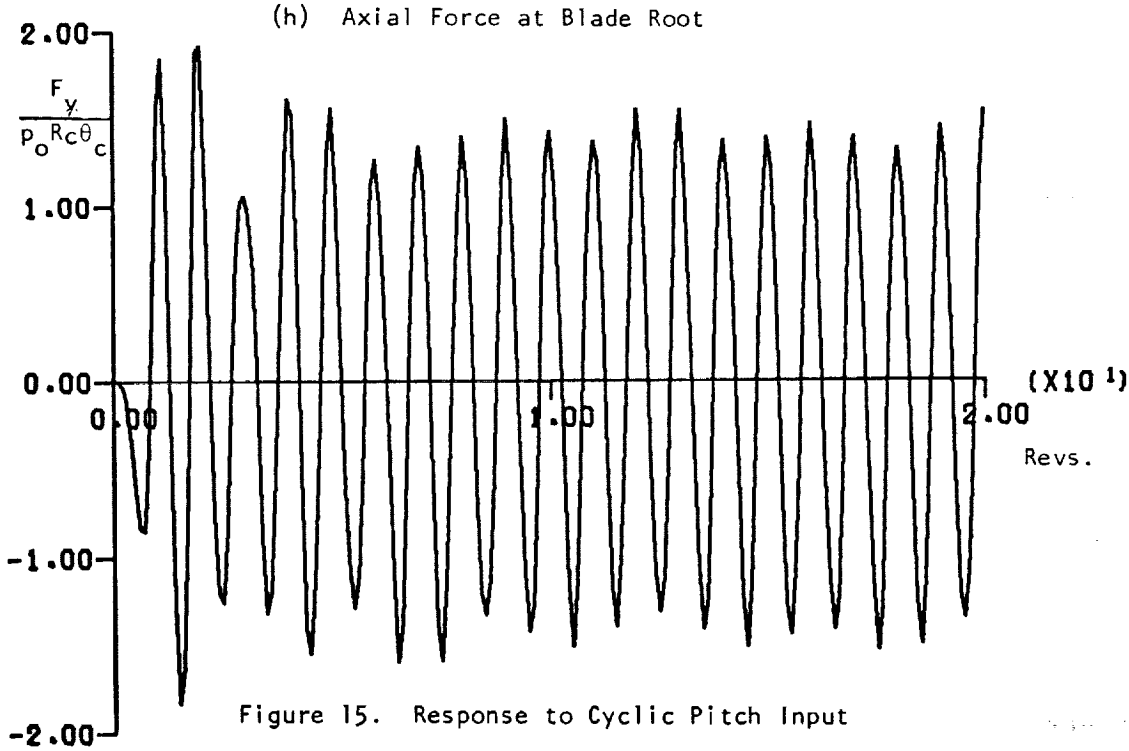

Figure 15. Response to Cyclic Pitch Input

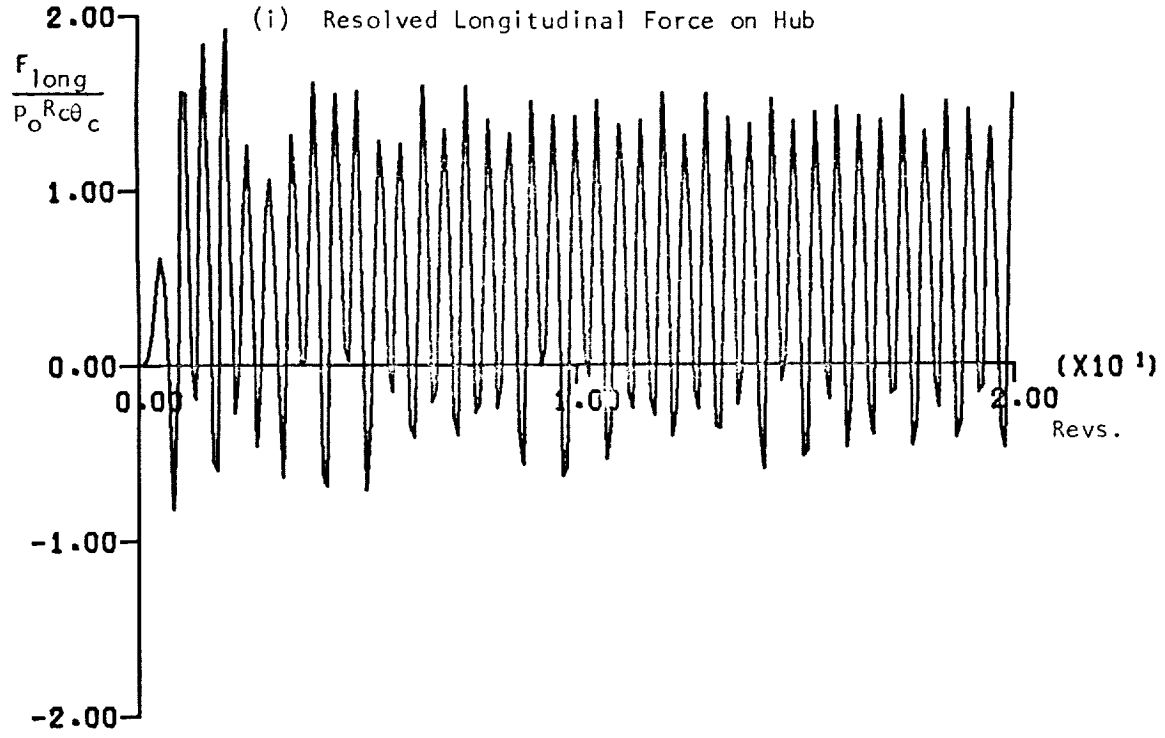

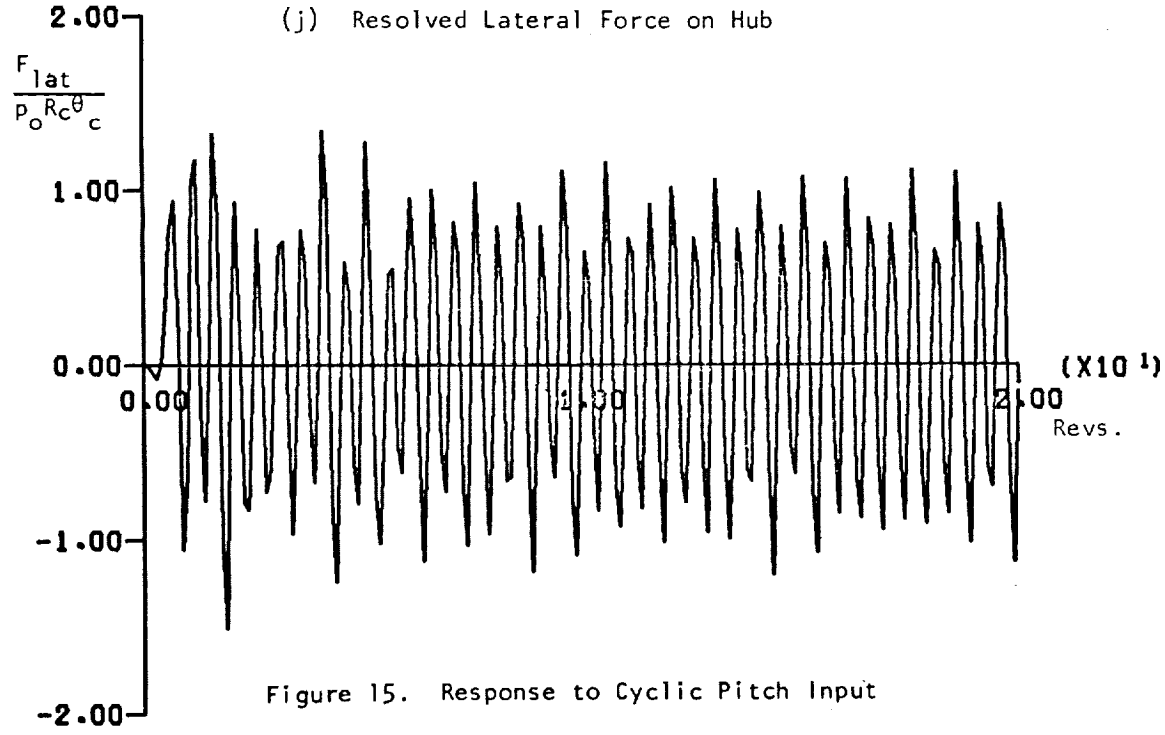

Figure 15. Response to Cyclic Pitch Input

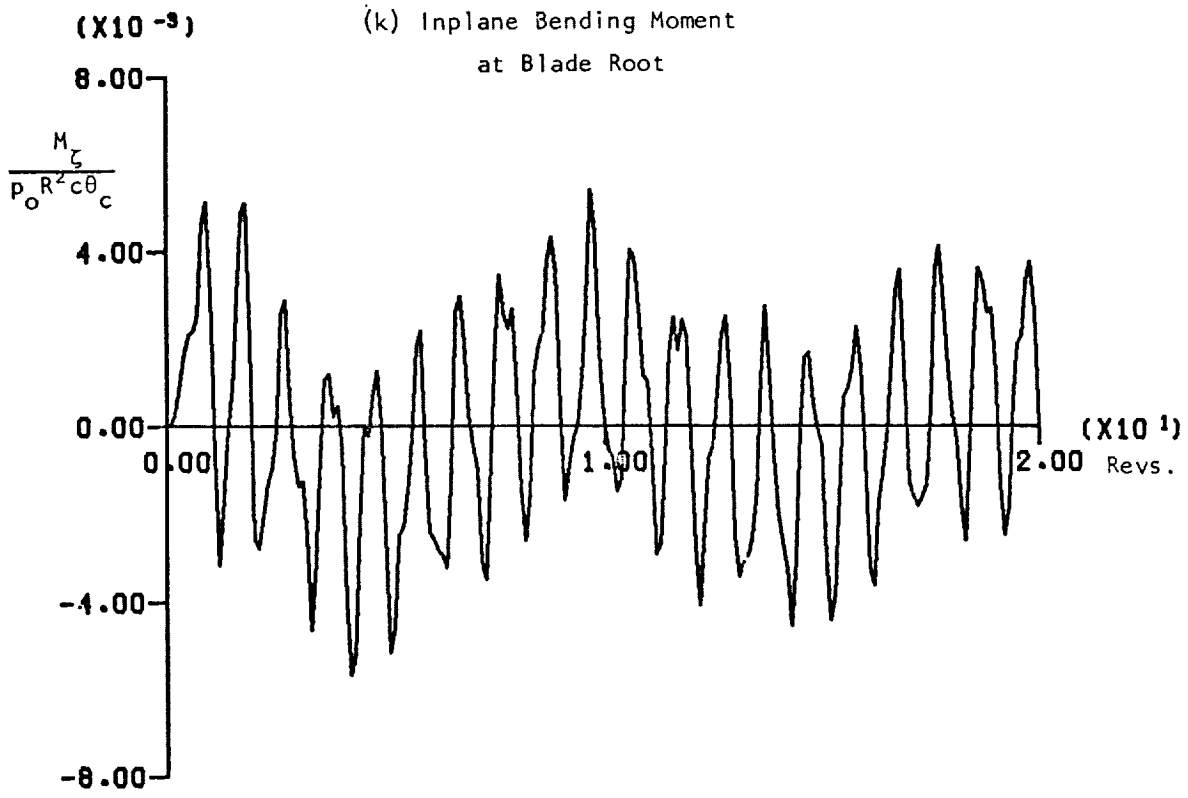

(k) Inplane Bending Moment at Blade Root

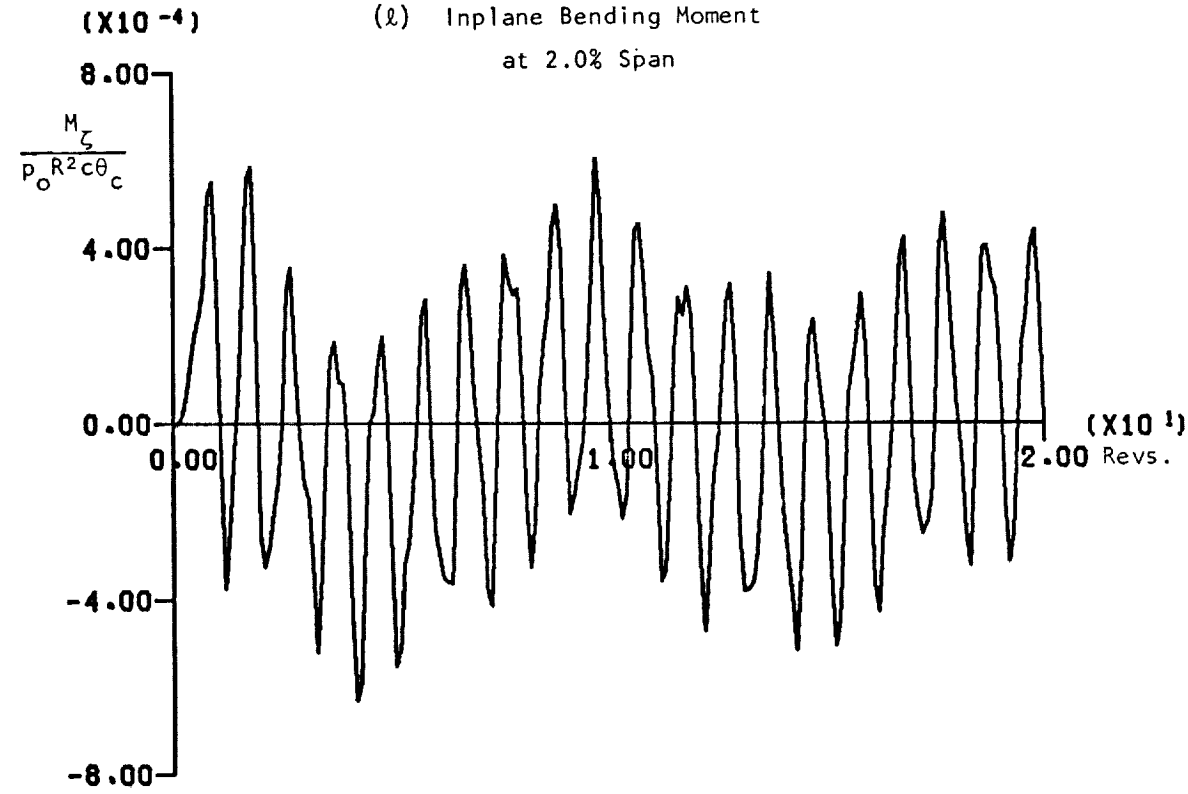

(ℓ) Inplane Bending Moment at 2.0% Span

Figure 15 Response to Cyclic Pitch Input

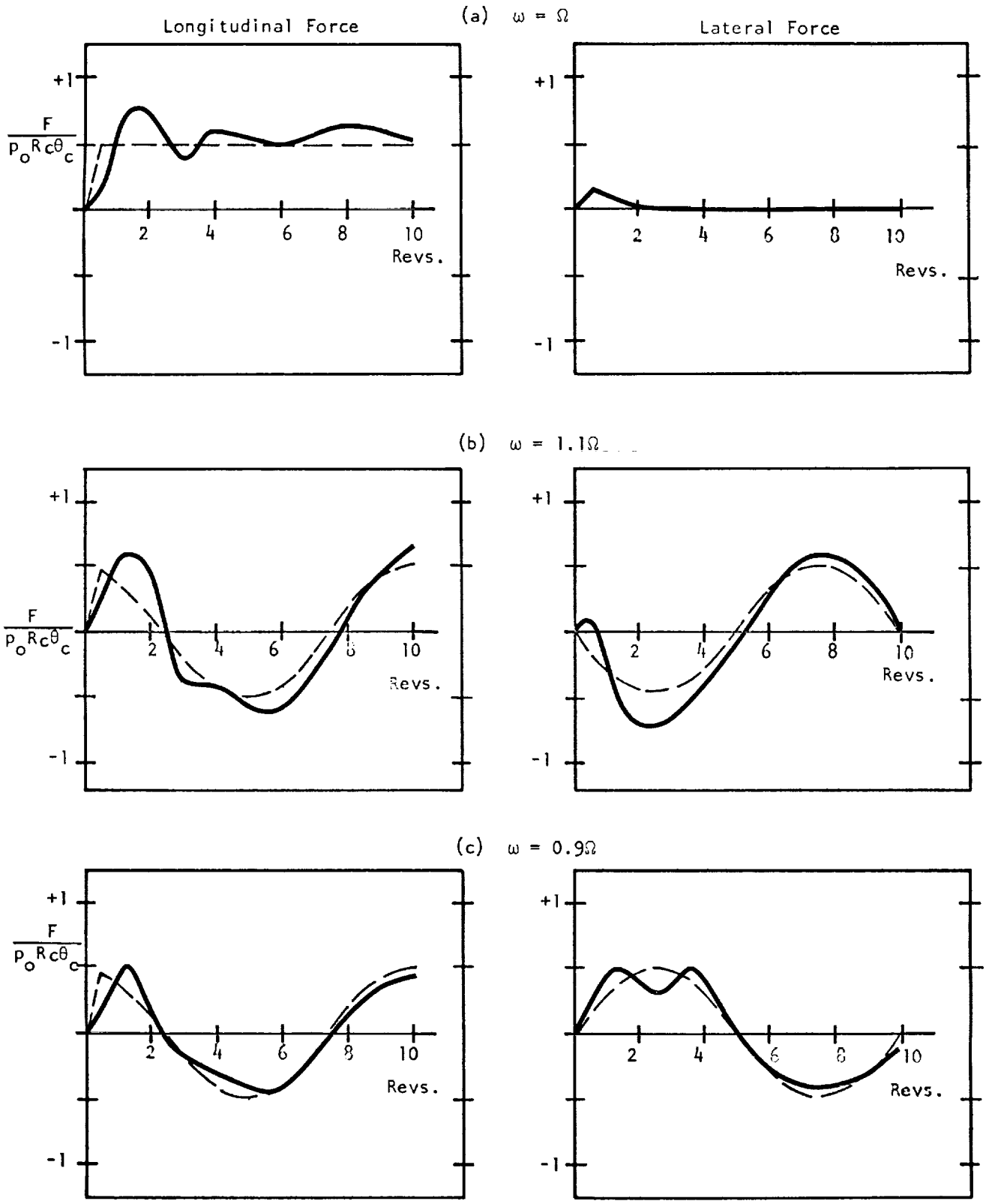

Figure 16. Force Resultants for Cyclic Pitch Input

Flexible Blade

Rigid Blade

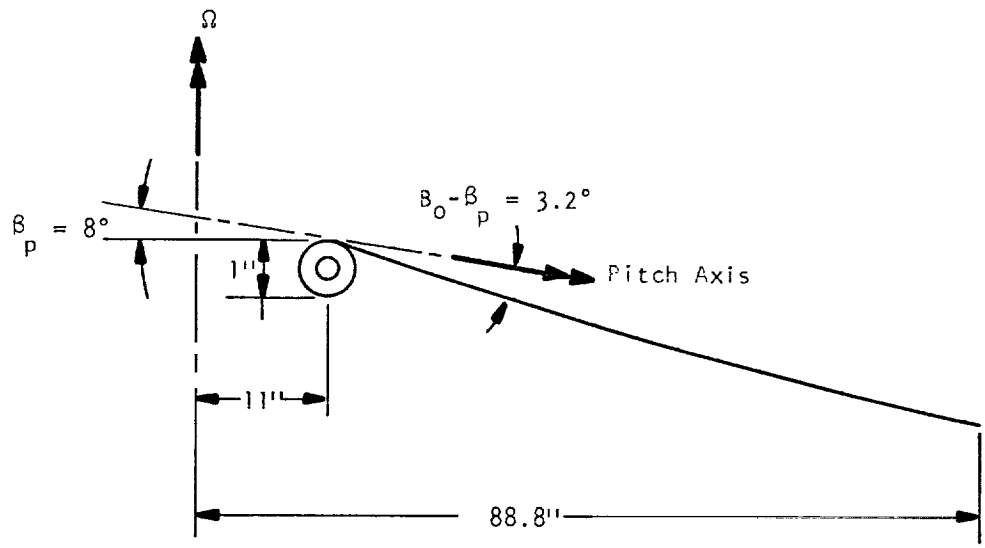

Blade Properties

Thickness: .001" (Kapton)

Chord, C = 1.938"

Weight/unit area = 1.08×10^{-4} lb/in^2 (Kapton plus paint)

Modulus of elasticity, E = 500,000 psi

Operating Parameters

Spin rate, $\Omega = 2\pi$ rad/sec

Stress at Centerline, $\sigma_o = 43.6$ psi

Coning angle at tip, $\beta_t = 6.33°$

Inplane Stiffness Parameter, $K = \frac{1}{12}\left(\frac{E}{\sigma_o}\right)\left(\frac{c}{R}\right)^2 = .454$

Figure 17. Heliogyro Blade Experiment

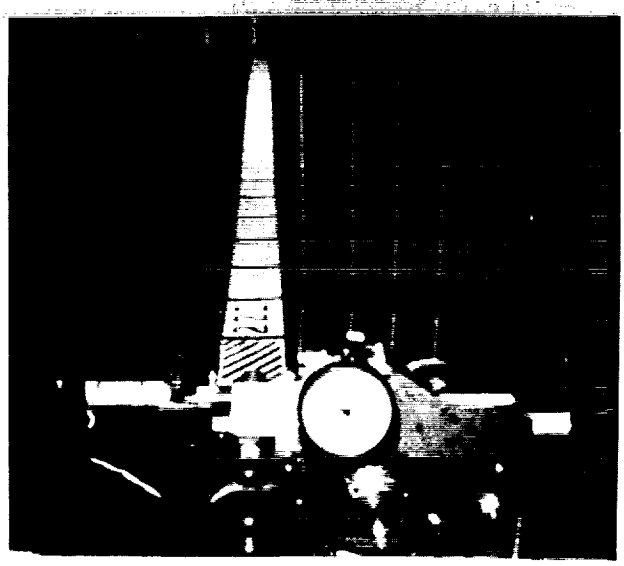

(a) $\theta_c = 0$

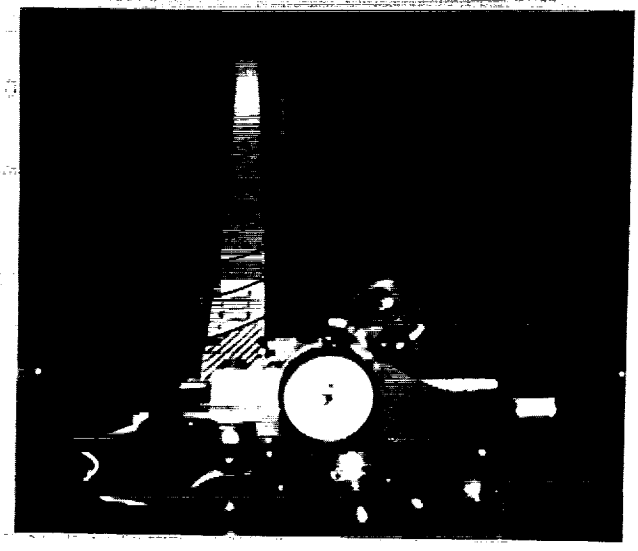

(b) $\theta_c = 25°$

Figure 18. Photographs of Rotating Blade in Test Chamber

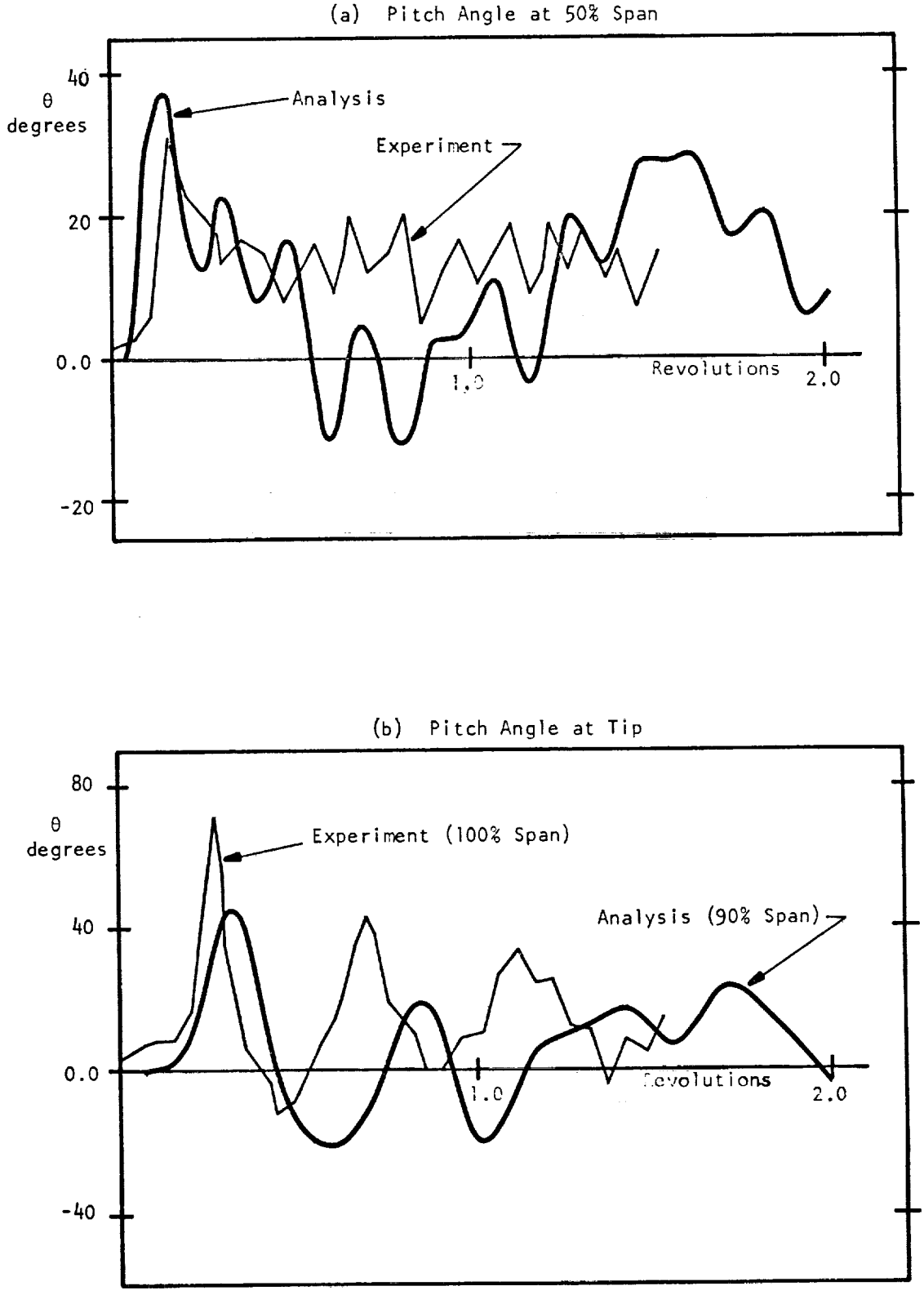

Figure 19. Response to an Abrupt 25° Change in Collective Pitch, $\beta_p = 8°$.

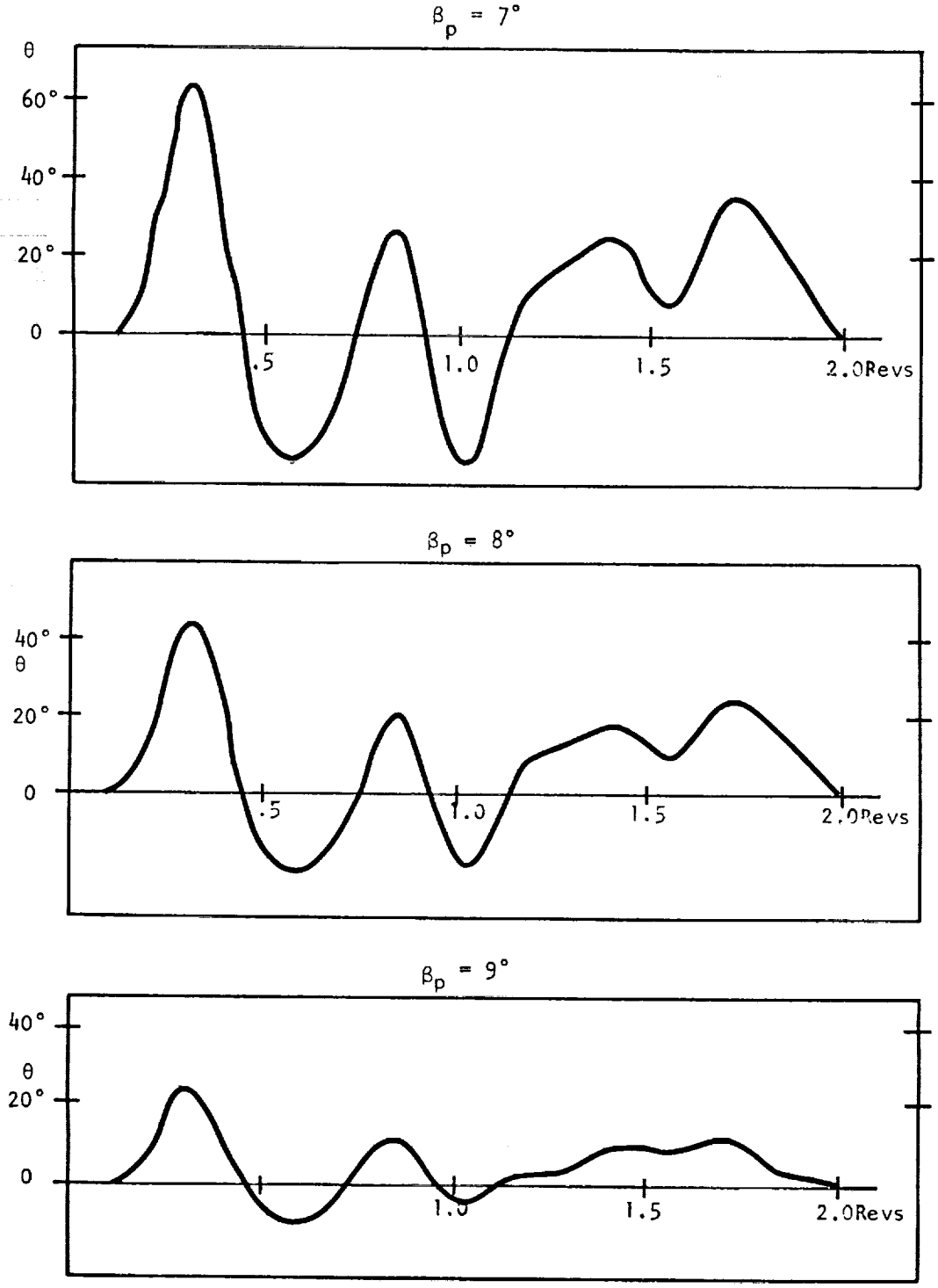

Figure 20. Effect of Pitch Axis Inclination on the Dynamic Pitch Response at the 90% Span